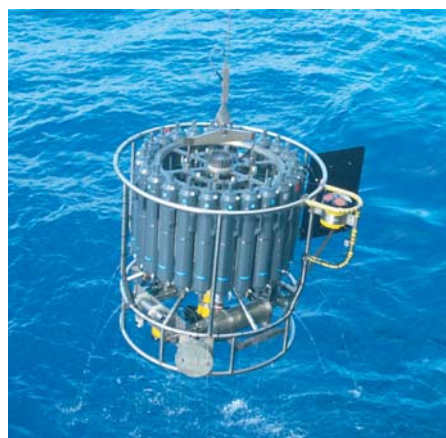# Influences of the 11-year solar cycle on the tropical atmosphere and oceans

Stergios Misios

Hinweis

Die Berichte zur Erdsystemforschung werden
vom Max-Planck-Institut für Meteorologie in
Hamburg in unregelmäßiger Abfolge heraus-
gegeben.

Sie enthalten wissenschaftliche und
technische Beiträge, inklusive Dissertationen.

Die Beiträge geben nicht notwendigerweise
die Auffassung des Instituts wieder.

Die "Berichte zur Erdsystemforschung" führen
die vorherigen Reihen "Reports" und
"Examensarbeiten" weiter.

Notice

*The Reports on Earth System Science are published
by the Max Planck Institute for Meteorology in
Hamburg. They appear in irregular intervals.*

*They contain scientific and technical contributions,
including Ph. D. theses.*

*The Reports do not necessarily reflect the
opinion of the Institute.*

*The "Reports on Earth System Science" continue
the former "Reports" and "Examensarbeiten"
of the Max Planck Institute.*

Influences of the 11-year solar cycle
on the tropical atmosphere and oceans

Stergios Misios

aus Ptolemaida, Griechenland

Hamburg 2012

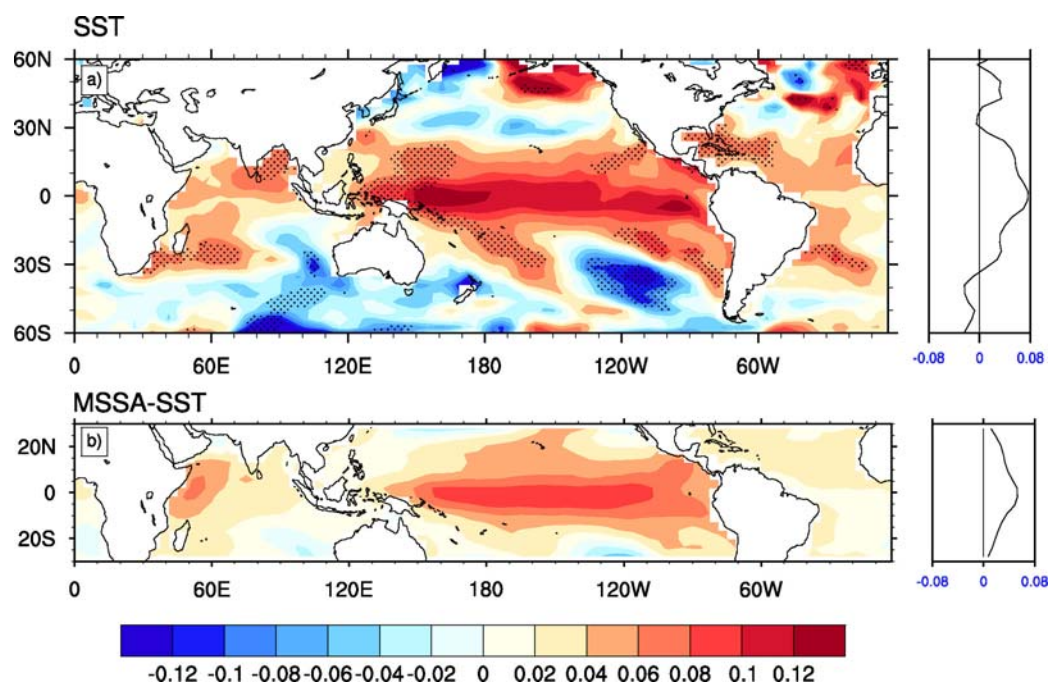Stergios Misios
Max-Planck-Institut für Meteorologie
Bundesstrasse 53
20146 Hamburg

Influences of the 11-year solar cycle
on the tropical atmosphere and oceans

Stergios Misios

Hamburg 2012

Abstract

The Sun is the main source of energy that fuels Earth's climate. Variations of the incoming total and spectral solar irradiance on decadal time scales should warm the surface and extensive research estimated a global-mean surface response of about 0.1 K from solar minima to solar maxima. Regional responses, however, can be manifold much stronger for dynamical reasons.

The response, if any, of the tropical Pacific Ocean to the 11-yr solar cycle forcing has drawn considerable attention in the recent years. Many studies indicated an El Niño-like warming, whereas other studies isolated a La Niña-like cooling during solar maxima. El Niño and La Niña are the two extremes of the El Niño-Southern Oscillation (ENSO). Detecting robust solar responses in the tropical Pacific is a not a straightforward task because naturally excited inter-annual or decadal oscillations can be taken as of solar origin. I find that the observed cooling in peak years of sunspot numbers is likely related to La Niña oversampling. If solar maxima favor, statistically, La Niña episodes, then El Niño-like warming should be detected in solar minima. Yet, observations do not support this transition. The Tropical Pacific Quasi-Decadal Oscillation (TPQDO), a natural oscillation of the tropical Pacific with signature similar to El Niño episodes, explains the observational evidence for a warmer tropical Pacific with increased solar cycle forcing. It is intriguing though that the observed TPQDO seems synchronized with the solar cycle over the last 50 years.

To systematically assess the response of the tropical Pacific to the 11-yr solar cycle, ensemble simulations with an atmospheric general circulation model with and without ocean coupling are carried out. The model is forced with realistic ozone and solar spectral irradiance changes from 1955 to 2006. The tropical-mean (30°S-30°N) surface temperature rises almost in phase with the solar cycle in the coupled ensemble simulations. In the Pacific, a basin-wide warming of up to 0.15 K from solar minimum to solar maximum is simulated, whereas the warming in the Indian and Atlantic oceans is weaker. The spatial solar signature at sea surface reminisces that of the simulated TPQDO. Our model generates a TPQDO of 12.3 years average period in simulations with constant solar forcing. The 11-yr solar cycle forcing, however, gives the pace, statistically, of the TPQDO. This is understood by the reduced surface easterlies in the western Pacific, which are simulated both in the coupled and uncoupled simulations. During solar maxima, westerly anomalies push the Pacific system to a state in which equatorial upper ocean heat is constantly flushed into the subtropics due to the divergence of Sverdrup transport. This solar-forced heat discharge lifts the thermocline over the entire Pacific, initiating the negative TPQDO phase in the years to follow. During solar minima, the stronger equatorial easterlies push the Pacific system to a state where heat is accumulated, favoring a positive TPQDO phase in the subsequent years. Hence, the solar-induced changes of the

surface winds set the pace, statistically, of the heat discharge and subsequently of the TPQDO.

In our coupled simulations with the 11-yr solar cycle forcing, the ENSO amplitude strengthens 2 to 4 years after the positive phase of the TPQDO. During the transition from negative to positive TPQDO phase, ENSO is less energetic. According to a primitive model of ENSO dynamics, this phase locking can be physically understood by decadal changes in the zonal wind stress and thermocline depth. Weaker zonal winds are leading the positive TPQDO phases, whereas a deeper thermocline is lagging the positive TPQDO phases. These changes should increase the growth rate of ENSO, resulting in stronger ENSO amplitudes during the declining phase of the TPQDO.

The simulated surface responses are generally weak. For this reason, solar signals in the stratosphere do not critically depend on ocean coupling. I find almost identical stratospheric temperature responses between ensemble simulations with and without ocean coupling. Even in the tropical lower stratosphere, where the strongest influence from surface solar signals is anticipated, qualitatively and quantitatively comparable changes in the two model configurations are detected. The solar signals in the tropical lower stratosphere extracted with multiple linear regression models, however, are affected by the solar cycle-ENSO collinearity. I identify a clear relationship between solar signals in temperature and the correlation between the solar cylce and ENSO predictors. Negative correlation is associated with higher temperature solar responses and vice versa. Although the bias induced by the solar cycle-ENSO collinearity is found weak in the coupled simulations, it could adversely affect any single short realization of the model and so it could in the observed record. In other words, the observed record is too short for unambiguous identification of solar signals in the tropical lower stratosphere with multiple linear regression models.

Zusammenfassung

Der Antrieb des Klimas auf der Erde ist die Sonne. Der Einfluss dekadischer Variationen der totalen und spektralen Sonneneinstrahlung auf die globale Oberflächentemperatur wird auf 0.1 K geschätzt. Regional kann dieser Einfluss jedoch durch eine Vielzahl dynamischer Prozesse verstärkt werden.

In den letzten Jahren wurde den Auswirkungen des 11-jährigen Sonnenzyklusses auf den tropischen Pazifik, so es solche gibt, vermehrt Aufmerksamkeit geschenkt. Viele Studien zeigen eine El Niñoähnliche Erwärmung während solarer Maxima, andere finden jedoch eine La Niña ähnliche Abkühlung. Aufgrund der vielen jährlichen und dekadischen Oszillationen im tropischen Pazifik ist es schwierig, robuste Signale zu isolieren. In der vorliegenden Studie zeigen wir, dass die beobachtete Abkühlung des tropischen Pazifiks in Jahren mit maximaler Sonnenaktivität durch gleichzeitig auftretende La Niña Ereignisse verursacht wird. Ein statistischer Zusammenhang zwischen den Maxima im Sonnenzyklusses und La Niña ähnlichen Ereignissen sollte im Umkehrschluss einen Zusammenhang zwischen solaren Minima und El Niñoähnlichen Ereignissen ergeben. Einen solchen Zusammenhang können wir jedoch nicht finden. Die Quasi-Dekadische Oszillation im Tropischen Pazifik (TPQDO) ist eine natürliche Mode, welche die beobachteten höheren Oberflächentemperaturen während der stärksten Sonnenaktivität erklären kann. Es ist allerdings bemerkenswert, dass die TPQDO in den letzten 50 Jahren mit dem Sonnenzyklus synchron verlief.

Um die Reaktion des tropischen Pazifiks auf den 11-jährigen Sonnenzyklus systematisch zu untersuchen wurden Ensembles von Simulationen mit einem globalen Atmosphärenmodell, ungekoppelt und gekoppelt mit einem Ozeanmodell, durchgeführt. Das Modell wurde mit realistischen Werten der Ozonkonzentration und der Sonneneinstrahlung von 1955 bis 2006 angetrieben. In den gekoppelten Simulationen ist der Anstieg der mittleren tropischen Oberflächentemperatur (30°S-30°N) beinahe in Phase mit dem Sonnenzyklus. άber den gesamten Pazifik gemittelt ergibt sich eine Erwärmung um 0,15K zwischen dem Minimum und dem Maximum der Sonnenaktivität. Die Erwärmung im indischen Ozean ist geringer. An der Oberfläche entspricht die räumliche Verteilung des solaren Signals dem der simulierten TPQDO. Ist die Sonneneinstrahlung im Modell konstant, wird eine TPQDO mit einer mittleren Periode von 12.3 Jahren simuliert. In den mit einem 11-jährigen Sonnenzyklus angetriebenen Simulationen entspricht die Periode der TPQDO der des Sonnenzyklusses. Dies kann mit einer Abnahme der Passatwinde im westlichen Pazifik, welche sowohl in den gekoppelten als auch in den ungekoppelten Experimenten simuliert wird, erklärt werden. Während der Maxima im Sonnenzyklus auftretende westliche Anomalien der Oberflächenwinde führen dazu, dass aufgrund der Divergenz des Sverdrup Transportes oberflächennahe Wärme im Ozean in die Subtropen gespült wird. Dieser durch den Sonnenzyklus verursachte Fluss führt zu

einer Hebung der Thermoklinen über den gesamten tropischen Pazifik, was wiederum einen negativen Ausschlag der TPQDO bewirkt. Stärkere Ostwinde, welche während solarer Minima auftreten, führen zu einer Akkumulation von Wärme im Pazifik und somit zu einer positiven TPQDO Phase in den darauffolgenden Jahren. Zusammenfassend lässt sich sagen, dass die durch den Sonnenzyklus beeinflussten Oberflächenwinde den Wärmehaushalt des Pazifiks bestimmen uns somit auch die TPQDO.

Treibt man das gekoppelte Atmosphären-Ozean-Modell mit dem 11-jährigen Sonnenzyklus an, kann man zwei bis drei Jahre nach einer positiven Phase der TPQDO eine Verstärkung der ENSO Amplitude beobachten. Während des ύbergangs einer negativen TPQDO Phase in eine positive TPQDO Phase ist das ENSO Signal schwächer. Ein einfaches dynamisches ENSO-Modell führt diesen Zusammenhang auf dekadische Unterschiede in der zonalen Windkraft und der Tiefe der Thermokline zurück. Schwächere zonale Winde führen zu einer positiven TPQDO, eine tiefere Thermokline hingegen verzögert diese. Dies verstärkt die Entwicklung von ENSO und resultiert in stärkeren ENSO-Amplituden auf dem absteigenden Ast der TPQDO.

Generell sind die simulierten Auswirkungen auf die Oberfläche sehr schwach. Aus diesem Grund sind die stratosphärischen Temperaturänderungen in den gekoppelten und den ungekoppelten Simulationen weitgehend gleich. Dies ist auch in der unteren tropischen Stratosphäre der Fall, wo man den stärksten Einfluss solar bedingter Oberflächenänderung erwartet. Untersucht man die untere Stratosphäre mit Hilfe multipler linearer Regression findet man eine Sonnenzyklus-ENSO-Korrelation. Wir finden eine klare Beziehung zwischen dem solaren Signal in der Temperatur und der Korrelation zwischen den Prädiktoren des Sonnenzyklusses und ENSO. Negative Korrelationen bedeuten einen stärkeren Einfluss auf die Temperatur und umgekehrt. Obwohl der Einfluss der Sonnenzyklus-ENSO-Kolinearität in unseren Simulationen schwach ist, könnte sie sowohl jeden kürzeren Modelllauf als auch die vorhandenen Beobachtungen beeinflussen. Mit anderen Worten, der Beobachtungszeitraum ist zu kurz um den Einfluss des Sonnenzyklusses auf die untere Stratosphäre mit Hilfe der multiplen linearen Regression zu identifizieren.

Table of Contents

Acronyms

AENS	Ensemble simulations with MAECHAM5
AOGCM	Atmosphere-Ocean GCM
CCM	Chemistry Climate Model
CENS	Ensemble simulations with MAECHAM5/MPIOM
CENS-ST	Ensemble simulations with MAECHAM5/MPIOM
CENS-T63	Ensemble simulations with MAECHAM5/MPIOM
DJF	December, January, and February
ECMWF	European Centre for Medium-range Weather Forecasts
EDAM	ENSO Decadal Amplitude Modulation
ENSO	El Niño Southern Oscillation
EOF	Empirical Orthogonal Function
ERA-40	ECMWF 40-year Reanalysis
ERSST	Extended Reconstructed Sea Surface Temperatures
F10.7	10.7 cm (2800 MHz) radio solar flux
GCM	General Circulation Model
MAECHAM5	Middle Atmosphere version of ECHAM5 GCM
MERRA	Modern Era Retrospective-analysis for Research and Applications
MPIOM	Max Planck Institute Ocean Model
MSSA	Multichannel SSA
NH	Northern Hemisphere
OASIS	Coupler for ECHAM5 and MPIOM
PC	Principal Component
QBO	Quasi-Biennial Oscillation
SSA	Singular Spectrum Analysis
SSN	Sunspot Number
TPQDO	Tropical Pacific Quasi-Decadal Oscillation
TSI	Total Solar Irradiance

Chapter 1

The Nature of the Problem

1.1   Introduction

When Galileo first observed spots revolving on the Sun's surface in 1610, he would have never imagined that his discovery would trouble the climate research few centuries later. For he had unnailed the established belief that the Sun, as a perfect celestial body, never undergoes any change. The very existence of sunspots proclaimed to the contrary. Present-day satellite and ground-based observations have returned a picture of a never-resting star. The solar variability is manifested in different spatial and temporal guises: chromospheric structures, prominences and flares are some examples. Nevertheless, more closely tied to Earth's climate are changes in total solar irradiance, spectral solar irradiance, total magnetic flux, and solar particle flux. These variables undergo quasi-periodic fluctuations and if large enough may result in traceable climatic fluctuations. For instance, the coincidence of the Maunder Minimum, a period of prolonged decline of sunspot activity (1645-1715), with the coldest spell of the Little Ice Age (1430 to 1850) has sparkled many intriguing questions about sun-climate linkages (Eddy, 1976).

If the solar variability caused substantial global or local changes centuries ago, there is no reason to argue against the possibility that it is still affecting Earth's climate. Since the early years of the 20th century and particularly after the 1950's, however, the global mean surface temperature has been increasing due to the constant release of human-made greenhouse gases (IPCC, 2007). In order to assess the impact of the anthropogenic forcing on global or regional scales, a better understanding of the sun-climate linkage is mandatory. Understanding, moreover, the response of important modes of internal variability to periodic forcing, such as the 11-yr solar cycle, could improve our skill for decadal predictions.

The investigation of possible relationships between solar variations on different time scales and climate has a long history. Various correlations with the 11-yr solar cycle have been claimed for an admittedly large number of meteorological variables (Pittock, 1978). Changes in river Nile flow, African droughts and temperature

variations in different regions are few only examples. Although statistically significant in many cases, correlations cannot provide physical significance whatsoever. These "nonsense-correlations", a term used by Yule (1926), result mainly from the shortness of the observed record as far as the solar-climate linkage is concerned. This is because quality controlled observations at particular locations span over few solar cycles at best, whereas global coverage of a few meteorological variables has been available only after 1979.

In recent years, intense research has concentrated on providing physical explanations of the observed solar responses (Gray et al., 2010). General circulation models have been proven an invaluable tool to confirm or reject details of the proposed mechanisms. Traditionally these models simulated the atmospheric responses to the solar cycle forcing but recent evidence of robust solar signals on tropical oceans call for new, carefully designed simulations with coupled atmosphere-ocean models. For this reason, in this dissertation I investigate the influence of the 11-yr solar cycle variability on the Earth's climate by the means of a comprehensive atmosphere-ocean model. I focus primarily at tropical latitudes, from the stratosphere down to the sea surface and below.

In the following sections of this chapter, a critical re-examination of the previously reported atmospheric and oceanic responses to the 11-yr solar cycle forcing is given. Based on the findings of this chapter, a number of interesting questions are posed, which are answered in Chapters 2, 3 and 4.

1.2 11-yr solar cycle variability and proposed mechanisms of solar-climate linkages

The Sun radiates approximately 1 W/m^2 more energy from the minimum to the maximum phase of the 11-yr solar cycle (Frohlich, 2006). This number is translated to ~0.1% variation of the Total Solar Irradiance (TSI) with an average value of ~1361 W/m^2 (Kopp et al., 2005). If the Earth's sphericity and global albedo (a=0.3) is counted, then 0.18 W/m^2 warms the surface in a global perspective. For reference, the annual cycle of TSI variation is 6.7%, which means extra ~16.1 W/m^2 at the Earth's surface. The amplitude of the 11-yr cycle TSI variation, therefore, is small and straightforward radiative balance calculations estimate a global-mean temperature increase of no more than 0.1 K from solar minima to maxima, unless climate feedbacks act to amplify the response (White et al., 1998; Douglass and Clader, 2002). Any regional responses, however, can be manifold much stronger either for dynamical or radiative reasons.

At cloud free regions of large atmospheric subsidence, such as the subtropical Pacific Ocean or the eastern tropical Pacific or the eastern tropical Atlantic, the 11-yr solar forcing can be much stronger (Salby and Callaghan, 2006a). General circulation models (GCMs) estimate that approximately 1 W/m^2 may heat the sea surface at these

regions (Meehl et al., 2008; Meehl et al., 2009). To compensate this radiative forcing, more moisture should be evaporated and carried by the trade winds to the convergence zones, where it should fuel the deep convection with extra energy, strengthening the meridional (Hadley) and zonal (Walker) overturning circulations of the atmosphere (Meehl et al., 2009). When the Walker cell speeds up, the anomalous stronger surface easterlies upwell more cold water in the eastern Pacific, reducing the surface temperature. Amplified subsidence and negative Sea Surface Temperatures (SSTs) in this region should further reduce the cloud coverage. This positive feedback could shift the Pacific system to a state that resembles the negative phase of the El Niño-Southern Oscillation (ENSO) phenomenon (van Loon et al., 2007; Meehl et al., 2009). This means that solar maxima may favor La Niña-like conditions. Although this mechanism sounds plausible, many independent analyses of historical SSTs isolated a basin-wide warming, which oscillates almost in phase with the 11-yr solar cycle (White et al., 1997; White et al., 1998; White and Liu, 2008b; Roy and Haigh, 2010). This warming resembles a positive ENSO phase or El Niño. Regardless of the exact sign of the SST solar response, solar signals at the sea surface could alter atmospheric circulations, influencing the stratosphere in a "bottom up" pathway.

Satellite measurements from 1979 onwards demonstrate a wavelength dependent 11-yr variability with stronger changes at short wavelengths of the solar spectrum (Lean et al., 1997). The variability in the extreme ultraviolen, for instance, can reach values of 100 % or even higher (Lean, 1991) but with little climatic importance since this part of the solar spectrum is entirely absorbed in the thermosphere and mesosphere. The variability in the ultraviolet (UV) is more relevant for climate studies due to its significant role on stratospheric ozone production (e.g. Chandra and McPeters, 1994). The recorded UV variability is weak and estimated to range from about 6 % at 200 nm to almost zero in the visible part of the solar spectrum (Lean, 2000), although recent observations of the spectral solar irradiances suggest that the UV variability may have been underestimated by an order of magnitude (Harder et al., 2009).

Higher ozone concentrations up to 4% have been observed in the upper tropical stratosphere (~1 hPa) when the Sun is more active (Soukharev and Hood, 2006; Randel and Wu, 2007). The synergetic effect of higher UV and ozone abundances in solar maxima, warms the upper stratosphere and strengthens the meridional temperature gradients in the stratosphere particularly in solstice seasons, when winter high latitudes plunge into darkness. Through thermal wind balance, the vertical gradient of the zonal-mean zonal winds is also altered with ensuing changes in the propagation and dissipation of planetary-scale atmospheric waves. Kodera and Kuroda (2002) proposed a positive feedback, which involves the interaction of planetary waves with the zonal wind anomalies. Their mechanism transfers the solar signal from the upper tropical stratosphere poleward and downward to the lower extra-tropical stratosphere, where it can affect dominant modes of atmospheric variability (such as the Northern Annular Mode). Hence, circulation patterns in the troposphere can be also affected because there is observational evidence that changes

of the Northern Annular Mode may penetrate into the underling troposphere within a few weeks (Baldwin and Dunkerton, 2001).

The interaction of the planetary waves with the background zonal wind fields has one more consequence; the slowdown of the Brewer-Dobson circulation in solar maxima. Hence, solar-induced circulation changes in the upper extra-tropical stratosphere could be linked to the tropical lower stratosphere through changes in tropical upwelling with ensuing changes in temperature and ozone (Kodera and Kuroda, 2002). This mechanism could explain the observational evidence for a second response maximum both in ozone and temperature in the tropical lower stratosphere in solar maxima (Crooks and Gray, 2005; Haigh et al., 2005; Soukharev and Hood, 2006; Frame and Gray, 2010). An intensification and a poleward extension of the Hadley circulation due to the increased static stability in lower stratosphere, could transfer solar signals further down into the troposphere (Haigh et al., 2005). In summary, there are well established mechanisms whereby the stratospheric signals could descend into tropospheric altitudes in a "top down" pathway. Both suggested pathways, the "bottom up" and "top down", could operate at the same time, amplifying the influence of the 11-yr solar cycle onto the Earth's climate (van Loon et al., 2007).

Another manifestation of the 11-yr solar cycle variability is the variation of the energetic particle precipitation as well as the reduction of the galactic cosmic rays bombarding the Earth's atmosphere. Alpha particles, protons, and electrons enter the atmosphere at high magnetic latitudes and influence mesospheric nitrogen abundances with subsequent effects on ozone concentrations in the boreal winter (Marsh et al., 2007). For an in-depth account of the subject see Kieser (2011). Another intriguing theory relates the intensity of galactic cosmic rays and the low cloud coverage (Marsh and Svensmark, 2000), however many scientists have questioned this linkage (e.g. Kristjansson et al., 2008). These mechanisms lay beyond the scope of this study and are not examined.

For a comprehensive review of the observational solar signals and the proposed explanations see Gray et al. (2010) and the following books:

- Schrijver C.J. and Siscoe G.L (eds.): Heliosphysics: Evolving solar activity and the climates of space and Earth, 2010,

- Calisesi et al. (2007): Solar variability and planetary climates, 2007,

- Pap J.M. and Fox P. (eds.): Solar variability and its effects on climate, 2004.

1.3 Re-examination of previously detected 11-yr solar signals in the tropical Pacific Ocean

The observation-based studies of Meehl et al. (2008) and van Loon et al. (2007) composited SSTs in single years of peak Sunspot Numbers (SSN) relative to climatological conditions (Figure 1.1a). They found negative December-January-February (DJF) SST anomalies on the order of -0.7 K over the eastern Pacific. These studies, however, did not explore the tropical Pacific response in the opposite extreme of the solar cycle, namely in years of minimum SSN. Assuming a linear response, the tropical Pacific should shift from negative SST anomalies (La Niña-like) in maximum SSN years to positive anomalies (El Niño-like) in minimum SSN years. Yet, observations do not substantiate such transition. The Extended Reconstruction SST (ERSST) version 3b dataset (Smith et al., 2008), for instance, indicates negative temperature anomalies both in composites of maximum and minimum peaks of SSNs, respectively (see Figure 1.1). This raises questions about the validity of the mechanism proposed by Meehl et al. (2008) and subsequently about the origin of the response. It appears that the Pacific response in the composite analyses is not directly related to the 11-yr solar cycle but caused by oversampling of La Niña events (Zhou and Tung, 2010). It is still possible that La Niña events are synchronized to, not excited from, the 11-yr solar cycle. White and Liu (2008a), for instance, suggested a non-linear resonance of the observed 3.6-yr and 2.2-yr ENSO periods on the 11-yr solar cycle.

Multiple linear regression analysis of the boreal winter SSTs (1880-2008) also identified cold water in eastern Pacific during solar maxima (Tung and Zhou, 2010). The studies of Tung and Camp (2008) and Zhou and Tung (2010) documented a somewhat comparable picture but for annual averages. The fact that independent analysis techniques (e.g. composites vs multiple regression) have detected similar cooling in the eastern Pacific could advocate for the robustness of the Pacific response. Yet, a scrupulous comparison of the SST responses in the western equatorial Pacific to increased solar cycle forcing reveals considerable inconsistencies. Composites returned a well-formed La Niña-like pattern during peaks of SSNs with negative SST anomalies extending into the western sector (see Figure 1.1a). The regression analysis, in contrast, returned a zonal SST dipole with positive anomalies in the western and negative anomalies in the eastern sector (we repeat the work of Tung and Zhou (2010) in Figure 1.2a).
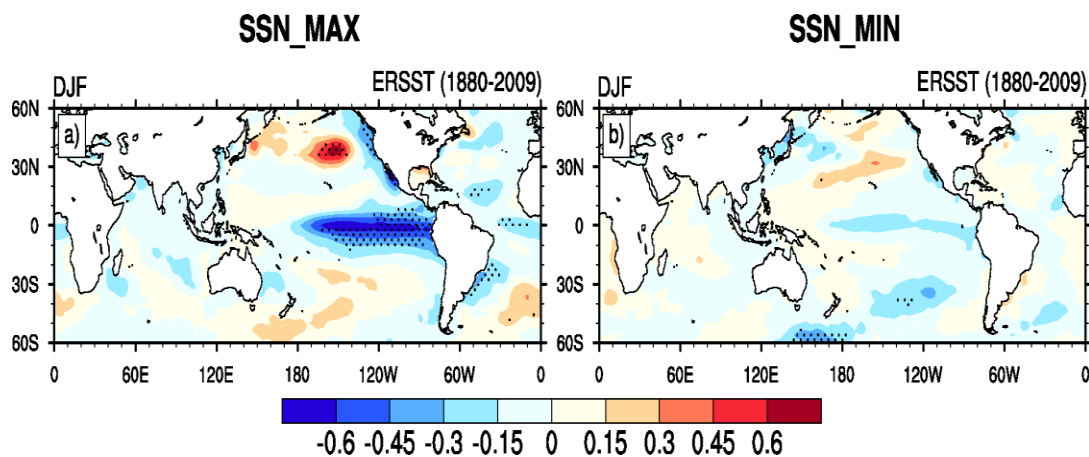
Figure 1.1: DJF sea surface temperature anomalies (K) from the ERSST v3b reconstruction (1880-2009) grouped to a) years of peak maximum sunspot numbers (1883,1893,1905, 1917,1928,1937,1947,1957,1968,1979,1989,2000) and b) years of peak minimum sunspot numbers (1889,1901,1913,1923,1933,1944,1954,1964,1976,1986,1996,2008). Anomalies are calculated with respect to the 1880-2009 climatology. A high-pass filter (156-months running averages have been subtracted) has been applied prior to the analysis in order to eliminate the non-linear positive trend (Thompson et al., 2008). Stippling indicates 95% significance according to a bootstrap test of 10000 surrogates. Figure 1.1a after van Loon et al. (2007).

The SST dipole found in Tung and Zhou (2010) could originate from decadal oscillations of the tropical Pacific unrelated to the 11-yr solar cycle. For instance, the ENSO amplitude undergoes a 10 to 15-yr variation over the observed period (Sun and Yu, 2009). In periods when ENSO becomes more energetic, the center of action of El Niños moves towards the coast of South America (Rodgers et al., 2004). In contrast, strong La Niña events are confined in the central Pacific. The residual effect of this spatial asymmetry is non-zero; positive SST anomalies in the eastern Pacific and negative SST anomalies in the central Pacific are observed during phases of stronger ENSO activity. Furthermore, the dipole is characterized by stronger temperature anomalies in the eastern Pacific (see Figure 9a of Sun and Yu (2009)). During periods of weaker ENSO amplitude, the dipole's polarity reverses.

We calculate the observed ENSO Decadal Amplitude Modulation (EDAM) from ERSST over the period 1880-2009. Although the quality of the ERSST reconstruction in the tropical Pacific should be considered less reliable before the 1950s, our analysis covers the full period to be consistent with earlier studies. The EDAM index is defined as the 8-yr low-pass Lanczos filtered (9 weights) time series of the annual Nino-3.4 amplitude (Yeh and Kirtman, 2005). The Nino-3.4 amplitude, in turn, is the modulus of the Nino-3.4 index (SST anomalies over the region 5°S-5°N, 120°W-170°W). Prior to the amplitude calculation, a 8-yr high-pass filter is applied on the Nino-3.4 index to eliminate any low-frequency variability (e.g. trend) but keeping the observed 3 to 7-yr ENSO related periodicities (Sun and Yu, 2009).

Figure 1.2a compares the observed EDAM index in DJF with the reconstructed TSI from 1880 to 2009 (Lean et al., 1995). For visualization reasons, the secular trend of the reconstructed TSI is removed. Periods of negative EDAM tend to coincide with solar maxima. This tendency is more pronounced after 1930. During the solar maxima in 1894, 1937, 1947, 1980, and 2000 the EDAM index takes peak negative values. The correlation between the EDAM index and TSI is -0.26, implying that the two indices are not independent. This means that multiple linear regression models cannot sufficiently separate the associated spatial SST patterns from each other. To demonstrate this, we repeat the multiple regression analysis of Tung and Zhou (2010) but with the EDAM index in place of TSI. The qualitative and quantitative similarity of the tropical Pacific response in Figures 1.2b and 1.2c supports our argument that EDAM is aliased to TSI. It is worth noting that the resemblance extends to the September-October-November season but it weakens over the other seasons (not shown). It seems, therefore, that the zonally asymmetric SST response in Figure 1.2b is likely attributed to EDAM and not explicitly to the 11-yr solar cycle.
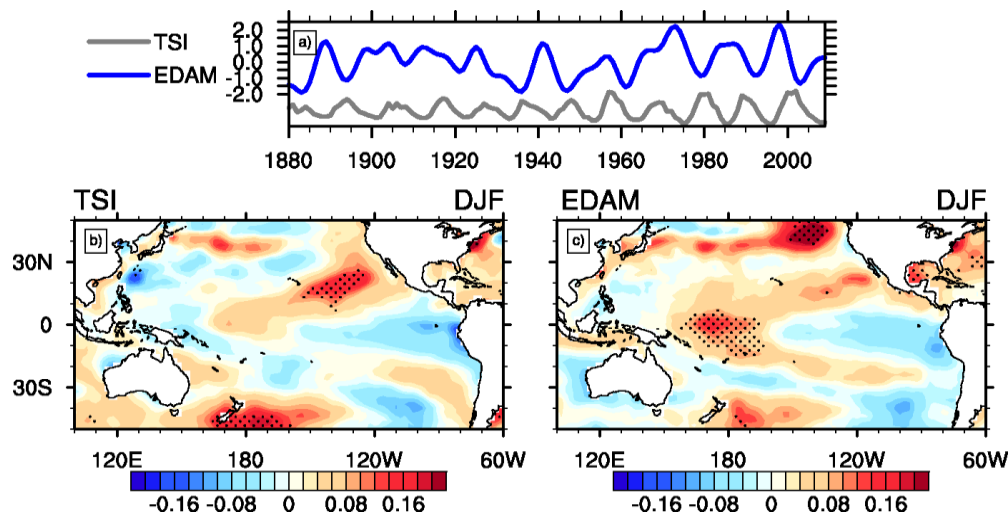
Figure 1.2: (top) Time series of the normalized EDAM index (blue line) in DJF. The detrended (high pass filtered) TSI from 1880 to 2009 is superposed for reference (grey line). (bottom) Regression coefficients of the boreal-winter SST anomalies (1880-2009) from the ERSST v3b dataset onto b) the unfiltered TSI and c) EDAM index. Units in K per standard deviation of the predictor. Stippling denotes 95% significance.

The leading Empirical Orthogonal Function (EOF) of the 7 to 15-yr band-pass filtered annual SST anomalies seems to oscillate in phase with TSI over the period 1955-1994. White et al. (1997) documented a broad-scale warming, both in meridional and longitudinal directions, located over the central and western Pacific. This spatial mode, however, is the Tropical Pacific Quasi-Decadal Oscillation (TPQDO) detected in SSTs and Sea Level Pressure (SLP) anomaly fields over the last century (Tourre et al., 1999; Allan, 2000; White and Tourre, 2003; White et al., 2003b). Note that the TPQDO is considered here as the basin-wide warming in the tropical Pacific Ocean that resembles the spatial structure of El Niño episodes and not the zonally SST dipole

associated with EDAM. White et al. (2003b) used the term QDO instead of TPQDO to describe this oscillation.

We isolate the TPQDO by employing joint EOF and Multichannel Singular Spectrum Analysis (MSSA) on the tropical (30°S-30°N) annual SST anomalies over the period 1950-2009. This period is chosen to avoid the discontinuity in the SST observations in the 1940's (Thompson et al., 2008) and because it overlaps with the period analyzed in White et al., (1997). Again, annual SST anomalies are taken from the ERSST reconstruction. MSSA has been extensively utilized in the past to isolate quasi-periodic phenomena (e.g. Moron et al., 1998; Ghil et al., 2002). A thorough description of MSSA is given in Appendix 2. It is suffice to note here that MSSA detects two oscillatory modes, which demonstrate spectral peaks at 12.5 years. The annual MSSA-filtered SST anomalies are then reconstructed by considering only this pair. Finally, the leading principal component of the reconstructed SSTs defines the TPQDO index. The spatial signature of the TPQDO is obtained by regressing the normalized TPQDO index onto the raw SST anomalies (units in K per one standard deviation of the TPQDO index: K/std). Our analysis method differs from the method of White et al. (1997) in the time filtering only; instead of using one of the conventional band-pass filters we use the MSSA.
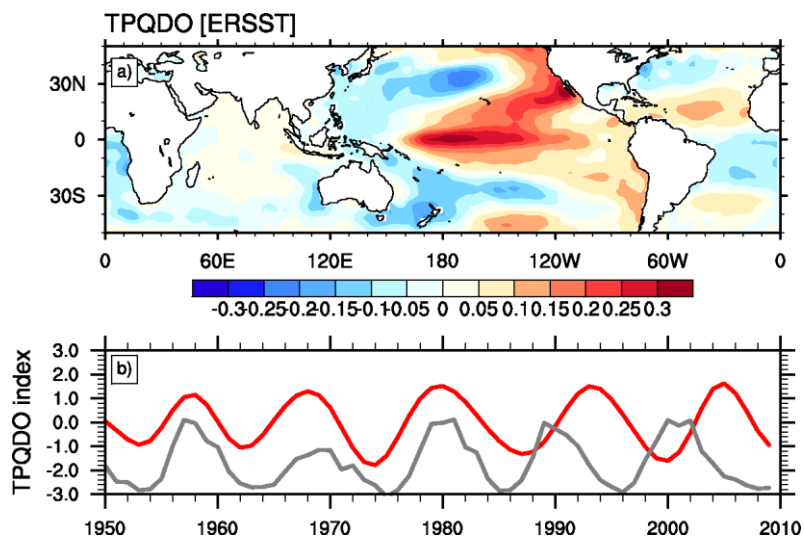
Figure 1.3: The TPQDO displayed as the regression coefficients (K/std) of the unfiltered SST anomalies from the ERSST v3b dataset onto the normalized TPQDO index. b) Time series of the normalized TPQDO index from 1950-2009 (red line). TSI is superimposed for reference (grey line).

TPQDO is associated with a relative uniform warming over the equatorial Pacific. Strongest positive anomalies are located in the central Pacific (up to 0.25 K/std) whereas the signal weakens in the eastern Pacific. Additionally, warm waters extend from the central Pacific towards the Gulf of California. The signal over the north Indian Ocean is much weaker compared to the signal in the Pacific. A latitudinal tripole of positive/negative/positive SST anomalies is developed over the tropical

Atlantic Ocean (Tourre et al., 1999). An important feature, not shown here, is the eastward propagation of the equatorial anomalies that has been documented also by White et al. (2003b). Given that the MSSA analysis can be viewed as a narrow band-pass filter, it is not surprising that the spatial patterns in Figure 1.3 are consistent with those from White et al. (1997). Our analysis, however, returns stronger signals.

A closer look in Figure 1.3 shows that the TPQDO index (red line) does follow closely the TSI (orange line) from 1950 to 1985, but from 1985 onwards the TPQDO index lags TSI to such an extent that during the positive phase of the solar cycle 23 (1998-2002) the tropical Pacific remains anomalously cold. Although numerical simulations proposed a solar excitation of the TPQDO (White and Liu, 2008b), many state-of-the-art atmosphere-ocean GCMs simulate a TPQDO with constant solar forcing, suggesting for an oscillation native to the tropical Pacific coupled system (Knutson and Manabe, 1998; Cibot et al., 2005; Tourre et al., 2005). TPQDO in these models and observations alike, was explained by the recharge/discharge mechanism of the ENSO phenomenon (Jin, 1997), operating on decadal time scales (Hasegawa and Hanawa, 2003). In Chapter 2, we show that a 12.3-yr TPQDO is naturally excited in our model, too. Nevertheless, the in-phase relationship between the 11-yr solar cycle and TPQDO over several decades remains an intriguing feature that must be further studied.

1.4   Re-examination of previously detected 11-yr solar signals in stratospheric temperatures from reanalysis products

There is statistical evidence for robust solar signals in zonal-mean temperatures in the stratosphere (Gray et al., 2010). For instance, data from the ERA-40 reanalysis (Uppala et al., 2005) over the period 1979-2001 shows a meridionally narrow area of positive temperature anomalies in the upper stratosphere with increased solar forcing (see Figure 1.4a). This warming is accompanied with a second significant warming in the lower tropical stratosphere (Crooks and Gray, 2005; Frame and Gray, 2010).

Newer reanalysis products show similar responses and some substantial differences. We apply a first-order auto-regressive multiple linear regression model on the recently released MERRA (Modern Era Retrospective Analysis for Research and Applications) product, which spans from 1979 to 2008 (Rienecker et al., 2011). This regression model, which has been used by Crooks and Gray (2005) and Frame and Gray (2010), considers six predictors: the 10.7 cm solar radio flux, the Nino-3.4 index, two independent indices to describe the Quasi-Biennial Oscillation (QBO) of the tropical stratosphere, the CO_2 concentration, and an index describing aerosol injections in the stratosphere from volcanic eruptions. The solar regression coefficients are normalized to 100 solar flux units (sfu) to ease comparison with

previous studies (Austin et al., 2008; Schmidt et al., 2010). For details about the regression model see Frame and Gray (2010) and Chapter 4.

The most striking differences between the temperature solar responses in MERRA and ERA-40 are identified in the upper stratosphere (above 5 hPa, Figure 1.4). Positive temperature anomalies in MERRA are not restricted over the tropical band, but extend over all latitudes. MERRA exhibits significant positive temperature responses at 60°N, whereas strong negative signals are seen in ERA-40. Obviously, this discrepancy reflects data inconsistencies between MERRA and ERA-40. Although recent modeling attempts with chemistry-climate models documented comparable temperature solar responses in the upper stratosphere (Austin et al., 2008), one must be cautious concerning the origin of the signals in Figure 1.4 because reanalysis datasets exhibit poor performance in the upper stratosphere and mesosphere (Manney et al., 2008).
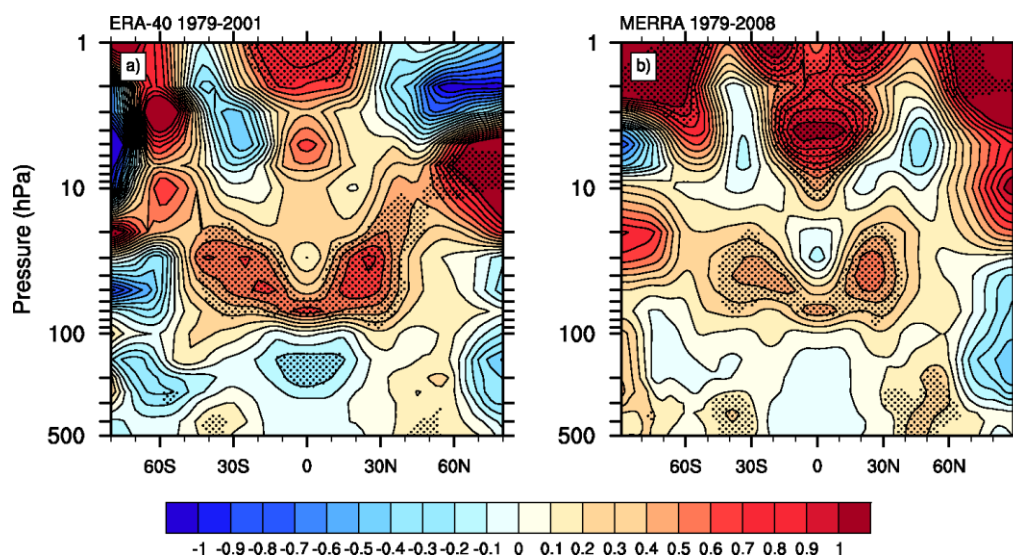
Figure 1.4: Regression coefficients (K/100 sfu) of the monthly temperature anomalies from a) ERA-40 (1979-2001) and b) MERRA (1979 to 2008) onto the 10.7 cm radio flux. The response of a typical solar cycle is obtained by multiplying with 1.33. Figure 1.4a after Frame and Gray (2010).

A significant warming in the tropical lower stratosphere is the other notable feature in Figure 1.4. This warming takes the form of two separate lobes located at 25 degrees latitude in each hemisphere. Although significant in both datasets (>95%), the magnitude of the warming is substantial weaker in MERRA. This is likely explained by the fact that no major volcano has been erupted from 2002 onwards. A number of possible explanations have been proposed to explain the observed positive temperature anomalies in the tropical lower stratosphere (Gray et al., 2010). On the basis that the predictors used in the multiple regression model are slightly dependent (correlated) over the analyzed period, this warming has been attributed to possible contamination (aliasing) of the 11-yr solar signal with the signal of volcanic eruptions, or ENSO, or QBO. Physical mechanisms have been suggested, too. The

most accepted dynamical mechanism explains this warming in terms of reduced upwelling. According to this mechanism (Kodera and Kuroda, 2002, see above) however, the temperature response should peak at the Equator and not in the subtropics. With the aid of carefully designed numerical simulations, the origin of the positive temperature solar responses in the tropical lower stratosphere can be assessed.

1.5   Thesis objectives

Our level of understanding of the mechanisms through which the 11-yr solar cycle forcing influences the climate system is characterized as low (IPCC, 2007), although considerable improvements have been scored in the recent years (Gray et al., 2010). The difficulty in detecting robust solar signals arises mainly from the shortness of quality-controlled observations, relative to the 11-yr solar cycle. For this reason numerous past studies investigated the response of the Earth's climate to variable total and spectral solar irradiances by means of GCMs of ranging complexity (Rind et al., 1999; Matthes et al., 2004; Langematz et al., 2005; Schmidt et al., 2006; Marsh et al., 2007; Austin et al., 2008; Rind et al., 2008; Matthes et al., 2010; Schmidt et al., 2010). The majority of these studies aimed at the atmosphere and particularly at the stratosphere where the strongest solar signals are expected. A limited number of simulations examined the responses of the Pacific Ocean to the 11-yr solar cycle but with contradicting results (Meehl et al., 2008; White and Liu, 2008b; Meehl et al., 2009; Bal et al., 2011).

What would we like to know more about? The response, if any, of the tropical Pacific to the 11-yr solar cycle forcing is unknown since many studies indicated an El Niño-like warming, whereas other studies isolated a La Niña-like cooling during solar maxima. Moreover, any sensitivity of the stratospheric solar signals to the solar signals at the surface has not been examined yet. In other words, the interaction of the "bottom up" with the "top down" mechanism need to be clarified. Obviously, the tropical lower stratosphere is the first place where one should look for signs of this interaction. For the aforementioned reasons, this study aims to systematically assess any possible 11-yr solar influences in the tropical oceans and stratosphere. One may phrase two general questions as follows:

- *How does the 11-yr solar cycle affect the tropical oceans?*

- *Does the stratospheric response to 11-yr solar cycle forcing depend on the solar signals in the tropical oceans?*

These questions can be further specified:

- *Do periods of increased solar activity favor, statistically, La Niña events?*

- *Is numerical modeling supporting the observed relationships between the 11-yr solar cycle, TPQDO, and EDAM?*

- *Can we rule out the possibility that the observed solar responses in the tropical lower stratosphere originate from solar cycle-ENSO aliasing?*

To answer these questions, we conduct a large number of ensemble simulations with the middle atmosphere version of ECHAM5 in two different configurations: stand-alone and coupled to the MPI ocean model. A detailed description of the model is given in the following chapters.

1.6   Thesis outline

All questions posed before are answered in the following 3 chapters. Each chapter is designed to be a separate paper itself; hence, some repetitions in the introductory and model description sections are unavoidable.

In Chapter 2, we try to answer if the 11-yr solar cycle has any measurable effect in the tropical oceans. Contrary to earlier suggestions for a La Niña-like response, we detect a basin-wide warming over the Pacific during solar maxima. This warming is related to a number of thermodynamical mechanisms and we establish a statistical linkage between the TPQDO and the 11-yr solar cycle. Hence, the question concerning the possible synchronization of the TPQDO to the solar cycle is addressed. A modified version of this chapter has been submitted to Journal of Climate (Misios and Schmidt, 2011) and is currently under revision.

Chapter 3 builds upon the findings of Chapter 2. Our model reveals that ENSO becomes more energetic during the declining phase of the TPQDO. A conceptual model of ENSO corroborates this finding.

In Chapter 4, it is examined whether the surface responses documented in Chapters 2 and 3 play any critical role on the simulated solar signals in the stratosphere. Our model gives a negative answer. In addition, we answer the third specific question. We clearly demonstrate that multiple linear regression tools cannot sufficiently separate solar from ENSO signals even when 52 years of data are analyzed. Finally, the dependence of the simulated solar signals on the levels of solar forcing, the horizontal resolution and the season is discussed. Part of the simulations presented in this chapter have been published in Schmidt et al. (2011).

The contributions of this thesis and possible directions of future research concerning the influence of the 11-yr solar cycle on the Earth's climate are summarized in Chapter 5.

Chapter 2

Mechanisms involved in the amplification of the 11-yr solar cycle signal in the tropical Pacific Ocean

2.1 Introduction

The possible influence of the 11-yr solar cycle on the Pacific Ocean has received considerable attention in the recent years, yet it remains under debate (e.g., van Loon et al., 2007; Meehl et al., 2008; Meehl et al., 2009; Roy and Haigh, 2010; Tung and Zhou, 2010). Due to the shortness of reliable observations of the tropical Pacific Sea Surface Temperatures (SST), which cover only few solar cycles (Deser et al., 2010), different analyses demonstrated either anomalous cooling or warming in the Pacific Ocean with increased solar activity. Beside this, modes of natural variability, like the El Niño-Southern Oscillation (ENSO), and external forcings such as volcanic eruptions, may veil solar signals in this region. Specialized experiments with general circulation models (GCMs), however, could bypass the aforementioned shortcomings because they can separately quantify the climatic effect of each forcing (Shindell et al., 2006; Meehl et al., 2008; Rind et al., 2008; Meehl et al., 2009). In this study, we conduct simulations with a coupled atmosphere-ocean GCM (AOGCM) to investigate whether and how the tropical oceans, particularly the Pacific Ocean, respond to the 11-yr solar cycle forcing.

More than a decade ago, the analysis of White et al. (1997) detected a band of positive SST anomalies in the tropical Pacific, oscillating almost in phase with the Total Solar Irradiance (TSI). This warming in observed data was initially attributed to direct solar heating but later, changes in latent and sensible heat fluxes were claimed to be responsible (White et al., 2003a). More recently, a somewhat comparable band of warm water along the equatorial Pacific was also indentified in reconstructions of boreal-winter SSTs (Roy and Haigh, 2010). White and Liu (2008b) further suggested that this warming is related to the solar excitation of the Tropical Pacific Quasi-

Decadal Oscillation (TPQDO) first identified by Allan (2000). TPQDO, however, is excited naturally in many AOGCMs even in the absence of the solar cycle forcing (Knutson and Manabe, 1998; Rodgers et al., 2004; Cibot et al., 2005).

In contrast, the work of van Loon et al. (2007) indicated that during peak years of sunspot numbers (SSN) the boreal-winter eastern Pacific is anomalously cold, resembling a La Niña-like cooling. Simulations of the twentieth-century employing AOGCMs without stratospheric dynamics gave additional support for a negative SST response with increased solar activity but the magnitude of the signal was much weaker compared to observations (Meehl et al., 2003; Meehl et al., 2008). The inclusion of stratospheric dynamics amplified the magnitude of the simulated cooling (Meehl et al., 2009). This led to the proposition that the stratospheric response to enhanced UV radiation and ozone changes ("top down mechanism") may act together with coupled atmosphere-ocean surface reactions to increased TSI ("bottom up mechanism") to amplify the solar signals on the sea surface (van Loon et al., 2007; Meehl et al., 2009). Both mechanisms are suggested to strengthen the Walker circulation, which eventually pumps cold water in the eastern Pacific more vigorously, reducing surface temperatures.

In summary, previous observational and modeling studies do not agree on the sign of the Pacific response to the 11-yr solar cycle. In an attempt to reconcile this discrepancy, it was suggested that different analysis techniques captured different phases of the solar cycle, resulting in solar signals of opposite sign. In this context, the Pacific warming of White et al., (1997) was interpreted as a delayed, wave-driven reaction to earlier cooling during peaks in solar forcing (Meehl and Arblaster, 2009).

One may ask whether the negative SST anomalies over the tropical Pacific reported by van Loon et al. (2007), do merely reflect an accidental sampling of La Niña events rather than a solar signal (see Figure 1.1). Although, van Loon and Meehl (2008) addressed this question and found evidence for a different stratospheric response compared to a typical La Niña signature, Roy and Haigh (2010) questioned these findings. Tung and Zhou (2010) argued that the 11-yr solar signal in the tropical Pacific should be regarded neither as El Niño-like nor as La Niña-like.

In this chapter, we investigate the response of the tropical oceans to the 11-yr solar forcing by conducting ensemble simulations with an AOGCM including comprehensive stratospheric dynamics. Particularly we try to answer whether the Pacific Ocean shifts to a La Niña-like state with increasing solar forcing. The answer we give is negative. We rather simulate a basin-wide warming concealed behind the natural inter-annual variability (ENSO), which is pinned down to synergetic effects of the water-vapor feedback and the ocean dynamics. The latter are governed by the same recharge/discharge mechanism that describes the ENSO phenomenon.

The rest of this chapter is organized as follows. In Section 2.2 we describe the model, the experimental setup, and the analysis procedures. In Section 2.3 spatial patterns of the solar signal in the tropical oceans are isolated, while the interpretation of these

patterns is given in Section 2.4. In Section 2.5, we briefly describe the nature of the simulated TPQDO and we build a physical relationship between the simulated tropical Pacific response to the solar cycle and the TPQDO. Finally, we discuss possible shortcomings of our model in Section 2.6 and our work is summarized in Section 2.7.

2.2 Data and Methods

2.2.1 *Model description and experimental design*

We performed ensemble simulations with the middle atmosphere version of the ECHAM5 (MAECHAM5) general circulation model (Manzini et al., 2006; Roeckner et al., 2006) coupled to the Max Planck Institute Ocean Model (MPIOM) (Marsland et al., 2003). The OASIS coupler without any flux correction is responsible for momentum, heat and freshwater exchanges between atmosphere and ocean (Valcke et al., 2003). The CO_2 concentration is fixed to 348 ppm. The atmospheric resolution is T31L90 denoting spectral truncation at wavenumber 31 (equivalent to a 3.75°x3.75°grid) and 90 vertical levels (up to 0.01 hPa), whereas the ocean curvilinear grid has 3 degrees resolution at the Equator and 40 vertical levels. We have chosen this fairly coarse resolution owing to the necessity for a large number of simulations. Compared to earlier modeling attempts (Meehl et al., 2008; Rind et al., 2008; Meehl et al., 2009), it is the first time when a fully AOGCM with spontaneously generated stratospheric quasi-biennial oscillation (Giorgetta et al., 2006) is employed to study effects of solar variability.

With respect to the model version described by Manzini et al. (2006), several modifications were introduced to MAECHAM5 in order to simulate a realistic and transient 11-yr solar cycle. More specifically, spectral solar irradiance changes conforming to those used in the CCMval (Chemistry and Climate Model Validation) activity (CCMVAL, 2010) and averaged over the model's shortwave, visible, and near infrared bands are implemented (Lean, 2000). This version is not coupled to a chemistry scheme to account for ozone photochemistry. Hence, ozone solar anomalies need to be specified. For this reason, we specify the annual cycle of solar-induced ozone anomalies simulated with HAMMONIA (Hamburg Model for Neutral and Ionized Atmosphere) in perpetual solar maximum/minimum conditions (Schmidt et al., 2010). The ozone anomalies are scaled with the 10.7 cm radio flux (F10.7) daily values and added to the standard ozone climatology. To avoid any contamination of the solar signal, no other external forcing is considered. This approach distinguishes our simulations from previous AOGCM studies in which time dependent volcanic and greenhouse gas forcings were additionally considered (Meehl et al., 2008; Meehl et al., 2009).

An ensemble of 11 realizations with realistic solar spectral variations from 1952 to 2006 has been carried out (CENS). Each run branches from different initial

conditions, taken from an unperturbed run (CTR) of 140 years. Our analysis focuses on the period 1955-2006; in other words, each ensemble member runs for 5 solar cycles and overall 55 solar cycles are simulated.

Additionally, a separate ensemble of 9 realizations of MAECHAM5 without ocean coupling is carried out (AENS). The model setup is the same as in the coupled simulations except that MAECHAM5 is forced with SSTs and Sea Ice Fraction (SIC) climatologies taken from CTR. The atmospheric initial conditions are those of CENS. Our analysis of AENS, however, is restricted to the 1958-2006 period due to spin-up effects most visible in the specific humidity. These simulations shall demonstrate the atmospheric response to solar forcing neglecting any atmosphere-ocean feedback. Note that we make use of AENS in Section 2.4.3 only.

2.2.2 *Evaluation of ENSO in MAECHAM5/MPIOM*

The coupled ECHAM5/MPIOM with lower lid (10 hPa) has been previously utilized in numerous studies including the CMIP3 simulations (e.g. Jungclaus et al., 2006). Here, for the first time, we document results from the middle atmosphere version of ECHAM5/MPIOM. Hence, we briefly compare the simulated mean state and inter-annual variability of the tropical Pacific Ocean, the main region of interest throughout this paper, against the ERSST v3b dataset (Smith et al., 2008).

Similar to the majority of the AOGCMs of this class (Latif et al., 2001; Reichler and Kim, 2008), our model shows a cold bias in the climatological state of the equatorial eastern Pacific. The comparison of the SST climatology of the CTR run versus the ERSST climatology (1880-2009) shows essentially the same pattern as in Figure 3a of Jungclaus et al. (2006), thus it is not shown here. The inclusion of the middle atmosphere does not alter significantly the precipitation patterns along the tropical Pacific. Double Intertropical Convergence Zones (ITCZs) are simulated, a common flaw of many AOGCMs (Latif et al., 2001; Guilyardi et al., 2003). To diagnose the inter-annual variability of the tropical Pacific, we evaluate the monthly Nino-3.4 index (SST anomalies averaged over 5°S-5°N and 120°W-170°W) in CTR. Figure 2.1 elucidates that the simulated ENSO is more cyclic compared to the observed one, given that in our model strong La Niña episodes occur after most strong El Niño episodes. Additionally, the simulated ENSO amplitude is much stronger (standard deviation of 1.28 K in CTR vs 0.7 K in ERSST), which complicates, as we see later, the detection of solar signals in the tropical Pacific. Nevertheless, the average period of simulated ENSO (43 months) lies within the observed range of 3 to 7 years.
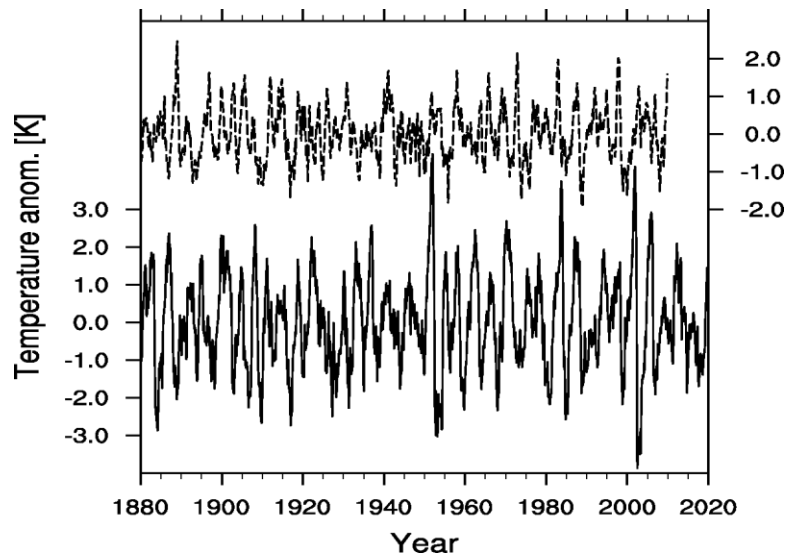
Figure 2.1: (dashed line) Time series of the observed monthly Nino-3.4 index from the ERSST v3b reconstruction over the period 1880-2009. A high-pass filter has been applied (substruction of 156-months running averages). (solid line) Time series of the simulated Nino-3.4 index in CTR. Time indexing is valid for observations only. Units in K.

2.2.3 *Analysis procedures*

Ensemble-mean monthly time series is derived by averaging over all ensemble members (eleven). The ensemble-mean seasonal cycle is similarly calculated. Hence, the deseasonalized ensemble-mean monthly anomalies refer to the deviations from the ensemble-mean seasonal cycle and accordingly, the annual anomalies are the yearly averages of monthly anomalies.

We regress annual anomalies of various meteorological variables onto the annual F10.7 over the period 1955-2006. Multiple linear regression techniques with various predictors (solar variability, ENSO, volcanic activity, etc.) have been extensively used in the past (e.g. Crooks and Gray, 2005; Roy and Haigh, 2010; Tung and Zhou, 2010). Despite the fact that 11 ensemble members are simulated, the ensemble-mean inter-annual variability of the Pacific is determined by ENSO (see Figure 2.2). We decided to include only F10.7 in the regression model. Multiple linear regression returns spurious spatial patterns when the ensemble-mean Nino-3.4 index is included, since F10.7 and Nino-3.4 are weakly correlated in CENS ($r=0.17$, 80% significance). A separate analysis with two uncorrelated predictors, the F10.7 and a high-passed Nino-3.4 (periodicities > 7 years are filtered out), leaves the spatial patterns deduced from the first method (F10.7 only) unchanged. The regression coefficients are scaled per 100 units of F10.7 (100 sfu) to ease comparison with previous studies. The response of a "typical" solar cycle could be derived by multiplying with 1.33. The statistical significance is examined with a standard t-test.

Complementary, we filter annual SST anomalies with the Multichannel Singular Spectrum Analysis (MSSA) to show the transient response of the tropical oceans to the solar cycle (Ghil et al., 2002). A detailed description of MSSA is given in Appendix 1. One advantage of the MSSA over linear regression techniques is that no a-priori information about the external forcing (e.g. the 11-yr solar cycle in this case) is required. The analysis is limited to tropical latitudes (30°S-30°N) for significant solar responses are detected only over these latitudes. A 10-channel MSSA with 14-yr window length calculates the Time Empirical Orthogonal Functions (T-EOFs) and the corresponding Time Principal Components (T-PCs). The 7th and 8th T-PCs (explaining 4.2% and 4.1% of the total inter-annual SST variability) exhibit a clear spectral peak at 10.9 years, which approximates the average solar cycle period from 1955 to 2006 (10.4 years). Moreover, this T-PC pair shows a phase-quadrature relationship that characterizes oscillatory modes (Plaut and Vautard, 1994). The first six T-EOFs describe ENSO and other intra-decadal frequencies. MSSA-filtered annual SST anomalies (hereafter MSSA-SST) are reconstructed considering only the 7th and 8th T-PCs/T-EOFs pairs. In essence, the MSSA analysis acts as a band-pass filter of narrow frequency range. By selecting a particular frequency (e.g. 10.9 years), however, MSSA may introduce spurious lags in the reconstructed time series because the length of every solar cycle is not constant but varies from 9 to almost 14 years. In Section 2.3.1, special attention is drawn to this potential caveat.

2.3   Tropical responses to solar forcing

2.3.1 *Overview of the simulated tropical solar responses*

Figure 2.2 highlights the difficulty of detecting solar signals in the equatorial Pacific, when short time series are considered. Due to the finite number of realizations (eleven) and the unrealistically large ENSO amplitude (see Section 2.2.2), a considerable fraction of the simulated ENSO variability survives. This is evident in Figure 2.2a, which shows the time evolution of the ensemble-mean equatorial (5°S-5°N) annual SST anomalies in CENS. Over the Pacific, positive anomalies up to 0.6 K follow negative anomalies of comparable magnitude and vice versa. It is very difficult to disentangle a solar signal in this plot. Any composite analysis with respect to a solar index would be prone to contamination from ENSO events.

ENSO may shade, however, the solar signal over the tropical Pacific Ocean. To inquire this possibility, we firstly smooth the annual SST anomalies with a 5-yr running mean filter. Given that the simulated ENSO has an average period of 4 years, a 5-yr window is a reasonable choice. In Figure 2.2b, the equatorial Pacific tends to warm (cool) in phase with higher (lower) solar forcing. This tendency is manifested more markedly during 1960-1967, 1978-1983, and 1993-2005.
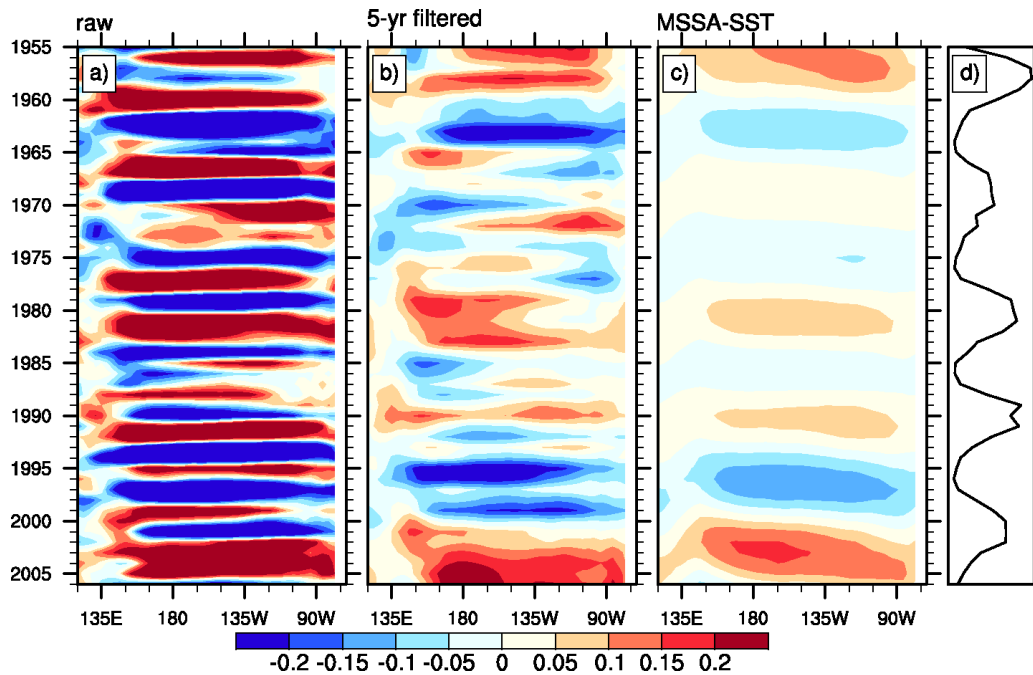
Figure 2.2: Hovmüller diagram of a) raw, b) 5-yr running averaged, and c) MSSA-filtered ensemble-mean annual SST anomalies at the Equator (5°S-5°N). Units in K. F10.7 is attached at the right side for reference (d).

As described in Section 2.2.3, MSSA is an alternative method to filter time series. The MSSA-SST reconstruction shows that, indeed, a weak solar signal is shaded by ENSO-induced variability because the equatorial Pacific warms (cools) almost in phase with increased (reduced) solar activity (Figure 2.2.c). The average peak-to-peak magnitude of the signal (0.13 K) is considerably lower than the SST variations in unfiltered data (1.2 K).

Unambiguous solar signals in particular locations can be detected even from the unfiltered SST anomalies. For example, the western equatorial Pacific (10°S-10°N, 130°E-150°E) shows a clear 11-yr solar variation. This region warms in phase with increased solar activity and the peak-to-peak amplitude of the 5-yr filtered time series is approximately 0.1 K (Figure 2.3). The correlation coefficient between the area-averaged SSTs and F10.7 is 0.4 (significance > 95%). In contrast, poor correlations are calculated for the central and eastern equatorial Pacific presumably due to the strong ENSO influence (not shown).
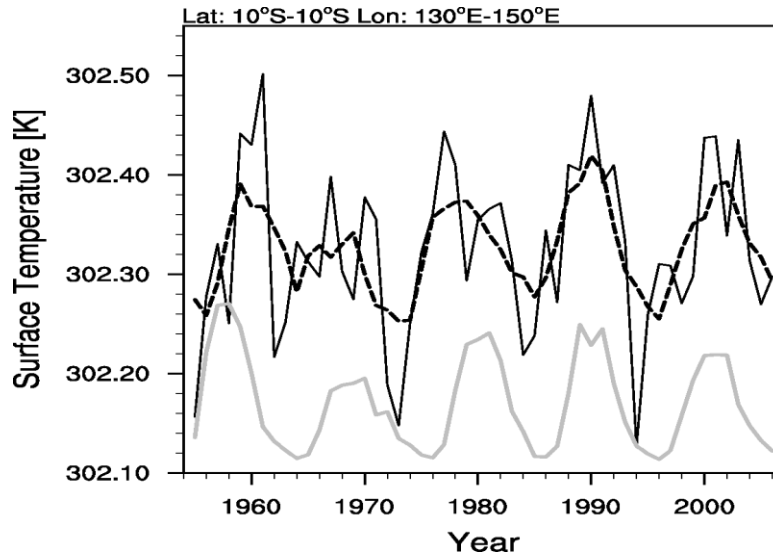
Figure 2.3: Time series of the ensemble-mean annual SST anomalies from 1955-2006 (solid black line) and its 5-yr running mean (dashed black line) over the western Pacific (10°S-10°N, 130°E-150°E) from 1955-2006. Units in K. F10.7 is superimposed for reference (grey line).

The tropical averaged (30°S-30°N) MSSA-SST together with the raw SST anomalies are presented in Figure 2.4. While it is impossible to distinguish a solar signal in the raw data, MSSA-SST oscillates almost in phase with F10.7. The tropical oceans warm (cool) with increased (decreased) solar activity with maximum amplitude of approximately 0.05 K. The filtered tropical SST response seems to lag the solar forcing. Indeed, the correlation coefficient between the MSSA-SST and F10.7 maximizes at lag +1 year (r=0.67). However, spurious lags can be introduced by the way MSSA-SST is constructed. To assess the validity of the MSSA reconstruction, we filter the annual F10.7 with the Singular Spectrum Analysis (SSA). The first and second T-PC pair captures an oscillation of 10.4 years that is, as already mentioned, the average period of the solar cycle over 1955-2006. The annual SSA-filtered F10.7 time series is reconstructed following a methodology similar to that described in Section 2.2.3. On the basis that the SSA-filtered F10.7 shows no spurious time-lag when compared to unfiltered F10.7, we conclude that the time delay of MSSA-SST, most notable after 1995, is a genuine feature of our simulations. SST solar responses lagging the 11-yr solar forcing by one to two years are theoretically expected (White et al., 1998).
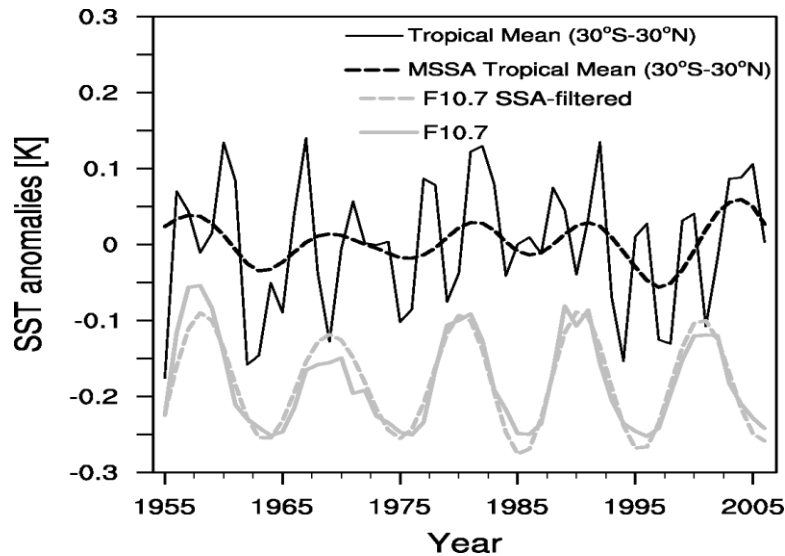
Figure 2.4: Time series of unfiltered ensemble-mean annual SST anomalies (solid black line) and MSSA-SST (dashed black line) averaged over the tropical oceans (30°S-30°N). Units in K. The unfiltered (solid grey line) and SSA-filtered (dashed grey line) annual F10.7 are superimposed for reference.

2.3.2 *Spatial patterns of surface temperature and precipitation*

Figure 2.5a displays the simultaneous regression coefficients of the annual SST anomalies onto F10.7. The tropical Pacific in CENS warms rather symmetrically with respect to the Equator but significant anomalies (>95%) are detected only in the western sector. Negative anomalies in the extra-tropics flank positive anomalies in the tropics. Over the north Indian and most of the tropical Atlantic Ocean, positive SSTs are also simulated but with weaker magnitude. Negative anomalies are seen off the Australian west coast. The zonal-mean SST response peaks at the Equator, reaching values of 0.08 K per 100 sfu. Although this work focuses on the tropical oceans, the signal in the extra-tropics and higher latitudes is shown for completeness. At the Aleutian sector, for instance, a dipole of cooling in the west and warming in the east is visible. A similar temperature dipole has been detected in reanalysis of surface air-temperature (Camp and Tung, 2007).

To verify the robustness of the solar signals in CENS, we present the regression coefficients of the MSSA-SST onto F10.7 (Figure 2.5b). The statistical significance is omitted because it exceeds the 95% threshold almost everywhere according to a t-test. Figure 2.5b is consistent with Figure 2.5a but some subtle differences are also indentified. The eastern Pacific seems to warm less compared in the MSSA-SST. Owing to filtering, the regression coefficients are now slightly weaker in the zonal average.

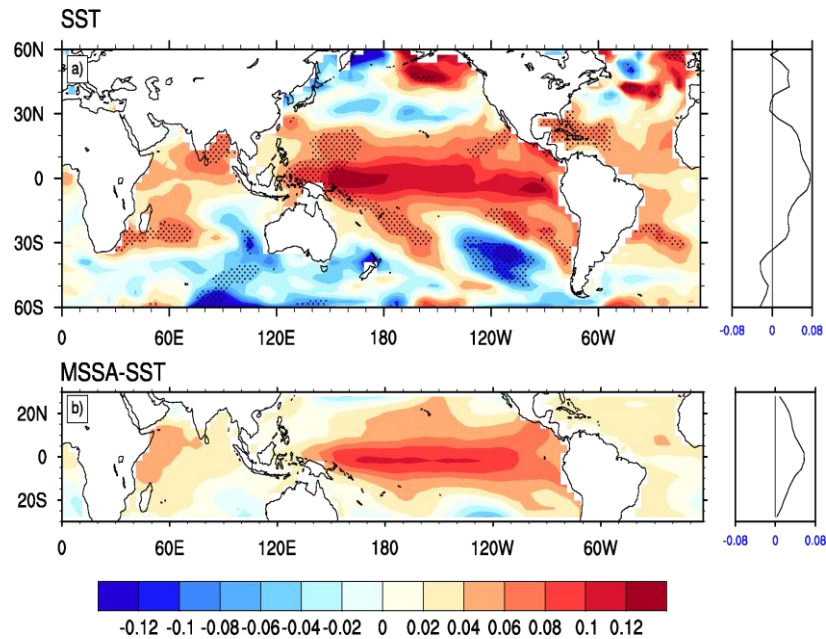Figure 2.5: Regression coefficients (K/100 sfu) of (a) the ensemble-mean annual SST anomalies and (b) the MSSA-SST anomalies, onto F10.7. Stippled areas in the top figure indicate 95% significance. Significance in the bottom figure is omitted because it exceeds the 95% level almost everywhere. Zonal averages are plotted in the right panels. The analysis in the bottom figure is limited over tropical latitudes for reasons explained in Chapter 2.3.2.

The tropical surface warming in both figures agrees well with the solar signal deduced from bathythermograph data over the period 1955-1994 (White et al., 1997). The similarity is not only qualitative but also quantitative. The maximum simulated warming in the equatorial Pacific (0.12 K/100 sfu) is consistent with the observed warming 0.15 K per 1 W/m^2 of TSI increase. The correspondence is not limited to the Pacific but also the solar signals in the tropical Indian and Atlantic oceans are qualitatively comparable. Although the simulated cooling/warming patterns in the tropical Indian and Atlantic Oceans agree with the solar signals deduced from the ERSST reconstruction, the tropical Pacific responses differ (Zhou and Tung, 2010). The eastern Pacific cools while the central equatorial Pacific warms with increased solar activity (see Chapter 1.3). In our simulations, the area off the coast of Peru and Chile shows weaker warming but no cooling. In Chapter 1.3, however, we discussed the potential contamination of solar signals in the tropical Pacific by decadal oscillations unrelated directly to the 11-yr solar cycle.

A warmer sea surface should increase the boundary layer moisture, which in turn may alter the hydrological cycle (Held and Soden, 2006). Simulated changes of total precipitation with increased solar activity are depicted in Figure 2.6. Over the western Pacific, the total precipitation increases by more than 0.2 mm/day/100 sfu. Although the signal is small and of low significance, its spatial pattern over the Pacific Ocean indicates stronger precipitation in the ITCZ. The zonal-mean solar response is positive at 10°N and slightly negative close to 20 degrees in both hemispheres. The positive-

negative dipole between 140°E-170°E implies a northward displacement of the South Pacific Convergence Zone. These changes are not unique in MAECHAM5/MPIOM and have been simulated with coupled models in the past (Shindell et al., 2006). A separate analysis of the seasonal dependence of precipitation changes identifies the strongest signal in June-July-August season, consistent with observations (van Loon et al., 2004). An explanation of the annual precipitation response is postponed until Section 2.4.2.
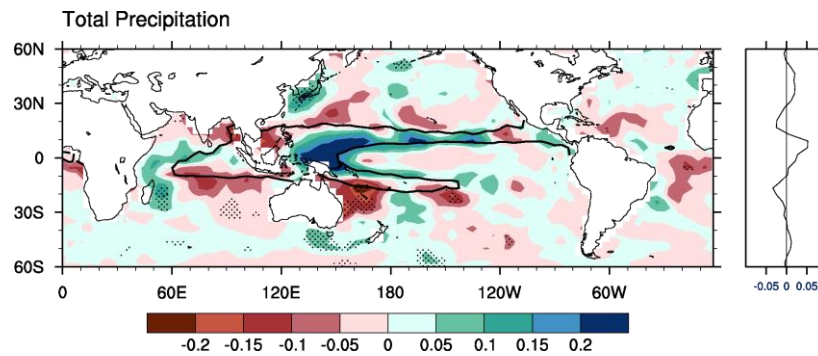
Figure 2.6: Regression coefficients (mm/day/100 sfu) of the ensemble-mean annual total precipitation onto F10.7. Stippled areas denote 95% significance. The thick black line outlines areas where the total precipitation climatology in CTR exceeds 6 mm/day. Zonal averages are plotted in the right panel.

2.4 Mechanisms responsible for surface warming

2.4.1 *Surface heat flux budget*

Insight into the physical mechanisms causing the warming in the tropics can be gained by compiling the different components of the surface heat flux budget. Increased solar insolation during years of enhanced solar activity should warm the surface, particularly over the cloud free regions (Meehl et al., 2008) and in areas where the cloud fraction is reduced (e.g. at the eastern Pacific, see later). Retorting to this warming, the oceans should release extra latent heat into the atmosphere. As seen in Figure 2.7a, the zonal-mean column-integrated water vapor, a quantity that reflects humidity changes in the boundary layer (Held and Soden, 2006), increases by 0.7 %/100 sfu over the inner-tropics (10°S-10°N) or by 0.7 %/0.08 K if the simulated SST changes are accounted. The latter value follows closely the Clausius-Clapeyron relationship. Moistening of the lowermost troposphere with increased solar activity has been documented in simulations with perpetual maximum/minimum solar forcing (Lee et al., 2009).

The enhanced near surface water vapor in solar maximum should diminish the clear-sky short-wave surface net flux (Q_{SW}) and enhance the long-wave surface net flux (Q_{LW}), respectively. Indeed, the clear-sky Q_{SW} over the inner-tropics is slightly reduced (-0.02 W/m^2/100 sfu), opposing the considerable increase of the clear-sky

Q_{LW} (0.3 W/m^2/100 sfu, see Table 2-1). Note that positive anomalies are directed downward. Overall, the positive water-vapor feedback is heating the sea surface by 0.28 W/m^2/100 sfu. Spatial details are depicted in Figure 2.7b.
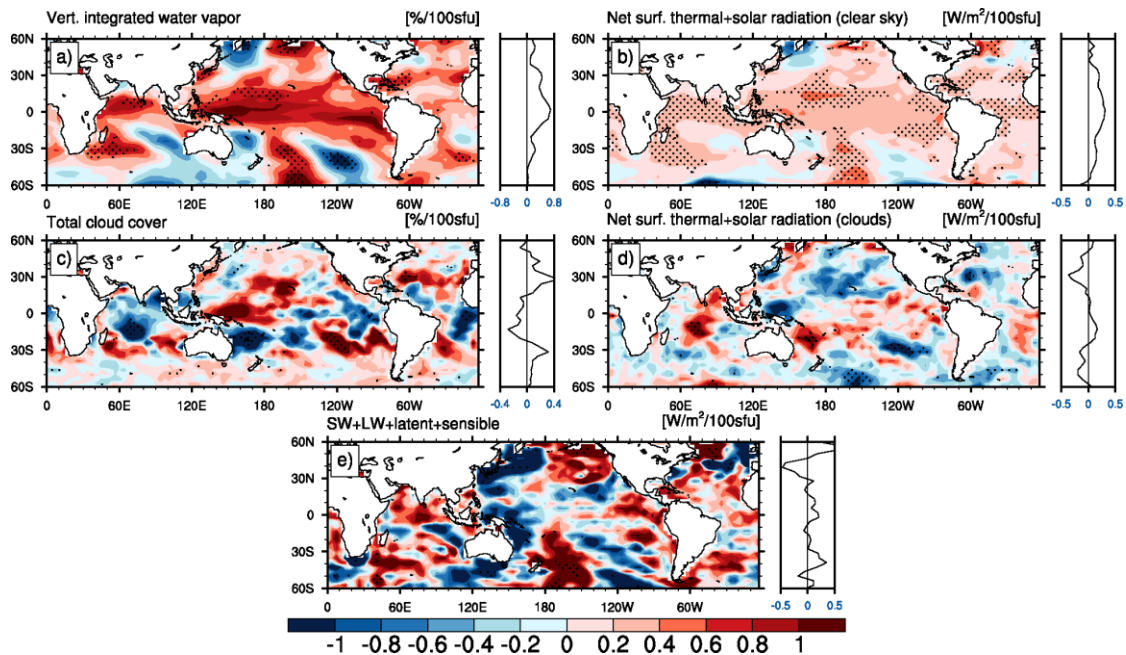
Figure 2.7: Regression coefficients onto F10.7 of the ensemble-mean annual a) vertically integrated water vapor (%/100 sfu), b) clear-sky net surface radiation flux due to water vapor changes (W/m^2/100 sfu), c) total cloud cover (%/100 sfu), d) net surface radiation flux due to cloud changes (W/m^2/100 sfu), and e) net short-wave, long-wave, latent and sensible surface heat fluxes (W/m^2/100 sfu). Stippled areas indicate 95% significance. Zonal averages are given in the right panels. In figures b), d), and e) positive values point downward.

Figure 2.7c displays reduced zonally averaged cloud fraction in the inner-tropics for increased solar activity. However, the response is zonally asymmetric. The cloud fraction increases by 1.6 %/100 sfu over the west Pacific while it reduces in the eastern Pacific. The latter reflects the reduction of low stratiform clouds (not shown), which can be explained by the thermodynamic considerations of Klein and Hartman (1993) that involve changes in static stability. Although this pattern resembles that of a stronger Walker circulation, the deep convection over the maritime continent is not getting stronger but, as shown below, it shifts somewhat to the east. Over the equatorial Indian Ocean, the negative cloud fraction anomalies are associated with stronger adiabatic heating due to enhanced descent of air (not shown).

The zonally averaged downward surface net flux due to cloud changes, Q_{SW} (cloud), increases by 0.19 W/m^2/100 sfu in the inner-tropics, whereas the Q_{LW} (cloud) flux decreases by 0.13 W/m^2/100 sfu. Note that the anomalous cloud forcing is calculated by subtracting clear-sky from all-sky Q_{SW} and Q_{LW}, respectively. The spatial patterns of Q_{SW}(cloud)+Q_{LW}(cloud) are depicted in Figure 2.7d, in which the negative sign denotes net increases in the upward direction. The change in cloud forcing averaged

over the inner-tropics is small (0.06 W/m^2/100 sfu) but spatially inhomogeneous for reasons explained before. Locally, strong radiative warming/cooling with values up to 1.6 W/m^2/100 sfu and -1.8 W/m^2/100 sfu respectively, is simulated.

Table 2-1 Intra-tropical (10°S-10°N) averages of the surface heat budget over oceans (W/m^2/100 sfu). The relative contribution of cloud cover and water vapor changes to Q_{SW} and Q_{LW} is given in the first and second column. The third column lists the net all-sky Q_{SW}, Q_{LW}, Q_{SE} and Q_{LT} surface heat fluxes. Positive values point to the ocean.

	Cloud cover	Water vapor	All sky
Q_{SW}	+0.19	-0.02	+0.17
Q_{LW}	-0.13	+0.3	+0.17
Q_{SE}	-	-	+0.03
Q_{LT}	-	-	-0.27
SUM	+0.06	+0.28	+0.1

Table 2-1emphasizes that in a zonally averaged perspective, the surface heating due to the water-vapor feedback is considerably stronger than the forcing due to cloud changes. This stems from the zonal uniformity of the former compared to the spatial heterogeneity of the latter. Locally (e.g. in the central and eastern equatorial Pacific), however, surface heating due to cloud changes outpaces the water-vapor feedback. The zonal mean radiative surface heating is balanced partly by stronger latent heat release (0.27 W/m^2/100 sfu, see Table 1). When changes in zonally averaged short-wave (Q_{SW}), long-wave (Q_{LW}), sensible (Q_{SE}), and latent (Q_{LT}) net heat fluxes are summed up over the inner-tropics, a net forcing of 0.1 W/m^2/100 sfu warms the ocean surface. The radiation balance calculations of White et al. (1998) estimated that 0.1 W/m^2 should increase the zonal-mean surface temperatures by about 0.03 K. Yet, the simulated warming in CENS is 2 to 3 times stronger, suggesting that another positive feedback is operating to amplify the Pacific response. This feedback shall be explained in the following chapter.

2.4.2 *Response of ocean dynamics*

To illustrate the response of the coupled atmosphere-ocean system, regression maps onto F10.7 of equatorial (5°S-5°N) annual zonal wind, ocean potential temperature, and vertical gradient of ocean potential temperature are shown in Figure 2.8. The

latter variable measures the sharpness and the depth of the thermocline (DiNezio et al., 2009).
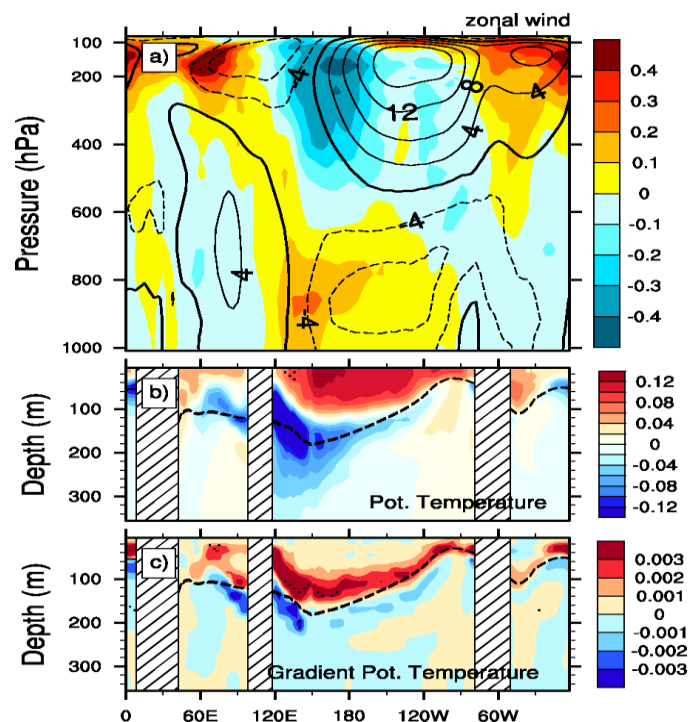
Figure 2.8: Regression coefficients (color shading) onto F10.7 of the ensemble-mean annual a) zonal wind (m/s/100 sfu), b) ocean potential temperature (K/100 sfu), and c) gradient of the ocean potential temperature (K/m/100 sfu) along the Equator (5°N-5°S). Contours in the top panel show the climatological zonal wind (m/s) from the CTR. The dashed lines in middle and bottom figures indicate the 20°C isotherm. Stippled areas indicate 95% significance. Note that figure (a) covers the troposphere-lower stratosphere (up to 90 hPa) while figures b) and c) show the upper 360 m of the ocean.

Over the equatorial Pacific, the Walker circulation is visible with easterlies in the lower troposphere and westerlies in the upper troposphere (contours in Figure 2.8.a). Negative anomalies (-0.4 m/s/100 sfu) at the upper branch of the Walker cell are accompanied by weak anomalous westerlies (0.2 m/s/100 sfu) in the lower troposphere. The strongest positive anomalies are simulated in the western Pacific just east of the zero-wind line and not at the core of the jet, indicating that the western branch of the Walker circulation, which is associated with deep convection, shifts to the east. Such an eastward displacement could explain the increased cloud fraction and precipitation anomalies over the western Pacific (Figure 2.7c). We note though that the signal is weak and of low significance.

To examine whether the strength of the Walker circulation is influenced by the solar cycle forcing, we calculate the zonal gradient of sea level pressure (SLP) between the western Pacific-Indonesian region (5°S-5°N, 80°E-160°E) and the eastern Pacific (5°S-5°N, 160°W-80°W), which is a common metric since it correlates to the upward velocity (Vecchi and Soden, 2007). Figure 2.9a depicts the regression coefficients of

the ensemble-mean SLP against F10.7. The signal in the western Pacific-Indonesian region is negligible but the SLP drops by about 7 Pa/100 sfu in the eastern Pacific. The simulated SLP response implies a weaker Walker circulation but the most notable feature is the eastward displacement of its western branch.
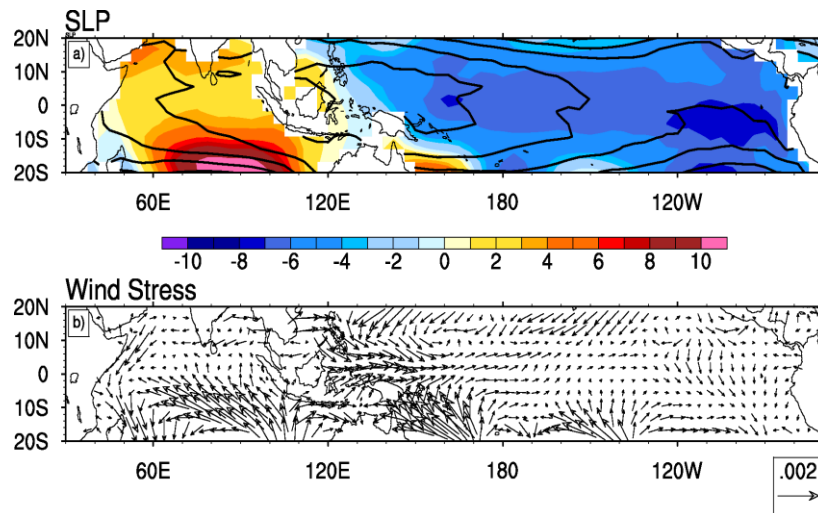
Figure 2.9: Regression coefficients onto F10.7 of the ensemble-mean annual a) sea level pressure (Pa/100 sfu) (color shading) and b) zonal and meridional wind stress (Pa/100 sfu). Contours in the top figure show the climatological sea level pressure from the CTR (2 hPa spacing; 1008 hPa isoline west of the Maritime Continent). Statistical significances are below 95% everywhere.

Such an eastward displacement causes anomalous surface westerlies and weakens the zonal wind stress along the western and central part of the equatorial Pacific (see Figure 2.9b) resulting in a number of oceanic responses. For example, a weakening of the equatorial surface currents and equatorial upwelling in concert with a reduced east-west tilt of the thermocline and a decreasing mean thermocline depth, is expected (Philander, 1981; Kirtman, 1997; McPhaden, 1999). In the following paragraphs, we demonstrate that such changes are simulated in the Pacific Ocean, indeed.

The subsurface warming in the upper layers of the Pacific Ocean reaches values of 0.12 K/100 sfu while the sign reverses in the deeper layers. The strongest cooling (-0.2 K/100 sfu) is located in the western Pacific at 160 m depth, around the mean thermocline position (Figure 2.8b). A dynamical mechanism causes this cooling. The thermocline shoals in the western Pacific due to the positive wind stress anomalies while the signal in the east is negligible. In other words, the east-west thermocline tilt is relaxed. At the same time, a basin-wide shoaling of the Pacific thermocline is simulated because positive anomalies of the potential temperature gradient flank the climatological thermocline depth at shallower layers (Figure 2.8.c). Additionally, a shallower thermocline in the eastern equatorial Indian Ocean is detected.

A lag-regression analysis of the potential temperature along the equatorial Pacific underlines the importance of thermocline depth changes in controlling the subsurface

response (Figure 2.10). At lag -5 years (meaning that F10.7 is leading temperature anomalies by 5 years), positive anomalies at 100-200 m depth are simulated in the western Pacific, which, as time progresses, extend to the east following the thermocline mean depth line (dashed line) and emerge at shallower levels (see Lag -5 to Lag -2). From Lag -2 to Lag 0, anomalously cold water builds up in place of warm water completing half a cycle. At Lag -1 the sub-surface positive anomalies reach the surface and over the next year the warming is amplified.
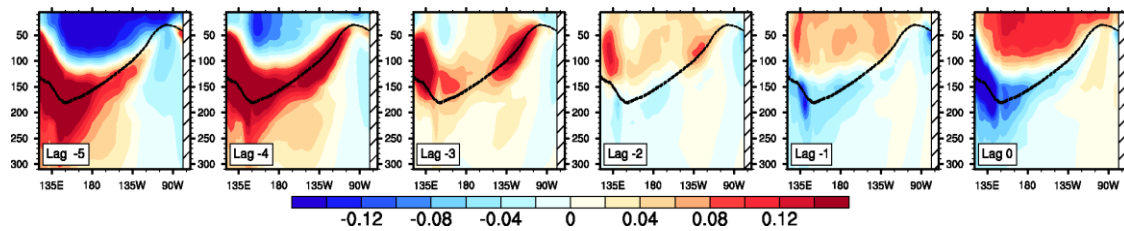
Figure 2.10: Time sequences of lagged regression coefficients onto F10.7 of the ensemble-mean annual ocean potential temperature (K/100 sfu) along the Equator (5°S-5°N). The vertical axis covers the upper 310 m of the ocean. Negative lag (in years) indicates that the F10.7 is leading the ocean potential temperature. No statistical significance is plotted.

The origin of this amplification is understood by examining the response of the shallow Pacific overturning circulation. Figure 2.11 shows the regression coefficients (shading) of the zonal mean (120°E-70°W) meridional velocity onto F10.7, together with its climatological profile (contours). With increased solar activity, a tendency for slower meridional circulation in the Pacific is simulated, affecting the surface cooling efficiency of the poleward heat transport. In accordance to slower meridional transport, the upwelling over the entire Pacific basin is reduced, with the strongest signal in the central and western sector (not shown). As expected, the NECC (North Equatorial Counter Current) weakens with ensuing surface warming (not shown) due to decreased heat flux divergence (DiNezio et al., 2009).

In the case of warm ENSO events, the thermocline shoals in the western but deepens in the eastern Pacific (DiNezio et al., 2009). In our simulations, on the contrary, the basin-wide shoaling of the thermocline balances its sinking in the eastern Pacific due to reduced surface easterlies. As proposed by DiNezio et al. (2010), these two opposing tendencies may yield a condition where the eastern Pacific is less prone to surface wind stress anomalies thus suppressing the efficiency of the Bjerknes feedback (Bjerknes, 1966) to amplify weak SST anomalies to an El Nino episode. Moreover, our analysis refutes the proposed mechanism of White et al. (2003a). We emphasize on the importance of ocean circulation changes, induced by reduced surface easterlies. The subsequent reduction of heat transport divergence warms the surface. The synergy of ocean circulation changes and the water-vapor feedback results in stronger warming over the Pacific Ocean when compared to the solar signals over the Indian and Atlantic oceans.
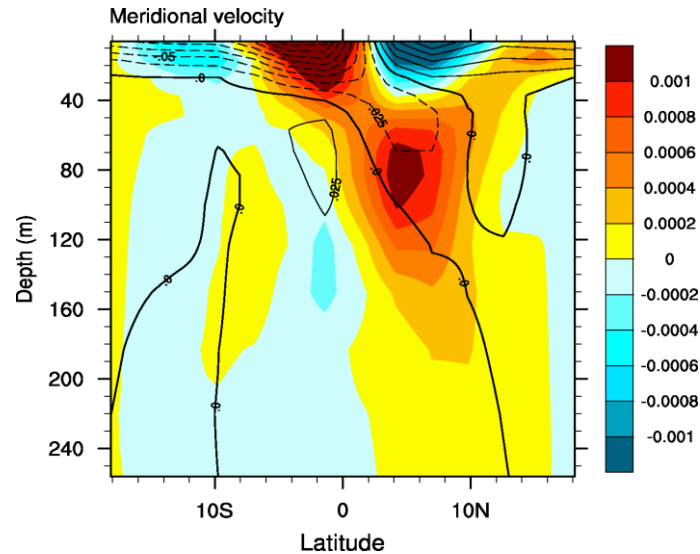
Figure 2.11: (shading) Regression coefficients (m/s/100 sfu) of the ensemble-mean annual meridional velocity (averaged over 120°E-70°W) onto F10.7. Climatological values from CTR are superimposed (contours) with solid/dashed lines to denote positive/negative values respectively (contour interval: 0.025 m/s). The vertical axis covers the upper 260 m of the ocean. Statistical significances are below 95% everywhere.

2.4.3 *Solar signals in the uncoupled simulations*

The previous section demonstrated the key role of the reduced surface easterlies, which result from the eastward shift of the region of deep convection. It remains to answer how this shift is physically explained. The ensemble simulations without ocean coupling (AENS) give an answer.

In Figure 2.12, which shows the regression coefficients of the equatorial zonal wind anomalies from AENS onto F10.7, the western branch of the Walker circulation moves eastward, resulting in weaker surface winds. This displacement is qualitatively similar to CENS. It seems therefore that ocean coupling is not needed to simulate a eastward shift of the Walker circulation. Changes in the atmosphere and not in the ocean are causing this response. In fact, increased stratification in the eastern Pacific (Clement et al., 1996) could act to weaken the solar signal as suggested by the stronger response in AENS. Simulations of the atmospheric and oceanic response to increasing greenhouse gas concentrations led to a similar conclusion (Vecchi and Soden, 2007; DiNezio et al., 2009).

It is difficult, however, to trace the origin of these atmospheric changes with the current set of experiments. Nevertheless, the suggestion of Held and Soden (2006) provides a plausible explanation. They suggested that under global warming, the zonally asymmetric component of the atmospheric overturning circulation should slow down in response to differential changes of global mean precipitation and low-troposphere water vapor. Simulations of global warming caused by increased greenhouse gas concentrations show a 2 %/K increase of global-mean precipitation

opposed to a 7 %/K increase of low-troposphere water vapor (Vecchi and Soden, 2007). To balance this difference, the atmospheric overturning circulation and particularly the Walker circulation is weakening and at the same time deep convection shifts to the east (Held and Soden, 2006; DiNezio et al., 2009).
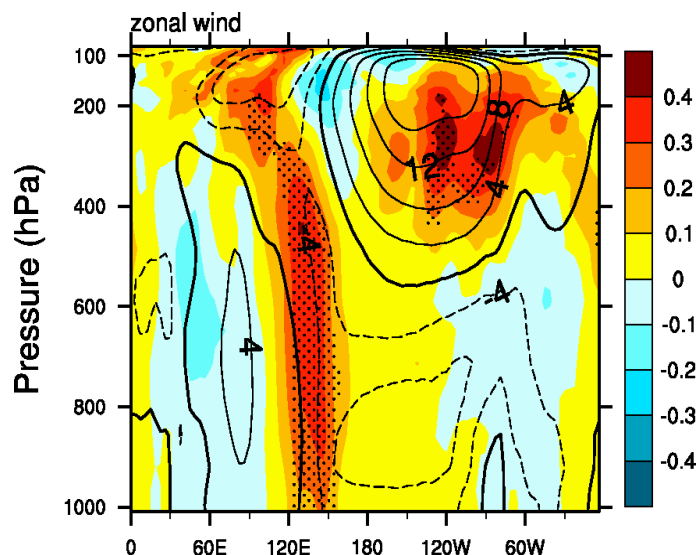
Figure 2.12: Regression coefficients (m/s/100 sfu) onto F10.7 of the ensemble-mean annual zonal wind (color shading) along the Equator (5°S-5°N) from AENS. Contours show the zonal wind (m/s) climatology from CTR. Compare to Figure 2.8a.

A globally warmer climate is also anticipated with increased solar activity (Gray et al., 2010). Our coupled simulations with MAECHAM5/MPIOM exhibit an increase of 0.03 K/100 sfu in global mean 2m temperature, 0.35 %/100 sfu in global mean vertically integrated water-vapor, and 0.04 %/100 sfu increase in global mean total precipitation respectively. These numbers translate to approximately a 10 %/K increase of the rate of low-troposphere water vapor (the vertically integrated water-vapor reflects humidity changes in the boundary layer) and a 1.4 %/K increase in total precipitation. Hence, the sensitivity of the rate of moistening and the rate of precipitation in our simulations is consistent with the simulated response due to increased greenhouse gas concentrations. Atmospheric thermodynamic constraints, therefore, may determine the response of the tropical Pacific Ocean to increased solar forcing. It must be noted that these derivations cannot be repeated for AENS because of the prescribed SSTs.

2.5 Linkages between the 11-yr solar cycle and the Tropical Pacific Quasi-Decadal Oscillation

2.5.1 *The Tropical Pacific Quasi-Decadal Oscillation in the control simulation*

As noted in Chapter 1.3, solar signals in the tropical Pacific can be mixed up with decadal oscillations, such as the Tropical Pacific Quasi-Decadal Oscillation (TPQDO), when short time series are analyzed. The possibility that the TPQDO is synchronized to the 11-yr solar cycle should not be excluded. Hence, it is reasonable to examine if the basin-wide weak warming illustrated in Section 2.3.2 is not merely a manifestation of the TPQDO.
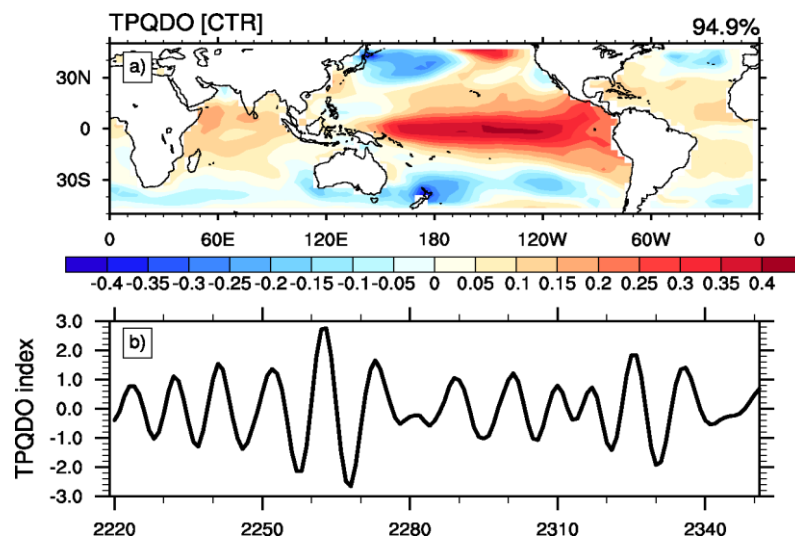
Figure 2.13: a) Regression coefficients (K/std) of the unfiltered SST anomalies from CTR onto the normalized TPQDO index. b) Time series of the normalized TPQDO index.

MAECHAM5/MPIOM internally generates a TPQDO with an average period of 12.3 years. The spatial signature of the TPQDO on tropical SSTs is isolated with a 10-channel MSSA of 17-yr window length. The chosen window length is dictated by the observed evidence for a ~12.5-yr TPQDO (see Chapter 1.3) and is longer compared to the window length used in Section 2.3 because the isolated oscillation has longer period (12.5-yr vs 10.9-yr). Similar to CENS, the first six T-EOFs in CTR describe ENSO and other intra-decadal frequencies whereas the 7th and 8th T-EOF/T-PCs pair (each T-EOF explains 4% of the inter-annual SST variability) exhibits a spectral peak at 12.3 years. This pair is associated to the TPQDO and is used to reconstruct annual SST anomalies. The leading PC (explains 95% of the filtered variability) of the reconstructed SST anomalies defines the TPQDO index (Figure 2.13b).

The spatial pattern of the simulated TPQDO is marked by a basin-wide warming up to 0.3 K/std, flanked by negative anomalies in the extratropics (Figure 2.13a). Over the

north Indian and most of the tropical Atlantic oceans the signal is positive but its amplitude is much weaker compared to the central Pacific warming. The examination of the TPQDO index indentifies pronounced multi-decadal variations. For instance, the amplitude of the simulated TPQDO becomes stronger from 2250 to 2280.
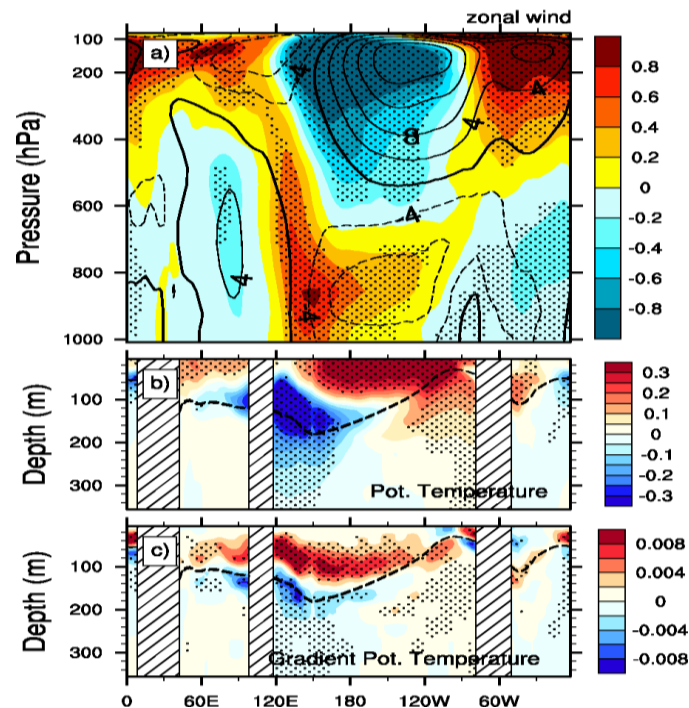
Figure 2.14: Regression coefficients (color shading) onto the TPQDO index of the annual a) zonal wind (m/s/std), b) ocean potential temperature (K/std), and c) gradient of the ocean potential temperature (K/m/std) along the Equator (5°N-5°S) from CTR. Contours in the top panel show the climatological zonal wind (m/s). The dashed lines in middle and bottom figures indicate the 20 °C isotherm. Stippled areas indicate 95% significance. Compare to Figure 2.8 but with different shading intervals.

The regression coefficients onto the TPQDO index of the annual zonal wind, ocean potential temperature, and the vertical gradient of ocean potential temperature at the Equator (5°S-5°N) are shown in Figure 2.14. The most-important features in this figure are: a) the positive zonal wind anomalies over the Pacific, which imply an eastward displacement of the Walker circulation, and b) the associated shoaling of the thermocline throughout the Pacific basin but most pronounced in the western part. There, the shallower thermocline depth causes negative temperature anomalies at 120 m depth. For brevity, the expected slowdown of the shallow Pacific overturning circulation due to the reduction of the wind stress divergence and the related changes of the surface currents are not shown.

TPQDO in MAECHAM5/MPIOM is explained by the recharge/discharge mechanism (Jin, 1997) operating, however, on decadal time scales. This is best elucidated by calculating the lag regression coefficients of the equatorial upper Ocean Heat Content (OHC) anomalies (5°S-5°N, 120°E-110°W integrated down to 310 m) and of SST

anomalies over the Nino-3.4 region onto the TPQDO index (Figure 2.15). As expected by the recharge/discharge theory, positive OHC anomalies precede positive SST anomalies. The time lag in our model is about 2 years. Moreover, the OHC rate of change (grey line) shows an out-of-phase relationship with the Nino-3.4 region SST anomalies (Knutson and Manabe, 1998; Hasegawa and Hanawa, 2003). From this point of view, the TPQDO can be perceived as an extension of the "classic" ENSO to lower frequencies (Tourre et al., 2005).
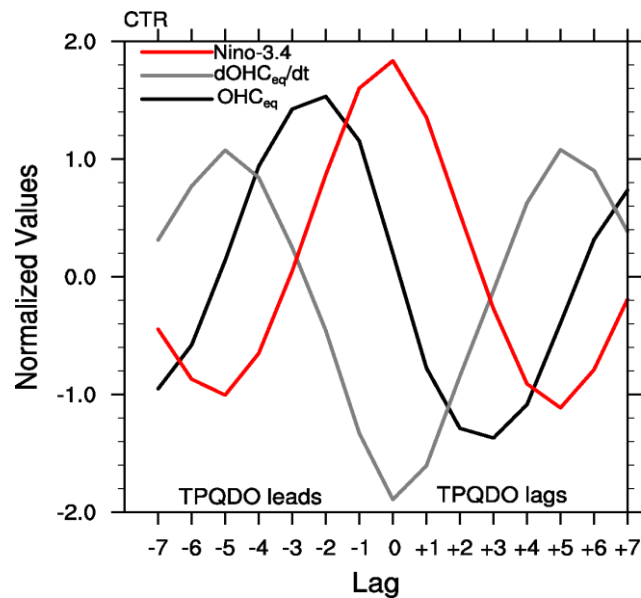
Figure 2.15: Lag regression coefficients onto the TPQDO index of the ocean heat content anomalies (OHC_{eq}) in the equatorial Pacific (5°S-5°N, 120°E-110°W) integrated from surface down to 310 m (black line), the temporal rate of change of OHC_{eq} (grey line), and the Nino-3.4 index (red line). Data are taken from CTR and all values are normalized to ease comparison. Negative lags means that the TPQDO index leads.

2.5.2 *Synchronization of the Tropical Pacific Quasi-Decadal Oscillation to the 11-yr solar cycle*

The solar-cycle-related tropical warming detected in CENS is qualitatively similar to the TPQDO-related warming (compare Figures 2.5 and 2.13). The same can be told for the zonal-mean zonal wind and ocean subsurface temperature responses (compare Figures 2.8 and 2.14). Furthermore, a separate analysis, not shown here, verifies that the dynamical oceanic responses illustrated in Section 2.4.2 are consistent with the recharge/discharge mechanism. Based on these findings, we suggest that the simulated warming over the tropical Pacific should be ascribed to the TPQDO. This means that the ensemble averaging cannot remove the TPQDO completely from the SST time series due to either physical reasons or sampling errors. The former suggests for the TPQDO-solar synchronization, whereas the latter implies accidental alignment of the TPQDO with the 11-yr solar cycle.
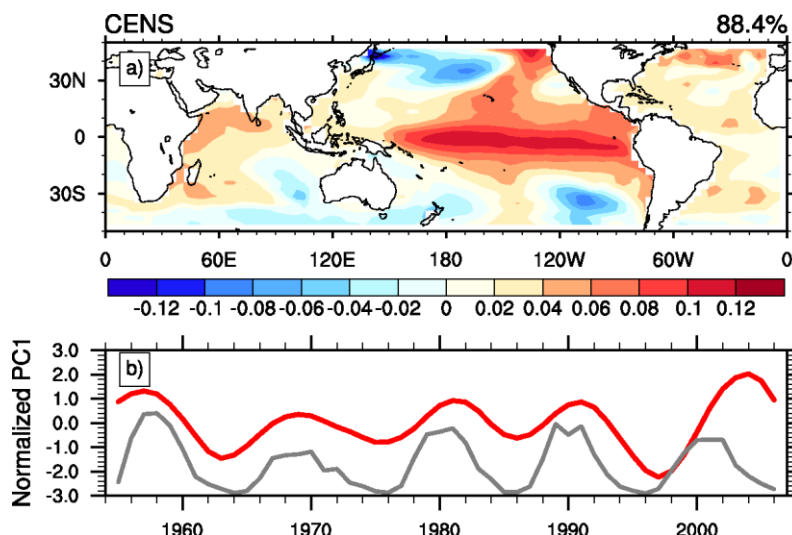
Figure 2.16: Time series of the simulated annual PC1 (red line) of MSSA-SST and F10.7 (grey line) over the period 1955-2006. The associated EOF1 is not shown but its spatial patterns are similar to Figure 2.5b. EOF1 explains 88.4 of the filtered variance. PC1 is essentially the same as the globally averaged MSSA-SST time series (Figure 2.4).

To examine whether the TPQDO is aligned by chance with the solar cycle, we device the following test. We first calculate the leading EOF of the MSSA-SST time series from CENS (explains 88.4% of the filtered variability, see Figure 2.16). The associated PC1, which describes the time evolution of the warming/cooling patterns seen in Figure 2.16, varies in phase with the 11-yr solar cycle (grey line) with a correlation coefficient that maximizes at lag of 1 year (r=0.65). The lag +1 correlation is then used as a metric to estimate the probability of deriving the same correlation coefficient in the CTR simulation in which the TPQDO is certainly not related to the 11-yr solar cycle.

Figure 2.17 displays the probability density function of the lag +1 correlation coefficient from 5000 synthetic ensemble-mean TPQDO indices, generated with the block-bootstrap resampling method. Every ensemble consists of 11 phantom members and every member is constructed by selecting randomly the first only year of a 52-yr chunk of the TPQDO index from CTR (Figure 2.13). Hence, the block size of the bootstrap test is 52 years. According to this conservative test, the lag +1 correlation coefficient calculated in CENS passes the 95% threshold. In other words, there is less than 5% chance that by superimposing randomly 11 model integrations without solar cycle forcing to obtain lag +1 correlation higher than 0.65. We conclude, therefore, that in CENS there is a physical linkage between the positive (negative) TPQDO phase and the positive (negative) 11-yr solar cycle phase.
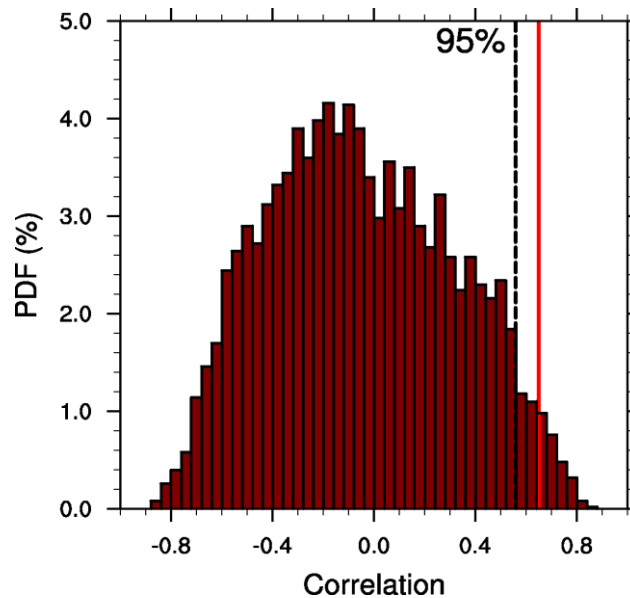
Figure 2.17: Probability density function (PDF) of the lag +1 correlation between the ensemble-mean (11 members) synthetic TPQDO index and F10.7. 5000 synthetic new ensemble-mean TPQDO indices have been generated by block bootstrapping. The block size is conservatively set to 52 years. Dashed black line shows the 95% level according to one-tailed t-test. Red line shows the lag+1 correlation in CENS (r=0.65).

To understand how the otherwise naturally excited TPQDO is synchronized to the 11-yr solar cycle, we recall that reduced surface easterlies (westerly anomalies) in the equatorial Pacific have been simulated in solar maxima regardless of ocean coupling. The critical role of the westerly anomalies on synchronizing, statistically, the TPQDO can be understood in the context of the recharge/discharge mechanism. During solar maxima, westerly wind anomalies push the Pacific system to a state where equatorial upper ocean heat content is constantly flushed towards the subtropics due to the divergence of Sverdrup transport. This solar-forced heat discharge lifts the thermocline over the entire Pacific initiating the negative TPQDO phase in the years to follow. In the opposite phase of the 11-yr solar cycle, the stronger equatorial easterlies push the Pacific system to a state where heat is accumulated, favoring a positive TPQDO phase in the subsequent years. Obviously, the same coupled mechanism between the equatorial winds and heat content anomalies generates the TPQDO in CTR. The difference in the CENS simulations is that the atmospheric response to the 11-yr solar cycle variability sets the pace of the heat discharge.

2.6   Potential model shortcomings

Though the amplitude of the simulated positive SST anomalies in the Pacific is consistent with observations (White et al., 1997), the globally averaged temperature response is substantially weaker. MAECHAM5/MPIOM shows a global (60°S-60°N) ocean surface warming on the order of 0.027 K/100 sfu or 0.036 K from solar

minimum to maximum (multiply with 1.33). This number is roughly half of the observed global ocean temperature response (0.08 K) to 11-yr solar forcing (White et al., 1997; Tung and Camp, 2008). If temperature changes over land surface are added, the simulated global temperature solar response increases slightly (0.03 K/100 or 0.04 K for solar maxima-minima). Yet, the signal remains considerably lower than the observed 0.1 K solar warming (Lean and Rind, 2008).

It is particularly challenging to understand why our simulations underestimate the global response while they give a reasonable signal over the Pacific when compared to the work of White et al. (1997). One reason could be deficiencies in simulating a realistic reduction of the global planetary albedo due to cloud changes with increased solar forcing. One of the major caveats of current AOGCMs, are uncertainties related to the parameterization of clouds. For example, the proper simulation of marine stratocumulus clouds in the eastern Pacific is still a major issue (Lin, 2007). It is also possible that physical mechanisms not accounted for or poorly represented in our model may contribute to this shortcoming.

One important deficiency of our model is the poor representation of the solar signal in the Northern Hemisphere winter stratosphere. Opposite to observations and earlier modeling attempts (Kodera and Kuroda, 2002; Matthes et al., 2004; Frame and Gray, 2010; Schmidt et al., 2010), the simulated polar vortex is anomalously weak with increased solar forcing resulting in negative zonal-mean zonal wind anomalies throughout the boreal winter. Moreover, a secondary maximum in the equatorial lower stratosphere temperature is not visible despite that the implemented solar-induced ozone concentration anomalies show a clear secondary maximum (Schmidt et al., 2010). Given that the "top down" propagation of the solar signal has been suggested that amplify the ocean-atmosphere responses to increased TSI (van Loon et al., 2007), this caveat could locally weaken the surface response. However, the global mean signal should remain unaffected.

2.7 Summary

The goal of this work is to better understand the tropical oceanic response to 11-yr solar variability. The focus is on the Pacific Ocean where coupled atmosphere-ocean interactions may enhance or diminish the response to 11-yr solar cycle forcing. To address this subject we analyze an ensemble of eleven simulations carried out with MAECHAM5/MPIOM. Simulations with an atmosphere-only version of the model are additionally considered. Both configurations are solely forced with realistic spectral irradiance changes over the period 1955-2006. This approach diminishes the risk of any solar signal aliasing by other external forcings (e.g. volcanoes, greenhouse gases).

Our analysis is primarily based on unfiltered data, yet band-pass filtering is complementary used to eliminate the ENSO signature in the central and eastern

Pacific. The western Pacific warms in-phase with increased solar activity. If solar maxima trigger, statistically, more La Niña events and the Pacific shifts to El Niño state in a couple of years later, as suggested by Meehl and Arblaster (2009), then this cold-to-warm transition is smeared out when filtering is applied. Our simulations, however, do not support this transition given that the simulated warming over the Pacific is independent of the filtering (see Figure 2.5).

Our simulations show that the tropical oceans warm when the Sun is more active and the warming is amplified over the Pacific. There, an almost basin-wide warming of 0.1 K/100 sfu is simulated. Both regression analysis and the Multichannel Singular Spectrum Analysis reasonably agree on the spatial patterns of the surface warming. In the subsurface western Pacific however, a counterintuitive dynamical cooling is detected. This implies that the solar signal may penetrate deeper than previously thought (White et al., 1997).

The simulated tropical response to solar forcing is pinned down to the synergetic effect of the water-vapor feedback, cloud changes and, most importantly, ocean dynamics. As the incoming solar radiation increases, the oceans evaporate more water into the atmosphere. The stronger downward LW and SW radiation due to increased humidity and cloud changes respectively, are sources for surface heating in the Indian and Pacific oceans. Hence, the suggestion of Meehl et al. (2008) concerning the contribution of the water-vapor is confirmed by our simulations. Changes of the surface radiation heat budget cannot explain the magnitude of the tropical Pacific warming. The surface response there is primarily administered by a number of oceanic reactions to anomalous westerlies. These westerlies are independent of the ocean coupling; alike to the coupled ensemble the deep convection moves to the east in the atmosphere-only ensemble, too. In MAECHAM5/MPIOM, the mean depth of the thermocline shoals and its east-west tilt relaxes responding to weaker surface easterlies. Additionally, the surface ocean currents and the near-equator shallow meridional circulation slacken. These changes should alter the oceanic heat transport, which together with the water vapor feedback amplify the surface warming over the Pacific Ocean in a similar fashion as for the Pacific's response to global warming due to increased greenhouse gas concentrations (Vecchi and Soden, 2007; DiNezio et al., 2009; DiNezio et al., 2010).

We find evidence that the simulated TPQDO, which is a natural oscillation of the Tropical system, is synchronized to the 11-yr solar cycle at least over the period 1955-2006. The westerly anomalies over the Pacific mediate the atmospheric response to 11-yr solar forcing down at the ocean surface. Hence, the dynamical changes identified in the Pacific should be ascribed to the TPQDO. This is consistent with the suggestion of White and Liu (2008b) but with a fundamental difference: the TPQDO in our model is not excited by but synchronized to the 11-yr solar cycle. The nature of this synchronization is statistical. This means that a large number of ensemble simulations with MAECHAM5/MPIOM are required to diagnose such synchronization. Obviously, the TPQDO is not synchronized to the 11-yr solar cycle

in every individual realization. The detected solar cycle-TPQDO synchronization in our model provides a new plausible mechanism to explain the synchronization of the observed TPQDO to the 11-yr solar cycle. The solar cycle could give the pace of the observed TPQDO from 1955 to 2006.

The discussion above implies that global warming due to increased TSI is likely to affect the atmospheric overturning circulation and particularly the Walker circulation with subsequent changes to natural oscillations of the Tropical Pacific system. Therefore, global surface changes drive regional signals. Hence, in our simulations stratospheric circulation changes induced by increased UV irradiance pose a minor, if any, effect on the simulated tropical surface warming. This means that the "top down" mechanism does not operate in our model.

The results of this chapter suggest that, firstly, the stronger surface heating in the Pacific Ocean should be ascribed to typical climate feedbacks and not to the increased solar irradiance per se, and, secondly, the atmospheric response to 11-yr solar cycle drives the ocean. Our model suggests that, statistically, the surface temperature over the Pacific Ocean warms with increasing solar activity.

Chapter 3

Synchronization of the ENSO decadal amplitude modulation to the 11-yr solar cycle

3.1 Introduction

The El Niño-Southern Oscillation (ENSO) is the dominant mode of inter-annual variability of the tropical Pacific Ocean (Philander, 1990). Every three to five years, the sea surface in the eastern Pacific warms anomalously, initiating an El Niño event, which under normal conditions lasts for 9 to 12 months. The opposite ENSO phase, which is characterized by cooling in the eastern Pacific, is called La Niña. The transition from El Niño to La Niña is controlled by the positive Bjerknes feedback and the negative thermocline feedback (Neelin et al., 1998).

ENSO is certainly not the only quasi-periodic phenomenon of the tropical Pacific coupled system. Historical reconstructions of the Sea Surface Temperatures (SSTs) going back to 1880 have revealed a number of oscillations on decadal and multi-decadal time scales (Zhang et al., 1997). Many studies have documented a 10 to 12-yr oscillation with ENSO-like spatial characteristics (Mann and Park, 1996; Allan, 2000; White et al., 2003b). This oscillation, which will be termed as TPQDO (Tropical Pacific Quasi-Decadal Oscillation) hereafter, shall not be confused with the Pacific Decadal Variability (Mantua et al., 1997) that, despite its ENSO resemblance, refers to multi-decadal time scales (20-50 years). White et al. (2003b) used the term QDO instead of TPQDO. It has been shown that the very same recharge/discharge mechanism that explains ENSO variability (Jin, 1996, 1998) describes TPQDO, too (Hasegawa and Hanawa, 2003; White et al., 2003b). Model simulations with coupled Atmosphere-Ocean General Circulation Models (AOGCMs) demonstrated that the TPQDO is a natural mode of the tropical Pacific (e.g. Knutson and Manabe, 1998; Tourre et al., 2005). Nevertheless, the fact that the observed TPQDO seems phase-locked to the 11-yr solar cycle from 1955 to present (Figure 1.3) sparked intriguing

questions about possible solar cycle-TPQDO linkages (White et al., 1997; White and Liu, 2008b). Although this possibility is still debated (Gray et al., 2010), in Chapter 2 we give evidence for a statistical synchronization of the TPQDO on the 11-yr solar cycle.

The periodic modulation of ENSO characteristics (e.g. amplitude frequency, onset) is another source of decadal variability in the tropical Pacific Ocean (Torrence and Webster, 1999; Yeh and Kirtman, 2004). The ENSO amplitude in particular, undergoes a 10 to 15-yr variation with a distinct signature in equatorial Pacific SSTs (Power et al., 1999; Torrence and Webster, 1999; Sun and Yu, 2009). Compared to moderate episodes, the center of action of strong El Niño episodes appears to be shifting towards the eastern equatorial Pacific. In contrast, the center of strong La Niñas moves towards the central Pacific (An and Wang, 2000). This asymmetry induces a dipole of anomalous cooling (warming) in the central (eastern) Pacific during periods when ENSO is more energetic (Sun and Yu, 2009). AOGCMs successfully simulated decadal modulations of the ENSO amplitude but not always for the same reasons (e.g. Rodgers et al., 2004).

The origin of the ENSO Decadal Amplitude Modulation (EDAM hereafter) is still debated. It has been suggested that tropical-extratropical interactions can generate such decadal changes (Gu and Philander, 1997) but more recent studies view EDAM as phenomenon native to the Pacific system (Timmermann and Jin, 2002; Newman et al., 2003; Rodgers et al., 2004). Yet, it is not clear whether EDAM is a non-linear or stochastically forced mode of the Pacific system. This is because the nature of ENSO remains unknown (Fedorov and Philander, 2001; Timmermann and Jin, 2002; Timmermann, 2003). If ENSO is a non-linear self-sustained mode, the ENSO amplitude should be modulated by slow changes of the Pacific state (e.g. Kirtman and Schopf, 1998). TPQDO, for instance, can be viewed as a slow variation of the tropical Pacific given its much longer period compared to ENSO. This theory predicts that a physical relationship between the TPQDO and EDAM could be established. In the case that ENSO is a stochastically forced damped mode, EDAM should be insensitive to background changes (e.g. Flugel et al., 2004).

A possible relationship between EDAM and the 11-yr solar cycle has been discussed two decades ago (Barnett, 1989) because EDAM fluctuates out-of-phase with 4 out of 5 most recent solar cycles (from 1955 onwards). This nominal anti-correlation extends back for another two solar cycles (solar cycles 17 and 18) and reappears for the period 1880-1920 (see Figure 1.2). One must be cautious, however, due to the low spatial quality of the SST reconstructions in the tropical Pacific before the 1950s (Deser et al., 2010). Moreover, uncorrected discontinuities during the 1940's could introduce spurious decadal variations (Thompson et al., 2008).

To examine whether a physical linkage between the 11-yr solar cycle and EDAM can be established, we carry out ensemble simulations with a comprehensive AOGCM forced only with realistic solar irradiances from 1955 to 2006. Obviously, these

simulations could confirm or reject any solar cycle-EDAM relationship over the simulated period only.

This chapter extends the analysis of Chapter 2. In Section 3.2 we describe briefly the model and analysis procedures. To understand the nature of the simulated EDAM, data from a control simulation without 11-yr solar forcing is first analyzed in Section 3.3. In Section 3.4, we analyze solar cycle-forced ensemble simulations and a physical relationship between the simulated EDAM, TPQDO, and the 11-yr solar cycle is established. This relationship is further explained in Section 3.5. Finally, findings of this study are discussed in Section 3.6 and summarized in Section 3.7.

3.2   Model description and analysis procedures

All simulations are performed with the middle atmosphere version of the ECHAM5 (MAECHAM5) general circulation model coupled to the MPI Ocean Model (MPIOM) (Marsland et al., 2003; Manzini et al., 2006; Roeckner et al., 2006). The OASIS coupler communicates momentum, heat and fresh water fluxes between atmosphere and ocean without any flux adjustment (Valcke et al., 2003). The horizontal resolution of MAECHAM5 is T31, denoting spectral truncation at wavenumber 31 (equivalent to 3.75°x3.75° grid) while the vertical resolution has 90 unevenly spaced layers extending up to 0.01 hPa. MPIOM's curvilinear grid has 3 degrees horizontal spacing at the Equator and 40 vertical layers. A Hibler-type dynamic/thermodynamic sea-ice model and a river run-off scheme are also included.

To simulate a realistic and time varying 11-yr solar cycle, solar spectral irradiances and solar-cycle-induced ozone anomalies are introduced in MAECHAM5 (see also Chapter 4.2.1). The spectral solar irradiances are taken from Lean (2000). Ozone anomalies are taken from HAMMONIA (Hamburg Model for Neutral and Ionized Atmosphere) simulations with perpetual maximum/minimum solar conditions (Schmidt et al., 2010). No other external forcing (e.g. aerosol loading form volcano eruptions) is imposed and the greenhouse concentrations are fixed to values typical for the 1990's. Chapter 2 and Appendix 3 provide more details about MAECHAM5/MPIOM.

In the first part, data from a 140-yr control run (CTR) with constant solar activity (set to 1367 W/m^2) is analyzed. Branching from CTR, we carry out an ensemble (CENS) of 11 members with 11-yr solar forcing from 1952 to 2006. Our analysis, however, is restricted over the period 1955-2006. Data from the CENS ensemble has been used in Chapter 2, too. Finally, we conduct idealized simulations with a two-box discharge/recharge model of ENSO (Timmermann and Jin, 2002) to facilitate the interpretation of CENS.

Empirical Orthogonal Functions (EOFs) are applied on unfiltered and 8-yr filtered annual SST anomalies (30°S-30°N, 100°E-70°W) to separate dominant modes of variability of the tropical Pacific. This task is repeated for CTR and CENS,

respectively. A Lanczos filter is used here, but results do not critically depend on the filter's type or on the cut-off frequency. EOFs are presented as the regression coefficients of the unfiltered SST anomalies onto the associated principal components (PCs). Before regressing, PCs are normalized to unit standard deviation (std).

The EDAM index is defined as the 8-yr low-pass filtered Niño-3.4 amplitude (Sun and Yu, 2009). The Nino-3.4 amplitude is defined as the modulus of the Nino-3.4 index (SST anomalies over 5°S-5°N and 120°W-170°W). Because the simulated surface temperatures show no apparent trend (unlike in observations, see Chapter 1.3), no high-pass filter is applied prior to the calculation of the Nino-3.4 index. The ensemble-mean EDAM index is the average of eleven individual EDAM indices. Note that all computations consider annual anomalies after the seasonal cycle is removed. Figure 3.1 only is based on monthly anomalies.

We select the 10.7 cm radio flux index (F10.7) to describe the 11-yr solar cycle variation. As in Chapter 2, ensemble-mean SST anomalies are regressed onto F10.7. The regression coefficients displayed in Figure 3.7 are scaled to 100 F10.7 solar flux units (sfu) to facilitate comparison with earlier studies.

3.3 ENSO decadal amplitude modulation in the control simulation

In this section, we investigate the nature of EDAM in CTR because the same analysis has not been yet undertaken for MAECHAM5/MPIOM. We show that EDAM in our model is an internal low-frequency mode of the tropical Pacific system excited from stochastic forcing. To understand the mechanism generating EDAM, however, the nature of the simulated ENSO needs to be examined first.

MAECHAM5/MPIOM in the selected configuration excites unrealistically strong El Niño and La Niña events with an average reoccurring period of 3.6 years. The standard deviation of the Nino-3.4 index in CTR is 1.28 K as opposed to 0.7 K from the ERSST v3b reconstruction (Smith et al., 2008). This overestimation is ascribed to the coarse horizontal resolution; realistic ENSO episodes are simulated in a finer grid configuration (Jungclaus et al., 2006). The probability density function (PDF) of the monthly Nino-3.4 in CTR is very symmetric (Figure 3.1). Albeit Nino-3.4 is positively skewed (γ=0.17), the probability of extreme El Niños (Nino 3.4 > 2 K, 4.17%) is not significantly higher than the probability of extreme La Niñas (Nino 3.4 < -2 K, 4.44%). The latter implies that ENSO in our model is stochastically excited. In contrast, the skeweness of the Nino-3.4 index in ERSST is 0.26 and extreme El Niño events occur more frequently than extreme La Niña events.
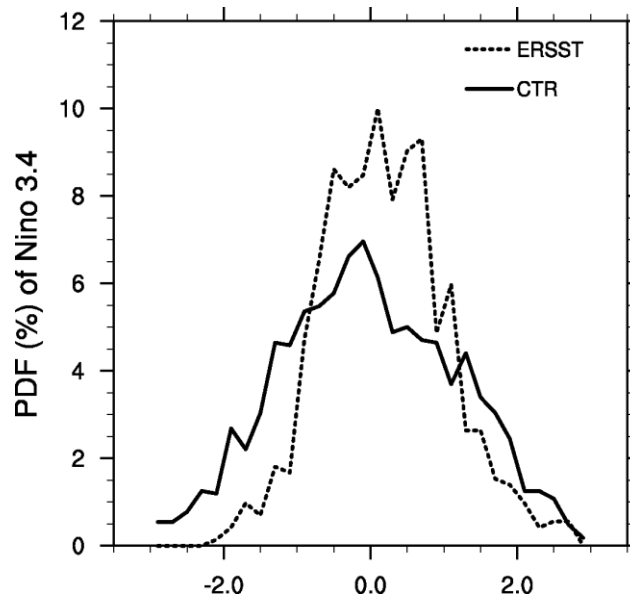
Figure 3.1: Probability density functions (PDFs) of the monthly Nino-3.4 index from the CTR (solid line) and ERSST v3b reconstruction (dashed line). The horizontal axis shows anomalies of the Nino-3.4 index (K).

The leading EOF of the tropical SST anomalies is characterized by the typical "horseshoe-like" signature of El Niño events (Figure 3.2a). As in many AOGCMs of this class (Guilyardi et al., 2009), the area of warm waters extends unrealistically far to the western Pacific. Moreover, the strongest SST anomalies are located in the central Pacific and not off the coast of Peru. The second leading EOF (Figure 3.2b) is characterized by a meridionally narrow warming confined to the eastern equatorial Pacific that resembles the declining phase of El Niño events (Rasmusson and Carpenter, 1982; Vimont, 2005).

The third leading EOF (CTR-EOF3) is of particular interest despite the fact that it explains only 5% of the inter-annual SST variability (Figure 3.2c). This mode displays cooling in the western (-0.3 K/std) and warming (0.3 K/std) in the eastern equatorial Pacific. Outside the tropical Pacific, in the tropical Indian and Atlantic oceans, the signal is negligible (not shown), implying that CTR-EOF3 is related to physical processes operating solely in the equatorial Pacific.

The skewness of the annual SST anomalies in the tropical Pacific, which measures the asymmetry of time series, shows spatial characteristics similar to CTR-EOF3 (Figure 3.3). Over the western sector negative anomalies tend to be stronger than positive SST anomalies; hence the negative skewness (γ=-1.8). The skewness is positive over the south-eastern Pacific (up to 0.4 at 100°W) because positive excel negative SST anomalies in this area. Compared to the observed skewness (Burgers and Stephenson, 1999), the region of negative skewness in MAECHAM5/MPIOM extends unrealistically to the west, whereas the magnitude of positive skewness is substantially smaller over the eastern Pacific. The former inconsistency results from the unrealistic extension of the simulated ENSO signature towards the western

Pacific. The latter inconsistency is explained by the fact that the simulated El Niño and La Niña events have comparable amplitude.
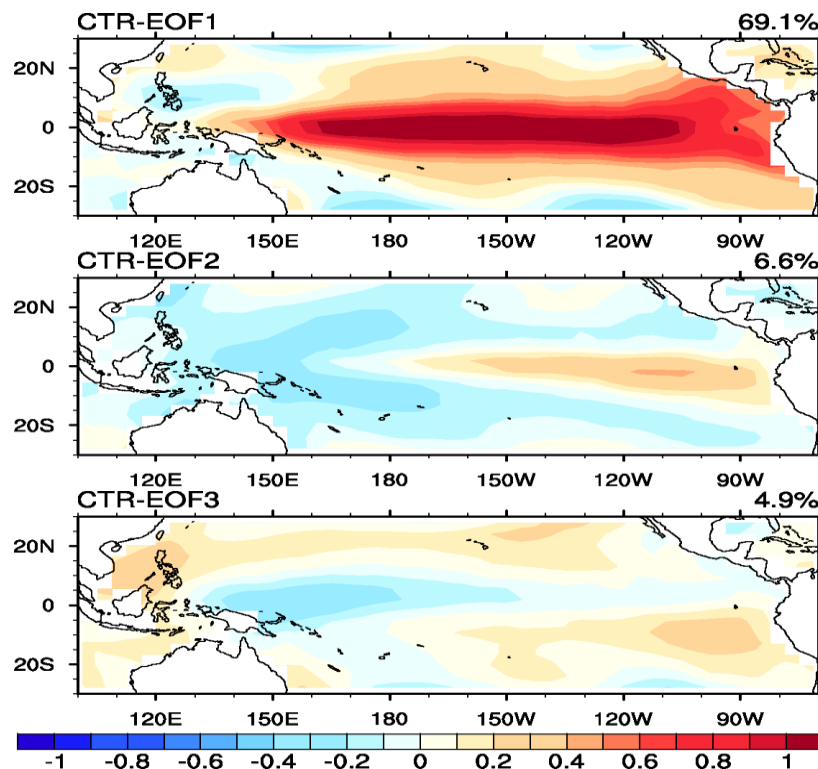
Figure 3.2: Leading three modes (CTR-EOF 1-3) of the annual SST anomalies in the tropical Pacific from CTR. EOF1 explains 69.1%, EOF2 explains 6.6%, and EOF3 explains 4.9% of the inter-annual variability. The spatial patterns are displayed as regression coefficients (K/std) of SST anomalies onto the corresponding PCs.
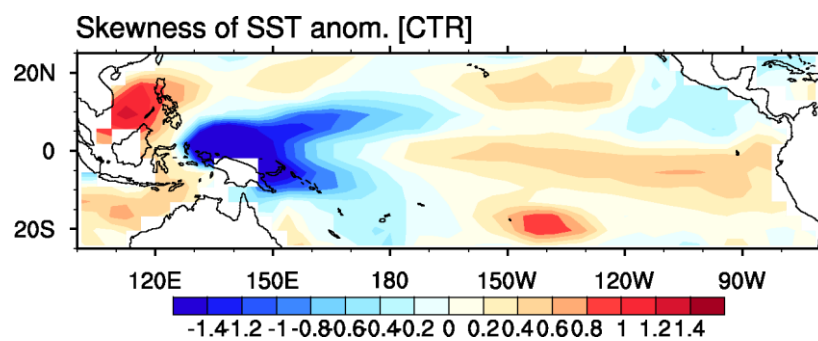
Figure 3.3: Skewness of annual SST anomalies over the tropical Pacific (30°S-30°N and 100°E-70°W) from CTR.

Albeit CTR-EOF3 seems trivial on inter-annual time scales, it becomes important on decadal time scales and appears as the second leading mode of the 8-yr low-passed SST anomalies (LP-CTR-EOF2, Figure 3.4b). LP-CTR-EOF2 explains 16% of the filtered variability and is well separated from the rest EOFs according to the North's rule of thumb (North et al., 1982). The spatial correlation between Figure 3.4a and 3.4b is high (r=0.87), and so is the correlation between the associated PCs (r=0.7, see

Figure 3.5). This suggests that both modes describe the same physical mechanism operating on annual and decadal time scales. Although not shown, we note that LP-CTR-PC2 exhibits a wide spectral peak at 14 to 17 years.

In observations and other model simulations, a cooling/warming dipole between the central and eastern equatorial Pacific on decadal time scales has been ascribed to EDAM (Timmermann, 2003; Cibot et al., 2005; Sun and Yu, 2009). In CTR, the regression coefficients of the annul SST anomalies onto the EDAM index exhibit a statistically significant dipole of positive (negative) anomalies in the eastern (western) Pacific. Positive and negative anomalies up to 0.3 K/std are simulated. This dipole is qualitatively and quantitatively similar to CTR-EOF3 and LP-CTR-EOF2. The spatial correlation coefficients are 0.82 and 0.97 respectively. Moreover, the EDAM index is highly correlated with LP-CTR-PC2 (r=0.77, see Figure 3.5). Naturally, EDAM is highly correlated with CTR-PC3 as well (r=0.53).
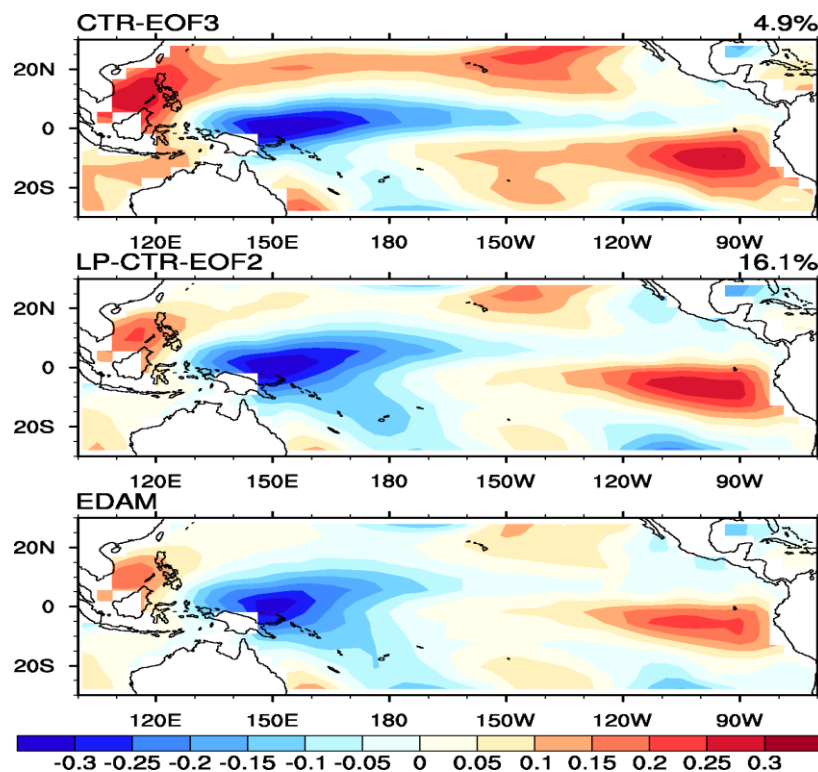
Figure 3.4: a) The third leading mode (CTR-EOF3) of the unfiltered annual SST anomalies. It is the same as Figure 3.2c but with different color scaling. b) The second leading mode (LP-CTR-EOF2) of the 8-yr low-pass Lanczos filtered SST anomalies. c) Regression coefficients of the unfiltered annual SST anomalies onto the EDAM index. CTR-EOF3 and LP-CTR-EOF2 are expressed as the regression coefficients of the corresponding PCs.

The simulated high correlation between EDAM and LP-CTR-EOF2 do not provide any possible cause-and-effect relationship because the latter could be the cause and not the result of the former. According to the examination of Meehl et al. (2001), a dipole of anomalous cold (warm) waters in the western (eastern) equatorial Pacific, as seen in Figure 3.4b, should weaken the ENSO amplitude because the zonal SST

gradient along the equatorial Pacific is reduced. On the basis that the cool/warm dipole in Figure 3.4c is associated with stronger, not weaker, ENSO amplitudes, we argue that LP-CTR-EOF2 is the result, not the cause, of EDAM. This conclusion is consistent with numerical simulations of Rodgers et al. (2004) and Cibot et al. (2005).
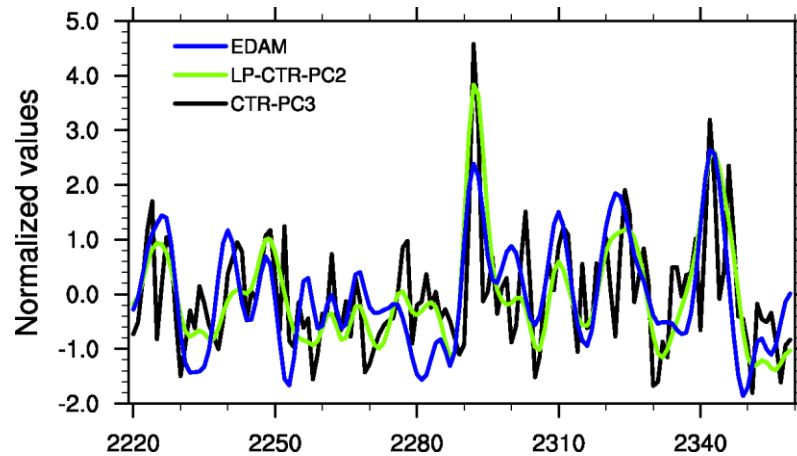
Figure 3.5: Time series of the normalized CTR-PC3 (black line), LP-CTR-PC2 (green line), and EDAM index (blue line). The spatial patterns associated with CTR-PC3, LP-CTR-PC2, and EDAM are depicted in Figure 3.4.

3.4 Synchronization of the EDAM to TPQDO in simulations with 11-yr solar forcing

We repeat the analysis of the previous section, but for the ensemble-mean annual SST anomalies from CENS. Figure 3.6 displays the third leading EOF of the unfiltered time series (CENS-EOF3) and the second leading EOF of the 8-yr low-pass filtered time series (LP-CENS-EOF2). The first two leading EOFs of the unfiltered SSTs describe ENSO-related variability and their spatial patterns are essentially the same as CTR-EOF1 and CTR-EOF2, respectively. This is expected since a considerable fraction of the ENSO survives even after 11 ensemble realizations (see Chapter 2.3.1). The leading EOF of filtered SSTs is characterized by an El Niño-like warming along the tropical Pacific and is associated to the TPQDO. This connection has been established in Chapter 2, albeit with a different methodology.

As in CTR, a dipole of cooling in the western and warming in the eastern equatorial Pacific is separated both in CENS-EOF3 and in LP-CENS-EOF2 (5% and 11.7% explained variability). The correlation coefficient between the associated PCs is high (r=0.92). Based on previous findings, the simulated SST dipole is expected to be physically related to EDAM. Indeed, the correlation coefficient between the ensemble mean EDAM index and the CENS-PC3 and LP-CENS-PC2 indices is 0.55 and 0.71, respectively (Figure 3.6a).
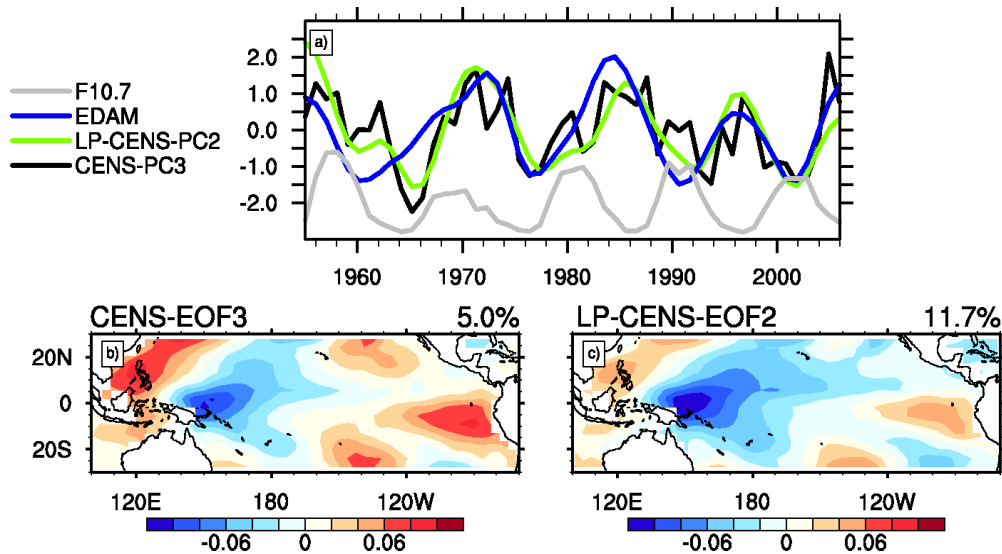
Figure 3.6: Time series (a) and the associated regression coefficients (K/std, b and c) of the third PC of unfiltered ensemble-mean annual SST anomalies, second PC of 8-yr filtered SST anomalies, and EDAM from CENS. The 11-yr solar cycle (F10.7) is superimposed for reference. All time series are normalized. CENS-EOF and LP-CENS-EOF explain 5% and 11.7% of the inter-annual SST variability, respectively.

The most interesting feature in Figure 3.6a is the out-of-phase relationship between the ensemble-mean EDAM index and the 11-yr solar cycle. It must be noted that similar phase relationship between EDAM and the solar cycle has been detected in observations from 1950 to 2009 (Figure 1.2). During the last three solar cycles (after 1980) the simulated ENSO becomes less energetic when the Sun is active, whereas this relationship seems to brake in the first two solar cycles. It is not surprising, therefore, that the simulated Pacific SST response to 11-yr solar forcing is zonally asymmetric from 1980 to 2006. Contrary to the almost uniform warming over the period 1955-2006 (see Figure 2.5), Figure 3.7 shows stronger temperature anomalies in the western (0.2 K/100 sfu) than in the eastern sector. Obviously, the amplified response results from the superposition of EDAM-related and TPQDO-related SST anomalies. The warming/cooling/warming pattern in the southern Pacific Ocean is another characteristic feature of the EDAM-related SST anomalies in our model (see Figure 3.4).

Why does the ensemble EDAM index seem to oscillate out-of-phase with the 11-yr solar cycle from 1980 onwards but not before? Certainly, this alignment could be a fluke of our simulations but in the following paragraphs, we argue that EDAM is phase locked with the TPQDO. TPQDO, however, synchronizes to the 11-yr solar cycle in CENS (Chapter 2) and for this reason EDAM seems linked to the 11-yr solar cycle.
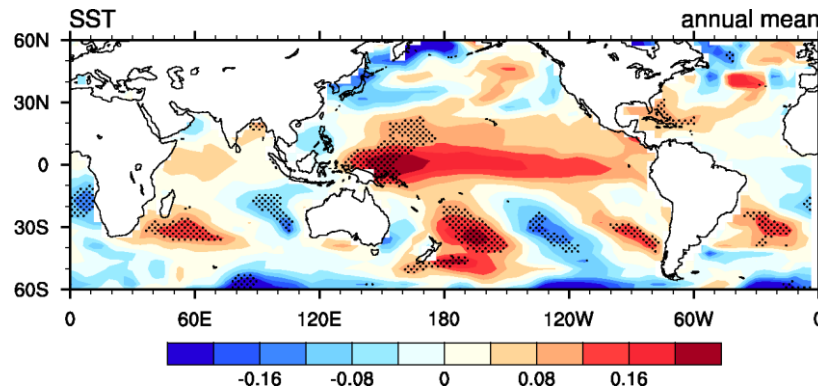
Figure 3.7: Regression coefficients against the annual F10.7 radio flux of the ensemble-mean annual SST anomalies (K/100 sfu) over the period 1980-2006. Stippled areas are statistically significant at the 95% level. Compare to Figure 2.5a.

Figure 3.8 compares the time evolution of the normalized TPQDO and EDAM indices. The TPQDO index has been calculated following the methodology discussed in Chapter 2.5.2. TPQDO oscillates in phase with the 11-yr solar cycle and the EDAM index lags the TPQDO index by 2 to 4 years. Starting from 1965, ENSO becomes more energetic during the declining phase of the TPQDO. Contrarily, weaker ENSO events are simulated during the rising phase of the TPQDO.
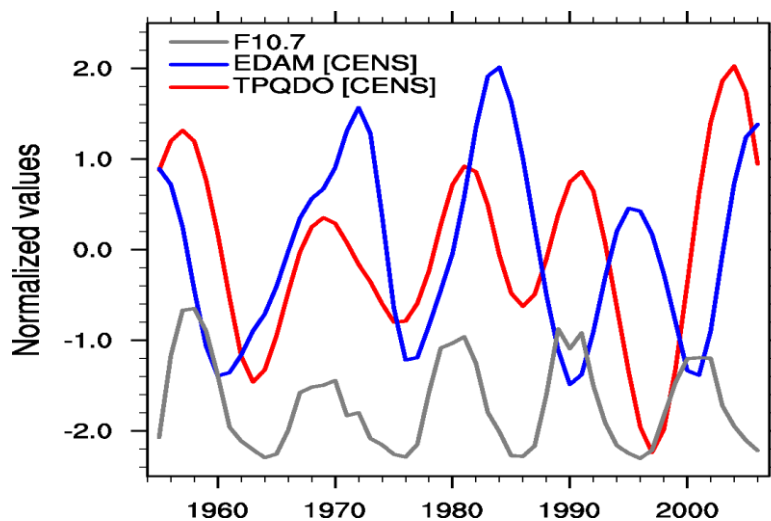
Figure 3.8: Time series of the ensemble-mean annual TPQDO (red line) and EDAM (blue line) indices over the period 1955-2006 from CENS. F10.7 is superimposed for reference (grey line). Both indices have been normalized to unit variance.

In Section 3.3, we argued that ENSO in MAECHAM5/MPIOM is triggered mainly by stochastic forcing. As such, a causal link between low-frequency changes of the Pacific and ENSO characteristics (e.g. amplitude) should not be anticipated. Note that here, the TPQDO is viewed as a low-frequency modulation of the Pacific background state given its much longer period compared to ENSO. On the other hand, the ENSO amplitude in CENS seems to be phase-locked to the TPQDO. The latter implies that

ENSO in these simulations is explained by self-sustained non-linear dynamics. To understand this apparent contradiction, we first inquire what phase relationship between the TPQDO and EDAM would be simulated, if ENSO results from self-sustained non-linear dynamics. A low-order model of the ENSO recharge/discharge theory is giving a physically plausible answer.

3.5 Phase-locking between EDAM and TPQDO in a low-order ENSO model

The low-order ENSO model (LO-ENSO) of Jin (1996) is a simple two-box non-linear model that calculates the surface temperature and thermocline depth anomalies in the western Pacific as well as the surface temperature anomalies in the eastern Pacific (T_e). The detailed formulation of LO-ENSO is given in Appendix 2. LO-ENSO takes into account the amplification mechanism of the zonal wind-SST interaction (Bjerknes, 1966) together with the out-of-phase, negative feedback of the heat recharge/discharge between equatorial and off-equatorial latitudes (Wyrtki, 1985).

As in the configuration used by Timmermann and Jin (2002), the wind stress variations related to the Walker circulation are set to zero. Furthermore, stochastic wind stress forcing is omitted in order to obtain a "pure" non-linear self-sustained oscillator. It is known that, depending on the configuration, LO-ENSO generates spells of strong El Niño events on decadal time scales, which can be explained in terms of homoclininc/heteroclinic chaos (Timmermann and Jin, 2002). The critical parameter that determines the transition from regular oscillatory behaviour to chaos is the strength (ε) of zonal advection of surface temperature anomalies, which is a free unitless parameter, ranging between 0.01-0.1 (Jin, 1998). In our experiments, ε is set to 0.0775. This value is dictated by the physical constraint that the thermocline in the eastern Pacific should not be lifted out of the sea surface. Under this configuration, a regular self-sustained ENSO oscillation with a period of 28 months and amplitude of 0.7 K is simulated (Figure 3.9a).

To initiate a decadal variability in LO-ENSO, we perturb the temperature equation of the eastern Pacific. For the sake of simplicity, we introduce a 11-yr sinusoidal warming with peak-to-peak amplitude of 0.12 K. This warming is consistent with the tropical Pacific SST solar response in CENS but results are independent of the specified amplitude. We run the model for 6800 months, but results for the last 400 months are presented for visualization reasons given that the signals in Figure 3.9 do not depend on the period analyzed.
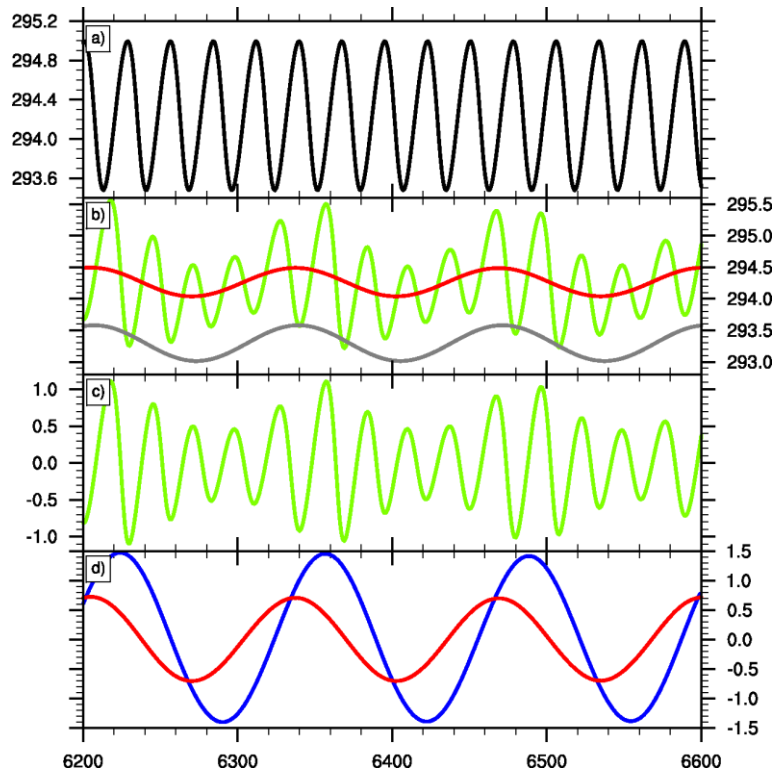
Figure 3.9: a) Time series of surface temperature (K) in the eastern Pacific (T_e) simulated with LO-ENSO without 11-yr forcing. b) Time series of T_e simulated with 11-yr solar forcing (green line) and 11-yr low-pass filtered (red line). The latter defines the TPQDO of LO-ENSO. The 11-yr forcing is superimposed for reference (grey line). c) Time series of T_e after the TPQDO is removed. d) Comparison of EDAM (blue line) and TPQDO (red line). Note that normalized values are used in the last panel. Time axis in months.

The time evolution of T_e shows interesting features when LO-ENSO is perturbed with 11-yr periodic heating (Figure 3.9b). Firstly, a low-frequency warming/cooling of 11-yr period (red line) that oscillates in phase with the imposed forcing (orange line) is simulated. The amplitude of this warming is around six times stronger than the imposed warming (0.27 K versus 0.06 K) suggesting for a non-linear amplification. This amplification is expected because the Bjerknes feedback shall always amplify any small perturbation. The low-frequency warming/cooling in the eastern Pacific is perceived as the TPQDO of the LO-ENSO model, although externally forced. The most striking feature in Figure 3.9b, however, is the amplitude modulation of ENSO. Note that ENSO time series is calculated after removing the TPQDO (Figure 3.9c). Overall, the maximum amplitude of ENSO episodes is not much stronger compared to the unperturbed run, but there are periods during which the ENSO amplitude is substantially suppressed. The simulated TPQDO and EDAM are phase locked; peaks of EDAM lag peaks of TPQDO by about 20 months (Figure 3.9d). Similar phase locking between EDAM and the TPQDO is simulated in a separate experiment in which both prognostic temperature equations are perturbed. Hence, the result is

robust. In this experiment, however, the TPQDO varies out-of-phase with the imposed periodic forcing.

The LO-ENSO setup in the previous experiment is highly idealized since the noise forcing is deliberately set to zero. Is the same phase relationship between the TPQDO and EDAM simulated in the presence of a Gaussian white noise? LO-ENSO gives a positive answer only for weak noise amplitudes compared to the prescribed periodic forcing. Figure 3.10a demonstrates that decadal modulations of the ENSO amplitude are stochastically excited, even in the absence of periodic forcing. This is consistent with the nature of EDAM in MAECHAM5/MPIOM. However, the inclusion of periodic warming (TPQDO) modulates the ENSO amplitude in such way that in most of the cases ENSO becomes more energetic in the declining phase of the TPQDO. The reverse is simulated during the rising phase of the TPQDO. Hence, the deterministic TPQDO-EDAM phase relationship in the absence of noise (Figure 3.9d) degenerates to a statistical relationship in the presence of stochastic forcing (Figure 3.10d). The stronger the noise the fewer the cases when ENSO becomes more energetic during the declining phase of the TPQDO.
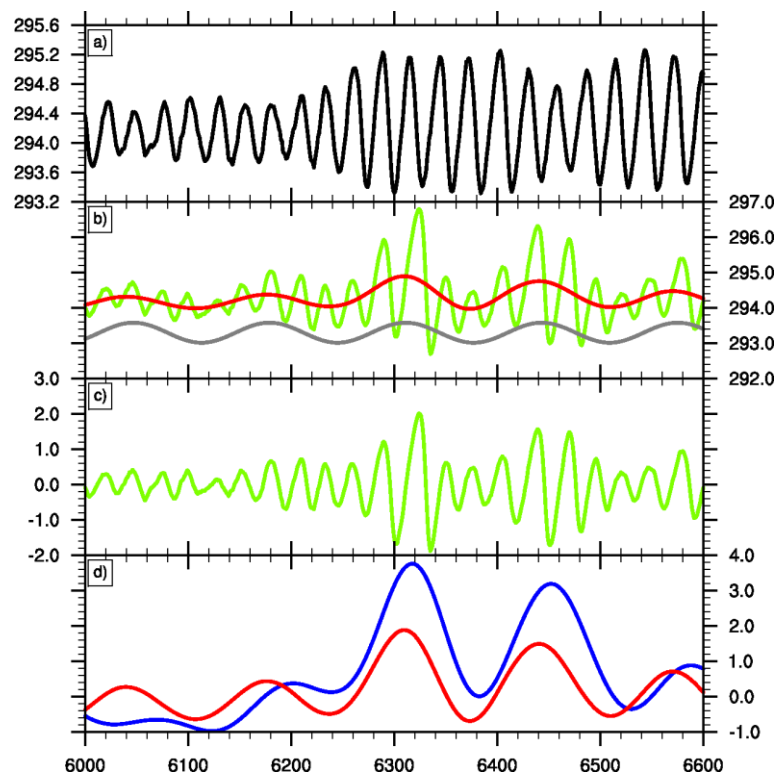
Figure 3.10: As in Figure 3.9 but from an experiment where a weak Gaussian white noise is added. Time axis in months. Note that this figure covers 200 more months.

Admittedly, LO-ENSO oversimplifies the nature of ENSO that is simulated with MAECHAM5/MPIOM. Moreover, TPQDO is externally forced in LO-ENSO, whereas it occurs naturally in MAECHAM5/MPIOM. Yet, the configuration of LO-ENSO with weak white noise is a valid approximation of TPQDO-EDAM relationship when ensemble simulations are analyzed. This is because atmospheric

noise in MAECHAM5/MPIOM is filtered out when ensemble-mean time series are considered. The higher number of ensemble simulations the lower the noise amplitude. Ensemble averaging should filter out the TPQDO as well if randomly excited. This is not the case, however, in the CENS because the TPQDO synchronizes, statistically, to the 11-yr solar forcing. Hence, the decadal evolution of the tropical Pacific system in CENS may be explained by non-linear dynamics in the presence of weak noise.

The stability analysis of Fedorov and Philander (2001) may provide a plausible framework to interpret the TPQDO-EDAM phase locking in LO-ENSO. They suggested that slow variation of the background state can change ENSO characteristics. These changes are sensitive to zonal winds and thermocline variations. In LO-ENSO, weaker zonal winds are leading the positive phase of the TPQDO, whereas deeper thermocline is lagging (~30 months) the positive phase of the TPQDO. According to Fedorov and Philander (2001), these changes should increase the growth rate of ENSO, causing stronger ENSO episodes. Hence, the positive phase of EDAM should peak in the declining phase of the TPQDO.

3.6 Discussion

The response of the tropical Pacific Ocean to the 11-yr solar cycle forcing has been severely debated in the recent years (Gray et al., 2010). Many studies documented either anomalous cooling (van Loon et al., 2007; Meehl et al., 2008; Tung and Zhou, 2010; Zhou and Tung, 2010) or warming (White et al., 1997; Roy and Haigh, 2010) in the eastern Pacific in solar maxima. In Chapter 1.3, we argued that the observed putative solar signals are likely associated to different oscillations of the tropical Pacific (Chapter 1.3). The previously reported warming during solar maxima should be ascribed to the TPQDO, whereas the cooling in the eastern Pacific during solar maxima is likely explained by oversampling of La Niña events. In other studies, the cooling in the eastern Pacific is explained by confusing EDAM-related with solar cycle-related SST responses. Hence, it is appropriate to address the possibility of a physically meaningful linkage between these oscillations and the 11-yr solar cycle.

TPQDO and EDAM are two modes of the tropical Pacific climate excited naturally in MAECHAM5/MPIOM and in many other AOGCMs as well (Knutson and Manabe, 1998; Rodgers et al., 2004; Cibot et al., 2005). Yet, the TPQDO in our simulations seems statistically synchronized to the 11-yr solar cycle. We propose that this synchronization may alter the amplitude of ENSO episodes. Positive EDAM phases lag positive TPQDO phases by 2 to 4-years.

Recently, Bal et al. (2011) simulated the response of the tropical Pacific to 11-yr periodic forcing with another AOGCM. They claimed that their simulations provide an additional confirmation of the mechanism suggested by Meehl et al. (2008), which associates a La Niña-like cooling with peaks of solar activity. A closer look on their

results, however, seems to confirm our suggestion on the possibility that the 11-yr solar cycle could, indirectly, modulate the ENSO amplitude. This is because Bal et al. (2011) reported stronger ENSO episodes, following peaks of the 11-yr solar activity by 1 to 2 years. It must be verified whether in their simulations peaks of solar activity coincide with peaks of the TPQDO, as it happens in our simulations. Interestingly, the ENSO amplitude was similarly modulated in every integration of their model. In contrast, MAECHAM5/MPIOM exhibits a statistical modulation. This non-trivial difference could be explained by the fact that Bal et al. (2011) used an unrealistically strong solar cycle forcing.

The obvious weakness of our simulations is the low magnitude of the response, which limits the statistical significance of our results. The simulated solar signals in the tropical Pacific are on the order of 0.15 K from solar minimum to solar maximum. As such solar signals can easily be confused with the background variability. This does not mean that stronger solar signals are expected, but it suggests that longer simulations covering 10 solar cycles at least are required before definitive conclusions can be made. Until the confirmation from other modeling studies the findings of this chapter should be considered speculative and certainly inconclusive. If the mechanism that we propose here operates also in reality, the knowledge of the solar activity may improve our skills on predicting periods of stronger or weaker ENSO episodes.

3.7 Conclusions

We have analyzed experiments performed with MAECHAM5/MPIOM in two configurations: with and without 11-yr solar cycle forcing. The main results are:

- In the solar-cycle-forced simulations, the Tropical Pacific Quasi-Decadal Oscillation (TPQDO) synchronizes, statistically, to the 11-yr solar cycle. TPQDO, in turn, modulates the amplitude of ENSO episodes. As a result, positive phases of the ENSO Decadal Amplitude Modulation (EDAM) follow positive TPQDO phases after 2 to 4 years and vice versa. In our simulations, the TPQDO-EDAM phase locking has a statistical character.

- According to a low-order ENSO model, this phase locking can be physically understood by decadal changes of the zonal wind stress and thermocline depth. In LO-ENSO, weaker zonal winds are leading the positive phase of the TPQDO, whereas deeper thermocline is lagging the positive phase of the TPQDO. These changes should increase the growth rate of ENSO, causing stronger ENSO episodes during the declining phase of the TPQDO.

Chapter 4

Stratospheric responses to the 11-yr solar cycle variability in MAECHAM5 with and without ocean coupling

4.1 Introduction

Stronger ultraviolet (UV) irradiance during the positive phase of the 11-yr solar cycle produces higher ozone abundances in the upper stratosphere due to the enhanced photolytic destruction of molecular oxygen. Higher UV and ozone levels should warm this region. Indeed, analyses of satellite observations indicated positive ozone and temperature changes on the order of 2.5 % and 1 K, respectively (Soukharev and Hood, 2006; Randel and Wu, 2007; Tourpali et al., 2007; Randel et al., 2009; Hood et al., 2010). Reanalysis datasets gave further evidence for positive temperature anomalies in the upper stratosphere, but the magnitude and location of the solar responses differ among different datasets (Chapter 1.4). General Circulation Models (GCMs) with chemistry schemes to account for ozone photochemistry, simulated consistent solar responses in the tropical (25°S-25°N) upper stratosphere (Matthes et al., 2004; Austin et al., 2008; Rind et al., 2008; Schmidt et al., 2010; Yamashita et al., 2010). Overall, there is a consensus about the radiative origin of the observed ozone and temperature increases in the tropical upper stratosphere (Gray et al., 2010). Yet, GCMs still face difficulties in reproducing the observed solar signals in high latitudes (e.g. Tsutsui et al., 2009). Given that the majority of the previous numerical studies employed atmosphere-only GCMs, it was proposed that the atmospheric response to the 11-yr solar cycle might depend on ocean coupling. The first objective of this chapter is to test this proposition.

Together with the temperature and ozone response maxima in the tropical upper stratosphere, many studies indicated significant second response maxima in the tropical lower stratosphere (TLS). Increased ozone up to 4% and positive temperature anomalies up to 1 K have been reported over the period 1979-2003 from the SBUV

(Solar Backscattered Ultraviolet) instrument (Hood, 2004; Soukharev and Hood, 2006). Additionally, the study of Crooks and Gray (2005) and its update that covers the period 1979-2008 (Frame and Gray, 2010), identified a meridionally broad structure of positive temperature anomalies (up to 0.7 K) at 40 hPa, which takes the form of two separate lobes located at 25 degrees latitude in each hemisphere (Chapter 1.4). The cause of this warming remains unsolved, although a number of possible explanations have been put forward. Investigating the origin of the second response maximum in the TLS is the second objective of this chapter.

Kodera and Kuroda (2002) interpreted the observed second response maximum in the TLS as a traceable sign of a slower Brewer-Dobson circulation during solar maxima. The proposed mechanism involves the interaction of zonal winds with planetary-scale atmospheric waves in the extra-tropical upper stratosphere and predicts positive temperature anomalies in the TLS owing to the reduction of adiabatic cooling. Separated by about a decade, the signals of El Chichón (1982) and Pinatubo (1991) could be misinterpreted as solar signals (Lee and Smith, 2003). However, the observed warming in the TLS remains robust even when longer times series are analyzed, although its magnitude weakens (Chapter 1.3). A different explanation invokes a non-linear interaction between the stratospheric Quasi Biennial Oscillation (QBO) and the 11-yr solar cycle (Salby and Callaghan, 2006b; Matthes et al., 2010).

Numerical simulations with GCMs have given evidence for slower Brewer-Dobson circulation during solar maxima (Haigh, 1996; Schmidt et al., 2010; Yamashita et al., 2010), supporting the mechanism suggested by Kodera and Kuroda (2002). Yet, the majority of past simulations failed to reproduce the observed solar responses in the TLS (Tourpali et al., 2003; Rozanov et al., 2005; Shindell et al., 2006; Rind et al., 2008). Recent simulations forced with time-varying solar spectral irradiance, observed SSTs, volcanic aerosols, and greenhouse gas concentrations reported improved agreement (Garcia et al., 2007; Austin et al., 2008). It is alarming, however, that solar responses in the TLS have been detected even in simulations forced with the observed SSTs only (Austin et al., 2008). This implies that either the observed SSTs include a solar component that is projected, indirectly, in the TLS (van Loon et al., 2007; Meehl et al., 2008) or the analysis methodology (multiple linear regression) introduces spurious signals.

It has been suggested that the tropical Pacific should shift to a La Niña conditions with increased solar activity (Meehl et al., 2008; van Loon and Meehl, 2008). La Niña episodes, which describe the negative extreme of the El Niño-Southern Oscillation (ENSO), warm the TLS. Hence, if the Pacific response to the solar cycle forcing is La Niña-like, the solar signals in the SST-only simulations of Austin et al. (2008) could be explained. In contrast, other studies detected positive temperature anomalies during solar maxima (White et al., 1997; Roy and Haigh, 2010). If the Pacific response to the solar cycle is El Niño-like, negative temperature anomalies should be detected in the

TLS. Our simulations suggest for a weak El Niño-like response in solar maxima (Chapter 2).

The majority of the aforementioned studies employed multiple linear regression models to isolate solar signals in observations. These models assume that all predictor variables are linearly independent; a requirement that is not always valid. Marsh and Garcia (2007), for instance, mentioned that the correlation coefficient between indices commonly used to describe the solar cycle and ENSO variations is significantly different from zero over the period 1979-2003 (r=-0.15). They suggested that some of the observed decadal variability in the TLS previously attributed to 11-yr solar variability might instead be related to the occurrence of ENSO events.

To recap, the origin of the second response maximum in the TLS is still under debate. Either it could be a genuine response to the solar cycle activity or it could be an analysis artifact. Moreover, surface responses to the 11-yr solar cycle variability may feed back to atmospheric responses. To inquire these issues, we conduct ensemble simulations with an AOGCM forced only with a realistic ozone and solar spectral irradiance over the period 1955-2006. Radiative forcing from a) the increasing greenhouse gas concentrations and b) the aerosol loading from volcanic eruptions are deliberately excluded to ease interpretation.

This study is separated into six sections including Introduction. In Section 4.2, a description of the model, experimental setup and analysis methodology is given. After a brief evaluation of the natural atmospheric variability in our model, we present annual temperature responses to the solar cycle forcing and we assess the ability of the multiple linear regression to disentangle solar from ENSO signals (Section 4.3). We analyze solar signals in boreal winter in Section 4.5. Results are discussed in Section 4.6 and the key findings of this study are summarized in Section 4.7.

4.2 Description of the model, experiments and analysis methods

4.2.1 *Model description*

All simulations are carried out with the middle atmosphere extension of the fifth generation of ECHAM (MAECHAM5). For thorough description about the numerics and physics of ECHAM5 see Roeckner et al. (2003; 2006). Manzini et al. (2006) provide details about the middle atmosphere version. Here, we make use of a version that is coupled to Max Planck Institute Ocean Model (MPIOM, Marsland et al., 2003). The OASIS coupler (Valcke et al., 2003) without any flux correction, is responsible for momentum, heat, and fresh water flux exchanges from the atmosphere to the ocean, whereas in the reverse direction, sea surface temperature, sea ice concentration, sea ice thickness, snow depth, and ocean surface velocities feed the atmosphere.

In most of the runs, MAECHAM5 has T31L90 resolution, denoting spectral truncation at wavenumber 31 (equivalent to 3.8°x3.8° grid) and 90 vertical levels (up to 0.01 hPa). In this configuration, MPIOM has 40 vertical levels and its curvilinear grid has horizontal resolution of 3 degrees near the Equator (GR30L40), which increases towards the model's poles placed over Greenland and Antarctica. In some runs, a finer horizontal grid, both for the atmosphere and the ocean component, has been chosen in order to evaluate the dependence of the simulated solar signal on the horizontal resolution. The resolution of MAECHAM5 in these experiments is T63L95 (equivalent to 1.9°x1.9° and 95 vertical layers), while the horizontal resolution of MPIOM reduces to 1.5 degrees at the Equator (GR15L40). Although the fine vertical resolution allows for a spontaneous QBO generation in both model configurations (Giorgetta et al., 2006), a latitudinal variation of the non-orographic gravity wave drag parameterization is applied to synchronize the average QBO period at 28 months. All simulations are conducted with present-day greenhouse gas concentrations.

Several modifications of the MAECHAM's radiation code are introduced in order to simulate a realistic and transient 11-yr solar cycle. More specifically, we implement daily spectral solar irradiances averaged over the model's shortwave, visible, and near infrared bands. The shortwave radiation parameterization accommodates 6 spectral bands, resulting in improved representation of ozone absorption compared to the older version (Cagnazzo et al., 2007). The solar input is taken from the Naval Research Laboratory model (Lean et al., 2005) and conforms with the recommendation of CCMVal (Chemistry and Climate Validation activity, CCMVAL, 2010). Because MAECHAM5 lacks of an interactive chemistry scheme, the effects of the solar cycle variability on ozone need to be parameterized. For this reason we add to the background ozone climatology the annual cycle of the solar-induced ozone anomalies taken from HAMMONIA simulations (Schmidt et al., 2010). Note that the ozone solar anomalies are scaled with the daily 10.7 cm solar radio flux (F10.7) to introduce 11-yr variation.

Figure 4.1a displays the percentage change of the specified annual ozone response to solar cycle (contours). Explained in full details by Schmidt et al. (2010), the ozone profile at tropical latitudes is characterized by two distinct response maxima at 5 hPa and 70 hPa, respectively. A comparable double-peaked tropical ozone response has been documented in analyses of satellite observations (e.g. Soukharev and Hood, 2006), but with different position, magnitude and latitudinal structure. Because of the uncertainty of the observed ozone solar estimates, which additionally suffer from limited meridional and vertical coverage, we decided to specify simulated ozone anomalies.
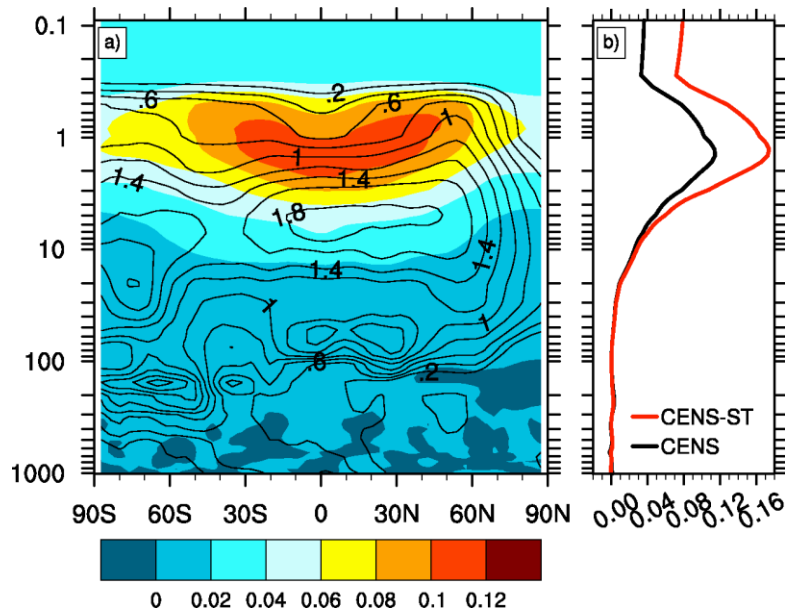
Figure 4.1: a) Changes of annual ozone (%/100 sfu, contours) and shortwave heating rates (K/day/100 sfu, shading) in the default configuration. b) Tropical (25°S-25°N) averages of the shortwave heating rates (K/day/100 sfu) in the default configuration (black line) and when the first spectral band of the MAECHAM5's radiation scheme (180-240 nm) is amplified by 2.5 times (red line). See Section 4.2.1 for details.

An increase of 100 solar flux units (sfu) of the F10.7 index heats the upper stratosphere by 0.12 K/day in the upper tropical stratosphere (Figure 4.1a). A separate analysis shows that approximately 60% of this value results from spectral irradiance changes while the remaining 40% results from ozone changes. These percentages are in accordance with idealized sensitivity experiments conducted with the radiation code of our model (CCMVAL, 2010). Owing to the coarse spectral resolution of the radiation scheme of MAECHAM5 (two bands between 185-440 nm), the simulated heating rates in the upper stratosphere are almost 45% weaker compared to those calculated with HAMMONIA (Schmidt et al., 2006). Similarly, the majority of the models that participated in the CCMval activity demonstrated increased heating rates at 1 hPa on the order of 0.14-0.17 K/day/100 sfu (CCMVAL, 2010). To overcome this shortcoming, we amplify the solar cycle variability only in the first spectral band of the radiation code of MAECHAM5 (185-250 nm) because this band is entirely absorbed in the stratosphere. The amplification factor is 2.5. With the amplified UV forcing, the shortwave heating rates reach values up to 0.18 K/day/100 sfu at 1 hPa (Figure 4.1b, red line), whereas the relative increase drops to 8% below 10 hPa. The first spectral band accommodates a tiny fraction of the Total Solar Irradiance (TSI) and hence the applied amplification causes negligible changes in the TSI variation.

4.2.2 *Experiments*

We carry out an ensemble of 9 runs with realistic and time varying solar forcing over the period 1952-2006. To remove any spin-up effect, however, data from 1955 to

2006 are only analyzed. Every member of this ensemble (CENS), which runs in T31L90-GR30L40 resolution, branches from different initial conditions taken from a 106-yr control simulation (CTR) with constant solar forcing. To assess the contribution of the oceans on the stratospheric solar signals, we conduct an ensemble of 9 runs without ocean coupling (AENS). AENS is forced at the lower boundary with monthly climatology of SSTs and Sea Ice Concentration (SIC) from CTR. Again, the full-simulated period spans from 1952 to 2006 but data from 1958 onwards are only considered. A superset of these coupled runs (11 members instead of 9 analyzed here) has been used in Chapter 2 and 3.

A twin ensemble to CENS but with the amplified UV forcing as described in Section 4.2.1 is additionally carried out (CENS-ST). CENS-ST simulations start from the same initial conditions as in CENS. The last set of coupled simulations (CENS-T63) is conducted with the same enhanced UV forcing as in CENS-ST but in finer horizontal resolution (T63L95-GR15L40). Every individual member of this ensemble branches from a control simulation (CTR-T63) and runs for 55 years (1952-2006) but data over the last 52 years are only used. The increased horizontal resolution is expected to improve the simulated stratospheric mean state and variability, particularly in the Northern Hemisphere (NH) high latitudes (see Section 4.3).

Table 4-1 Numerical Simulations

Experiment	Resolution	Forcing	Simulated years
CTR	T31L90-GR30L40	No solar cycle	106
CTR-T63	T63L95-GR15L40	No solar cycle	106
CENS	T31L90-GR30L40	Transient (1955-2006)	9*52
AENS	T31L90	Transient (1958-2006), SST and SIC from CTR	9*49
CENS-ST	T31L90-GR30L40	Transient (1955-2006), stronger SW forcing	9*52
CENS-T63	T63L95-GR15L40	Transient (1955-2006), stronger SW forcing	15*52

Table 4-1 lists all simulations conducted for this study. Hereafter, every ensemble group is called "experiment" and CENS is the reference experiment to which AENS and CENS-ST should be compared. CENS-T63 should be compared to CENS-ST since the magnitude of the 11-yr solar forcing is the same. Overall, we simulated 2369 model years and 201 solar cycles. Our approach differs from past modeling studies considering the atmospheric response to the 11-yr solar cycle in two important respects: a) the model setup is much simpler because it neglects the radiative effects

of variable greenhouse gas and aerosol concentrations and b) ensembles with such a large number of members are realized for the first time.

4.2.3 *The multiple linear regression model*

We analyze zonal averages of various meteorological variables after the respective seasonal cycle is removed. Ensemble-mean monthly and yearly anomalies are derived by averaging over all individual ensemble runs. In this way, four different ensemble-mean time series are available (CENS, AENS, CENS-ST, and CENS-T63).

Solar signals in every ensemble member are extracted with a multiple linear regression model that includes a first order autoregressive term as suggested by Crooks and Gray (2005). This model (MRA-AR1) reads:

$$Y(t) - \varphi \cdot Y(t-1) = \mu + \sum_{i=1}^{4} b_i \cdot (x_i(t) - \varphi \cdot x_i(t)) + \varepsilon(t)$$

where Y is the deseasonalized monthly time series in every latitude and pressure level, b_i the regression coefficient of each predictor x_i, φ the auto-regressive term, μ the constant term, and $\varepsilon(t)$ a white noise residual. Because the seasonal cycle has been subtracted, μ is set to zero. In such a formulation, the AR1 process is fitted to the errors of the regression of Y on x_i. MRA-AR1 considers 4 predictors: the F10.7 that describes the 11-yr solar cycle, the Nino-3.4 index (SST anomalies over 5°S-5°N and 170°W-120°W) that describes ENSO, and two orthogonal indices to account for the QBO. These two indices, which sufficiently capture the descending nature of QBO, are the first and the second principal component of the zonal-mean zonal winds anomalies in the equatorial stratosphere (15°S-15°N, 70-2 hPa), after the linear contribution of the solar cycle variability has been removed. Naturally, no ENSO term is used in AENS. All predictors are normalized to unit standard deviation except of F10.7, which is scaled to 100 solar flux units (sfu) to facilitate comparison with previous studies. Solar responses should be multiplied by 1.3 to get the magnitude of a "typical" solar cycle. A t-test statistic determines the statistical significance at 95%.

4.3 Stratospheric mean state and variability in MAECHAM5/MPIOM

Before analyzing the solar-cycle-forced experiments, we briefly evaluate the stratospheric mean state and variability in MAECHAM5/MPIOM. The study of Giorgetta et al. (2006) demonstrated that the main observed stratospheric features are adequately simulated in a version of MAECHAM5 without ocean coupling. Oceanic coupling introduces, overall, small changes when compared to the atmosphere-alone version and to ERA-40 reanalysis (Uppala and Coauthors, 2004). Both model configurations, T31L90-GR30L40 and T63L95-GR15L40, generate a well-positioned polar night jet in January with core speeds nearly identical to those in ERA-40 (bias

about 2-3 m/s, not shown). In July, however, the core of the Southern Hemisphere westerly jet is positioned poleward in the low-resolution model. This bias is alleviated when higher horizontal resolution is used; yet, the maximum jet speed is 18 m/s weaker compared to ERA-40 (not shown).
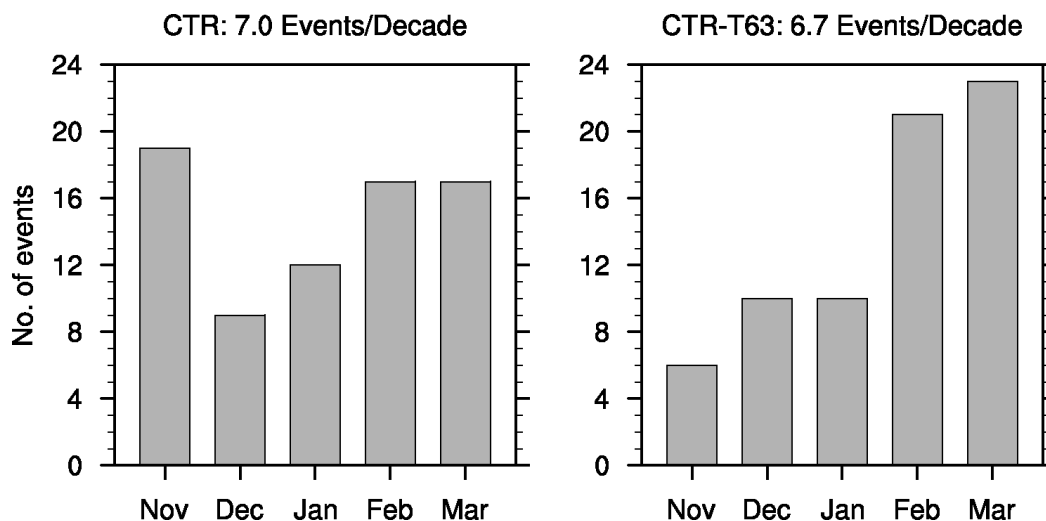

Figure 4.2: Number of sudden stratospheric warmings occurring in CTR (left) and CTR-T63 (right).

One striking difference between the two model configurations pertains to the distribution of the Sudden Stratospheric Warmings (SSWs) during the course of the boreal winter (Figure 4.2). Although the average SSW occurrence rate in the two control experiments remains the same (~0.7 yr^{-1}), most SSWs in CTR occur in November, whereas the peak occurrence rate shifts towards the late winter in CTR-T63 (February and March). As such, the distribution of SSWs in CTR-T63 is much closer to the observed (Charlton and Polvani, 2007), which implies that the overall extra-tropical stratospheric variability during winter is improved with increased horizontal resolution.

A considerable fraction of the extra-tropical stratospheric variability is linked to processes of the tropical stratosphere such as the QBO (e.g. Holton and Tan, 1980) and ENSO (e.g. Manzini et al., 2006). The standard deviation of the tropical-mean monthly temperature anomalies is shown in Figure 4.3a. The first region of high variability between 1 and 10 hPa is associated with the QBO. The origin of the second narrow peak at 70 hPa is more complicated. Certainly, a considerable fraction of the inter-annual variability at these altitudes is related to ENSO. AOGCMs with stronger ENSO intensity, defined as the standard deviation of the monthly Nino-3.4 index, should exhibit higher temperature variability in the TLS. The amplitude of ENSO in CTR is much higher than in CTR-T63 (1.27 K vs 0.95 K). For this reason, the inter-annual temperature variability at 70 hPa is higher in CTR. The influence of ENSO diminishes above 40 hPa. Yet, ENSO by no means is the only process affecting the TLS. This is best elucidated by analyzing a 70-yr control atmosphere-only simulation

(ACTR) with the same configuration as in CTR but with the climatological SST and SIC used in AENS (this run is not listed in Table 4-1). The temperature standard deviation drops as much as 70% in the troposphere but by merely 40% at 70 hPa, where a second peak is still present. This peak reflects the inter-annual variability of seasonal phenomena (e.g. upwelling), which are linked to extra-tropical processes as well as to the QDO.
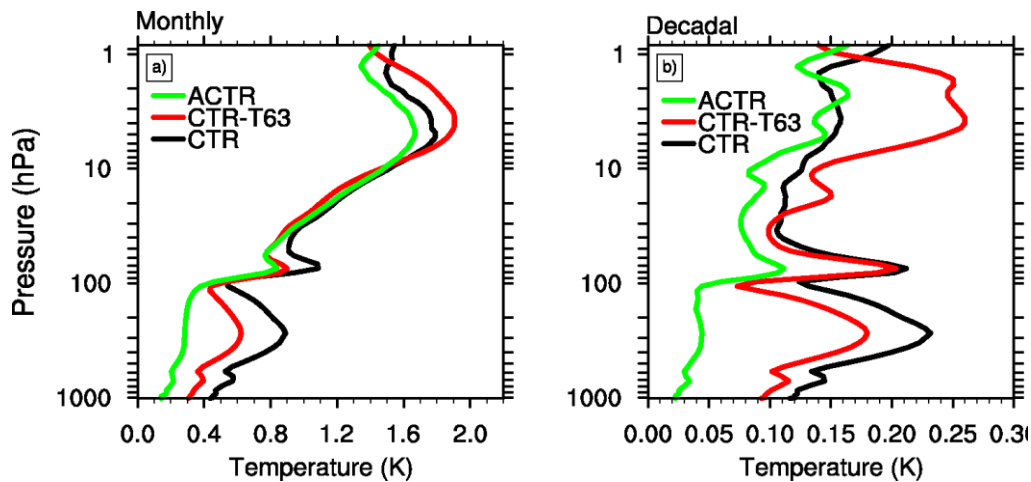
Figure 4.3: Standard deviations of a) monthly and b) decadal tropical-mean (25°S-25°N) temperature anomalies in CTR (black line), CTR-T63 (red line) and an uncoupled 70-yr long experiment (ACTR, green line).

On decadal time scales, the standard deviation of temperature anomalies at 70 hPa gets values up to 0.22 K in both CTR and CTR-T63, whereas it reduces to the half in ACTR (Figure 4.3b). Decadal profiles are calculated after a low-pass Lanczos filter with 10-yr cut-off is applied. Natural temperature variations on the order of 0.22 K in the coupled simulations could be erroneously interpreted as solar signals in short simulations even without an explicit 11-yr solar cycle forcing. Nevertheless, we will show in Section 4.4.2 that the ensemble averaging minimizes this error. A detailed investigation about the sources exciting decadal variability in the TLS is beyond the scope of this study, but in the coupled simulations they could be related to decadal fluctuations of ENSO.

4.4 Annual temperature responses to the 11-yr solar cycle forcing

4.4.1 *Ensemble-mean global responses*

The time evolution of the ensemble-mean global-mean annual temperature anomalies from the surface up to 0.1 hPa is displayed in Figure 4.4. Solar cycle-related variations throughout the stratosphere and lower mesosphere are detected in all experiments. As expected from the vertical profile of the specified ozone changes

(Figure 4.1a), temperature anomalies peak at 1 hPa in all cases. The amplified UV solar forcing in CENS-ST results in stronger signals compared to CENS. For instance, the simulated warming at 1 hPa is 0.2 K stronger in CENS-ST during the maximum phase of solar cycle 19 (1955-1957). The magnitude of the temperature anomalies is comparable between CENS-ST and CENS-T63.
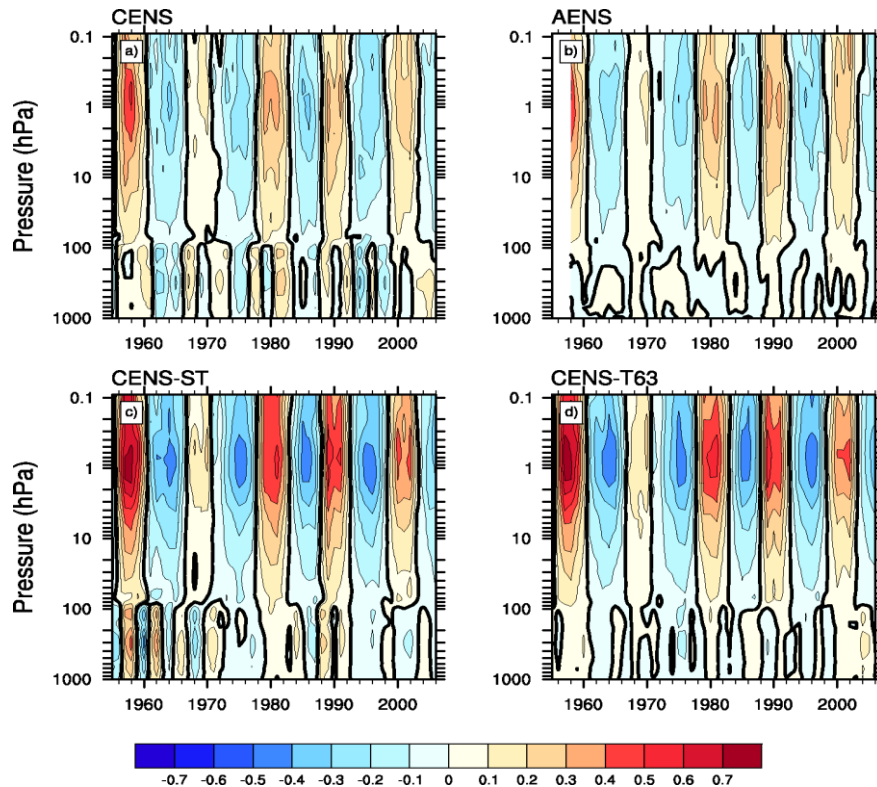
Figure 4.4: Pressure-time sections of the ensemble-mean global-mean annual temperature anomalies (K) in a) CENS, b) AENS, c) CENS-ST, and d) CENS-T63 over the period 1955-2006.

ENSO overprints on the solar signals in tropospheric heights in CENS and CENS-ST. This is expected because we already demonstrated in Chapter 2 that averaging over 11 ensemble runs is not sufficient to filter out the ENSO signal, because ENSO in this model configuration is unrealistically strong. Hence, the time evolution of the tropospheric temperature anomalies in CENS and CENS-ST mirrors El Niño and La Niña events. Nevertheless, there is a tendency for warm (cool) troposphere in phase with warm (cool) stratosphere in CENS-T63. This is understood by recalling that a) the simulated ENSO amplitude weakens with increased horizontal resolution, and b) CENS-T63 includes six more ensemble members. In AENS, the constant surface boundary forcing should mute the solar signals in the troposphere particularly in the lower troposphere. Yet, global-mean temperature anomalies of comparable magnitude with CENS-T63 that penetrate down to 200 hPa at least are also detected.

Figure 4.5, which displays the ensemble-mean solar regression coefficients calculated with MRA-AR1, reveals negligible dependence of the stratospheric solar signals on ocean coupling. Temperature changes up to 0.5 K/100 sfu at 1 hPa are simulated in

both CENS and AENS. The magnitude of these changes is considerably lower than the temperature responses estimated from observations (Randel et al., 2009; Frame and Gray, 2010), although the exact magnitude of the observed changes is not well constrained (Chapter 1.4). This is expected because the simulated solar heating rate anomalies are weak in the default configuration (Section 4.2.1). A warming/cooling vertical dipole at 80°N is simulated in these experiments. Obviously, this reflects changes during the winter season.
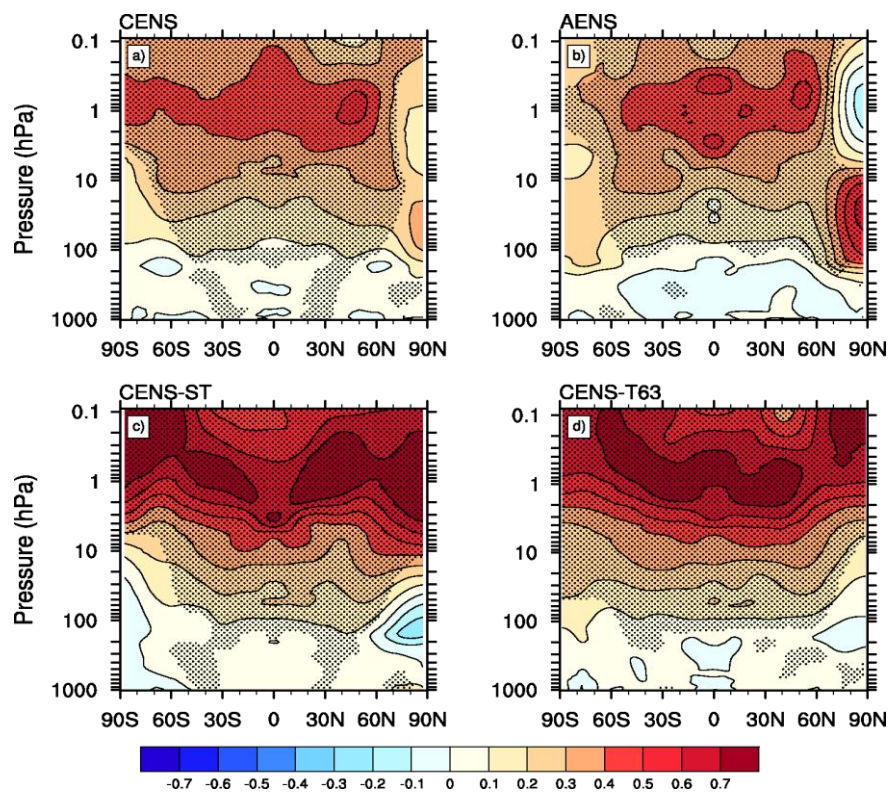
Figure 4.5: Ensemble-mean solar regression coefficients (K/100 sfu) of the annual temperature anomalies in a) CENS, b) AENS, c) CENS-ST, and d) CENS-T63. Shading denotes 95% significance.

The amplified solar UV forcing in CENS-ST and CENS-T63 warms the equatorial upper stratosphere by 0.8 K/100 sfu at 1 hPa, which is translated to 1 K warming for minimum to maximum phase of a typical solar cycle. The reported upper stratospheric warming in previous modeling attempts ranges from 0.7 K to 1.3 K depending on the magnitude of the ozone changes (Tourpali et al., 2003; Austin et al., 2008; Rind et al., 2008; Schmidt et al., 2010). In contrast to CENS and AENS, the response of the lower stratosphere in the NH high-latitudes is characterized by negative temperature anomalies both in CENS-ST and CENS-T63 but the significance is low.

At tropospheric heights, weak and generally insignificant temperature anomalies are simulated (less than ±0.1 K/100 sfu). In the experiments with ocean coupling (CENS, CENS-ST, and CENS-T63) two significant vertical columns of positive temperature anomalies appear at mid-latitudes. The temperature anomalies in CENS-T63 do not

pass the 95% significance level but pass the 90% level (not shown). In contrast, the significance is low in AENS. Interestingly, the multiple linear regression analysis of Haigh (2003) identified similar vertical columns of significant positive temperature anomalies at the same latitudes but with considerably higher magnitudes (~0.5 K).

4.4.2 *Ensemble-mean responses at tropical latitudes*

In this section we analyze solar signals averaged over tropical latitudes (25°S-25°N). Figure 4.6 illustrates time series of the ensemble-mean annual temperature anomalies at three pressure levels (1, 10, and 70 hPa). Averaging over tropical latitudes filters out a considerable fraction of the QBO signal; yet, semi-regular biannual oscillations (saw-like) are still visible. Solar signals can be traced at all pressure levels with magnitudes increasing with increasing altitude. Temperature anomalies up to 1 K are detected at 1 hPa, whereas the solar cycle signature is less visible at 70 hPa because it is shaded by ENSO and QBO in the coupled experiments and by QBO in AENS. Most notably in the CENS-ST (orange line in Figure 4.6), the cumulative La Niña-like event in 1960 and the subsequent El Niño-like event in 1962 dominates the temperature anomalies during the declining phase of solar cycle 19 (1954-1964). The ENSO influence diminishes in the middle (10 hPa) and upper (1 hPa) stratosphere.

Figure 4.7 displays profiles of the ensemble-mean profiles of the tropical temperature to increased solar cycle forcing. The magnitude of the response increases from the upper troposphere to the TLS, where it remains constant between 80 hPa and 40 hPa. From the TLS to the upper stratosphere, the magnitude increases monotonically, reaching values up to 0.7 K/100 sfu in CENS-ST and CENS-T63. The congruence of the CENS-ST and CENS-T63 profiles throughout the tropical stratosphere is remarkable. The same can be told for CENS and AENS. The TLS is cooler by about 0.05 K/100 sfu in the latter experiments, implying that the amplified UV forcing is influencing the TLS. For reasons not yet understood, the tropospheric responses in CENS are similar to CENS-ST, whereas the signal in CENS-T63 matches that of AENS.

Reanalysis datasets exhibit a temperature response maximum in the TLS and a subsequent local minimum in the tropical middle stratosphere (Frame and Gray, 2010). Apparently, none of the ensemble-mean temperature profiles is consistent with the observed profile because they exhibit a response plateau in the TLS. The latitudinal dependence of this plateau is weak and averaging over equatorial latitudes (5°S-5°N) returns a similar picture.
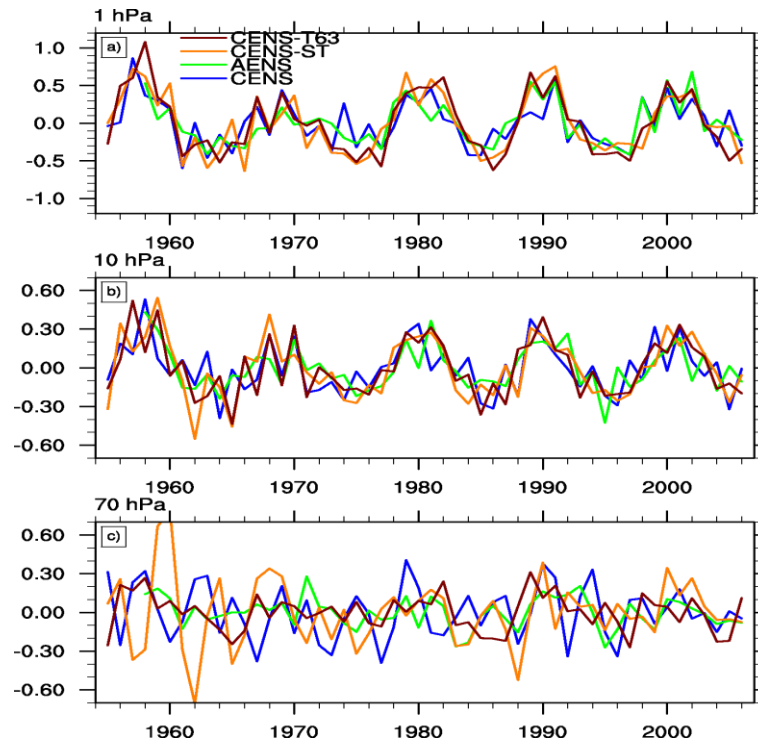
Figure 4.6 Comparison of the ensemble-mean annual temperature anomalies (K) in the tropics over the period 1955-2006 in CENS (blue), AENS (green), CENS-ST (orange), and CENS-T63 (brown) at three pressure levels: a) 1 hPa, b) 10 hPa, and c) 70 hPa.
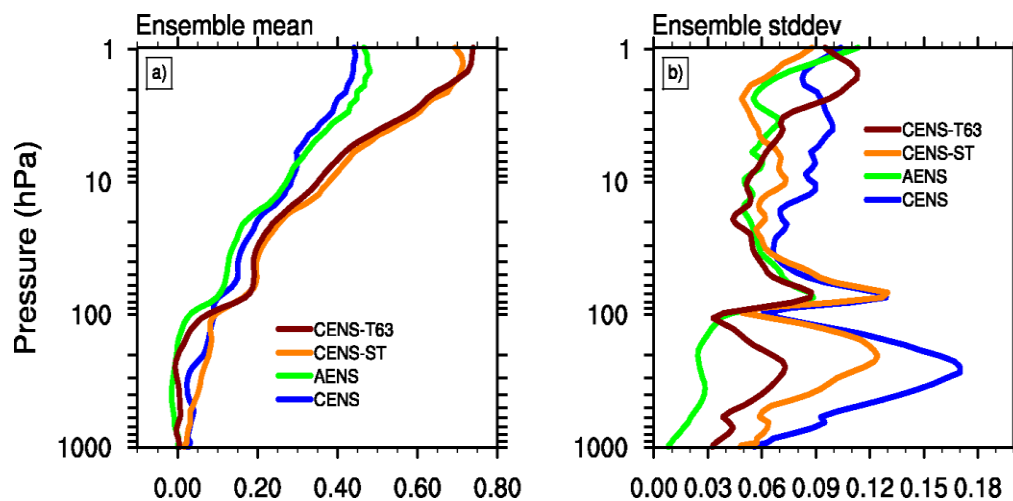
Figure 4.7: Profiles from CENS (blue), AENS (green), CENS-ST (orange), and CENS-T63 (brown) of a) the ensemble-mean tropical-mean temperature solar regression coefficients (K/100 sfu) and b) inter-ensemble standard deviation (K/100 sfu).

The simulated warming in the TLS is of radiative origin since stronger UV forcing yields stronger warming. A separate analysis highlights the minor role of circulation changes to the heat budget of the TLS. Perhaps more importantly, opposite to what one would expect from the mechanism of Kodera and Kuroda (2002), we detect anomalous upwelling in the TLS during solar maxima (not shown). The simulated

anomalous upwelling is likely related to the weak El Niño-like response of the tropical Pacific to the solar cycle forcing (Chapter 2). In the modeling study of Rind et al. (2008), the annual temperature response in the TLS to the solar cycle forcing was also related to radiative (i.e. short- and long-wave heating) and not to circulation changes. In the following sections, however, we make clear that tropical temperature profiles in individual ensemble members do not necessarily follow the ensemble averaged profile. This is implied in Figure 4.8b already, where the inter-ensemble standard deviation of the temperature solar responses at 70 hPa in CENS has comparable magnitude with the ensemble-mean response.

4.4.3 *Variability of the solar responses among ensemble members*

Thus far, we have analyzed ensemble averages. In this perspective, none of the experiments demonstrated a clear second temperature response maximum in the TLS. The tropical-mean temperature regression coefficients onto F10.7 in many individual ensemble members, however, do exhibit second response maxima in this region (Figure 4.8). One member of CENS-ST shows temperature changes at 70 hPa on the order of 0.4 K/100 sfu. Most of the ensemble members exhibit positive peaks at 70 hPa; negative peaks occur in six runs only.

Three notable features in Figure 4.8 must be understood. Firstly, the spread of the solar signals in the troposphere is much smaller in AENS than in all simulations with ocean coupling, among which CENS-T63 exhibits the weakest variation (see also Figure 4.7b). Secondly, all but one member of CENS-T63 show positive temperature anomalies at 70 hPa and the solar signal is almost identical in 13 runs (~0.2 K/100 sfu). In contrast, higher inter-ensemble standard deviations are seen in CENS and CENS-ST (Figure 4.7b). Thirdly, there is an apparent tendency for positive temperature anomalies in the TLS together with negative anomalies in the upper tropical troposphere and vice versa. This relationship reminisces of the ENSO signature and could suggest that MRA-AR1 is not able to adequately separate solar from ENSO signals. If this is true, the solar signals detected with MRA-AR1 should depend on the correlation coefficient between the F10.7 and Nino-3.4 indices used in MRA-AR1.
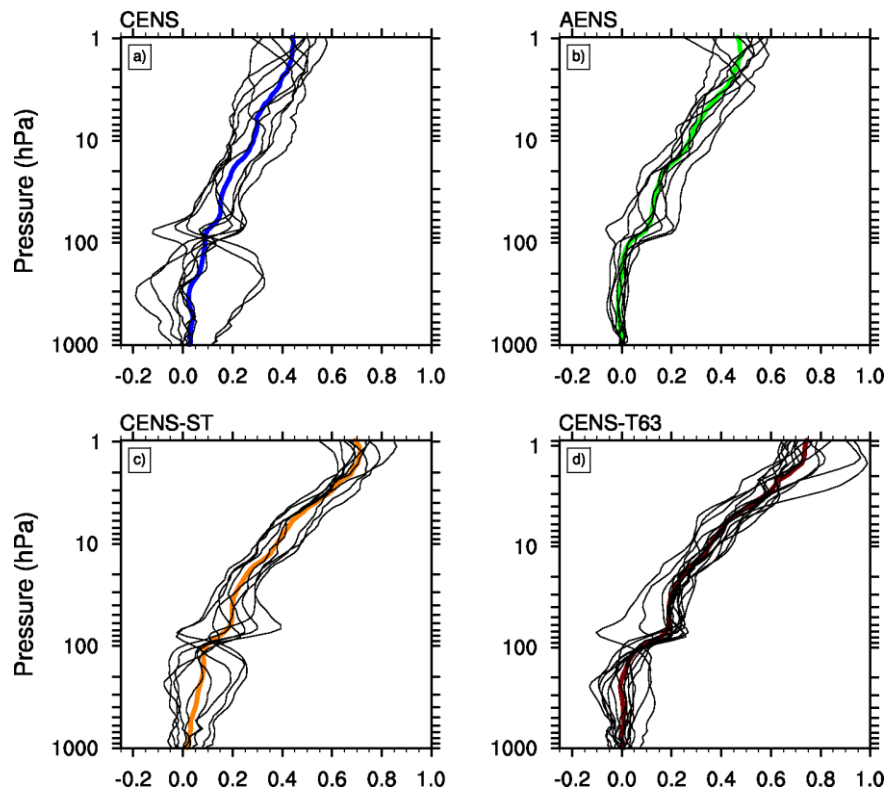
Figure 4.8: Profiles of tropical-mean annual temperature solar responses (K/100 sfu) in every ensemble member (black thin lines) and the associated ensemble means (thick color lines) in a) CENS, b) AENS, c) CENS-ST, and d) CENS-T63.

Indeed, two ensemble members taken from the CENS-T63 experiment advocate this dependence. While the temperature solar responses are almost identical in the upper stratosphere, they deviate considerably below 20 hPa. The correlation between F10.7 and the respective Nino-3.4 is weak but positive (r=0.1, red line in Figure 4.9) in the only run that MRA-AR1 resulted in negative anomalies in the TLS. In this particular run, the tropical troposphere warms with increasing solar activity. Contrarily, positive (negative) solar responses are calculated in the second ensemble member, which is characterized by negative correlation (r=-0.2, blue line in Figure 4.9). The solar response in the tropical troposphere and lower stratosphere match to those anticipated from ENSO events; negative (positive) temperature anomalies at 70 hPa (150 hPa) for an El Niño event. A La Niña event has the opposite effect. Hence, these two runs put forward the notion that MRA-AR1 solar cycle estimates are inflicted by the correlation between the Nino-3.4 and F10.7 indices.
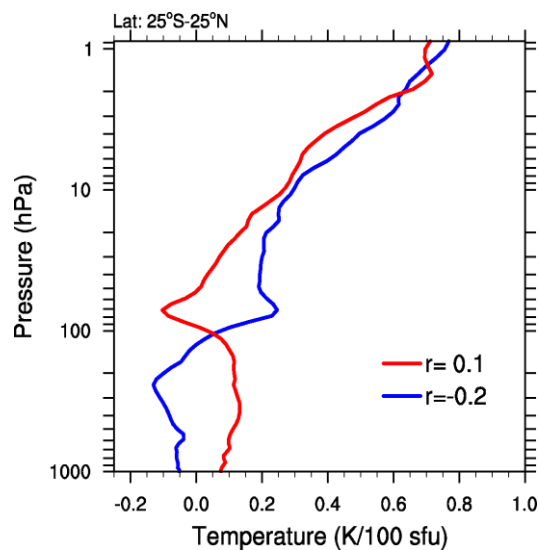
Figure 4.9: Comparison of the tropical temperature responses (K/100 sfu) to 11-yr solar cycle forcing in two selected members of CENS-T63 that show positive (r=0.1, red) and negative (r=-0.2, blue) correlation coefficient between F10.7 and the respective Nino-3.4 index.

The implied linear relationship between the sign of the regressed solar responses in the TLS and the correlation coefficient between F10.7 and Nino-3.4 is not restricted to these two examples only, but there is an evident tendency in all experiments with ocean coupling (CENS, CENS-ST, and CENS-T63). Although the ensemble mean solar response in CENS is relatively weak compared to the other experiments (see Figure 4.7a), we blend all coupled runs to maximize the size of the sample in hand (sample size: 33).

Figure 4.10a displays the tropical-mean solar regression coefficients of temperature anomalies at 70 hPa as a function of the correlation between F10.7 and the corresponding Nino-3.4. If all red dots are projected onto the vertical axis of zero correlation, the distribution of the solar regression coefficients, as expected, is skewed positive with mean value of 0.16 K/100 sfu. The mean correlation is zero. The least square regression line (red line in Figure 4.10a) intercepts at 0.17 K/100 sfu and its slope is -0.06 K/100 sfu per 0.1 correlation increment. A standard t-test rejects the null hypothesis of zero slope with 95% confidence. It seems, therefore, that MRA-AR1 is deriving biased estimations of the solar cycle response. If this argument holds true, we expect that a) MRA-AR1 would detect putative solar signals even in simulations without explicit solar cycle forcing b) the relationship between the solar regression coefficients and the correlation between F10.7 and Nino-3.4 would be similar to the solar-forced experiments.

Figure 4.10: Scatter plots with linear regression lines (red lines) of the solar regression coefficients of the tropical temperature (K/100 sfu) at 70 hPa versus the correlation coefficient between F10.7 and Nino-3.4 in the case that the Nino-3.4 term is a) included or b) excluded from the MRA-AR1. Red dots from the CENS, CENS-ST, and CENS-T63 experiments. Black, violet and pale-green dots from a 12-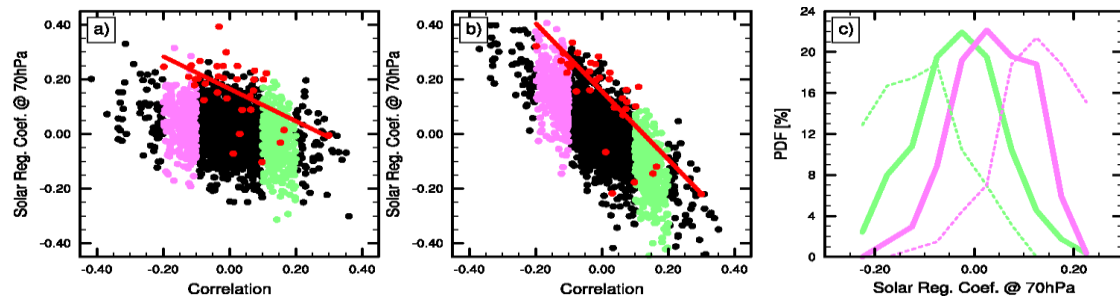month block bootstrap re-sampling of CTR and CTR-T63, respectively (see text for details). c) Probability density functions (PDFs) of the regression coefficients in case of weak positive correlations (0.1< r <0.2, pale-green) and weak negative correlations (-0.2< r <-0.1, violet). Thick lines refer to (a) and thin dashed lines to (b).

To test this hypothesis we repeat the previous analysis on 1700 new synthetic temperature time series (850 from CTR and 850 from CTR-T63) generated with a block bootstrap resampling (Efron, 1993). We select a block size of 12 months to allow annual sampling. Each new time series covers 52 years. The "solar cycle signals" at 70 hPa are then derived with the MRA-AR1 model, even though we know a priori that no real solar cycle signals exist. The new correlation coefficients span from -0.4 to +0.35, whereas the maximum false solar regression coefficients are comparable to those detected in the solar cycle-forced simulations (black, pale-green and violet dots in Figure 4.10a). As expected, the probability density functions (PDFs) of both the regression and correlation coefficients have zero means. A least-square regression analysis calculates zero intercept and negative slope that passes the 95% significance level according to a t-test (-0.024 K/100 sfu per 0.1 correlation increment).

Figure 4.10c underlines that MRA-AR1 introduces spurious signals even when the Nino-3.4 index is weakly correlated with F10.7. The PDF of the "solar" regression coefficients (thick pale-green line) from the control experiments in all cases that exhibit small but positive correlations (0.1< r <0.2) shifts to negative values and its mean estimate is significantly different from zero, although zero solar signals should be detected. In contrast, the PDF moves towards positive temperature anomalies when the correlation is weakly negative (-0.2< r <-0.1). Albeit robust, the overall bias is small. This is not necessarily the case, however, when the Nino-3.4 index is excluded from MRA-AR1. The regression line of the coupled simulations with solar cycle forcing (red line in Figure 4.10b) becomes steeper with slope of 0.12 K/100 sfu per 0.1 correlation increment (compare to -0.06 K/100 sfu per 0.1 correlation increment in Figure 4.10a). Accordingly, the associated PDFs in Figure 4.10c deviate more

drastically and stronger positive (negative) putative solar signals are calculated for weak negative (positive) correlations (Figure 4.10c). This means that the bias of the solar regression coefficients due to the solar cycle-ENSO collinearity is amplified when the ENSO predictor is excluded from MRA-AR1. The intercept of the regression line in Figure 4.10b, however, changes marginally in comparison to the intercept in Figure 4.10a (0.17 K/100 sfu vs 0.16 K/100 sfu). In other words, the ensemble-mean temperature response is an unbiased estimate.

Based on this analysis we can explain now the three features in Figure 4.10 highlighted before. Certainly, the specified SST climatology in AENS should damp the solar signals in the troposphere, resulting in a weaker inter-ensemble variability compared to coupled simulations. Yet, this is not the only reason. The inter-ensemble variation is inflated in the experiments with ocean coupling from biaseas introduced by the ENSO and solar cycle collinearity. An unrealistically strong ENSO amplitude should cause stronger temperature variability in the TLS and subsequently, stronger biases in the solar regression coefficients. This is the reason why CENS-T63 demonstrates the smallest inter-ensemble variability among the coupled experiments.

Multiple linear regression models, depending on the correlation between the solar cycle and ENSO predictors, could significantly overestimate or underestimate the calculated solar signals in the TLS when the ENSO predictor is neglected. By adding the ENSO predictor in the regression model, the collinearity bias is substantially reduced but not eliminated. It is not surprising, therefore, that the modeling study of Marsh and Garcia (2007), which employed the WACCM (Whole Atmosphere Community Climate Model) forced with the observed solar cycle and SSTs from 1950 to 2003, documented stronger positive ozone responses in the TLS to 11-yr solar cycle when the observed Nino-3.4 predictor was removed from the regression model. Since the observed Nino-3.4 index correlates negatively with F10.7 over the period 1979-2003 (r=-0.15), our analysis suggest that the ozone response needs to be reduced. However, the new value is still biased because it refers to non-zero correlation. Perhaps, this explains why the simulated solar response was further decreased over the period 1950-2003, when correlation is essentially zero.

4.4.4 *Time dependence of the temperature responses to the solar cycle*

The large number of ensemble simulations provides the opportunity to investigate the dependence of the simulated solar signals on the analyzed period. For this reason, the full 52-yr period is split into two 26-yr sub-periods covering 1955-1980 and 1981-2006, respectively and then, the tropical-mean temperature regression coefficients onto F10.7 are recalculated with MRA-AR1. In AENS, the first sub-period starts in 1958.

In broad terms, the dependency of the ensemble-mean tropical-mean responses on the simulated period is weak throughout the atmosphere (< 0.02 K/100 sfu). The signals deviate mainly in the TLS. Individual ensemble runs, however, do show strong dependency on the simulated period (not shown). This is not surprising because the probability of strong correlation between the F10.7 and Nino-3.4 predictors is higher when data form shorter time series are considered.
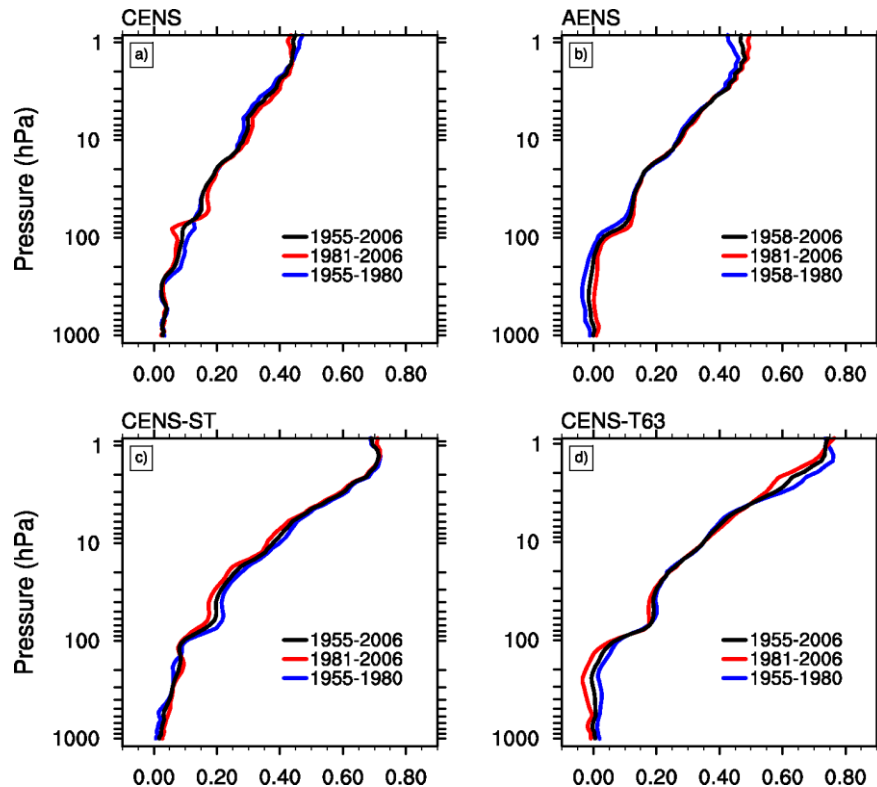
Figure 4.11: Ensemble-mean tropical-mean solar regression coefficients of annual temperature anomalies (K/100 sfu) over the periods 1955-2006 (black), 1955-1980 (blue), and 1981-2006 (red) in a) CENS, b) AENS, c) CENS-ST, and d) CENS-T63.

Austin et al. (2008) noted that the correlation coefficient between the observed SSTs and the solar cycle is positive over the period 1960-1981 (r~0.38) but negative from 1982 to 2003 (r=-0.11). In many simulations of their study, the temperature response to the solar cycle was either negative or weakly positive in the former period, whereas much stronger positive anomalies were detected in the latter period. Based on our simulations we suggest that the influence of the 11-yr solar cycle does not change with time; what changes is the correlation between the ENSO and solar cycle predictors. When single realizations are analyzed with multiple linear regression models, weaker (stronger) temperature solar responses in the TLS are expected during periods characterized by positive (negative) correlations. This bias is alleviated, however, when large ensembles of 9 or more members are considered. Ensemble averaging returns robust annual solar responses, even in the case of short model integrations (e.g. 26 years).

4.5   Stratospheric response during NH winter

In the previous section, we presented annual temperature responses to the 11-yr solar forcing. In this section, our interest moves to the boreal-winter season because we want to investigate the seasonal dependence of the temperature responses in the TLS to the solar cycle. Figure 4.14 displays profiles of the tropical-mean solar regression coefficients during January and February (JF). Compared to annual counterparts (Figure 4.8), the JF solar responses are substantially more scattered, particularly in the middle and upper stratosphere. In CENS-T63, for instance, the regression coefficents at 2 hPa range from slightly negative to strongly positive values (1.3 K/100 sfu). In many cases, this discrepancy is attributed to the fact that the number of the data points of JF averages is twelve times smaller than in monthly averages. Moreover, solar signals may be confused with QBO signals in few ensemble runs; otherwise is difficult to explain why increased levels of solar activity cool the tropical upper stratosphere given that the ozone solar response in our simulations is prescribed.
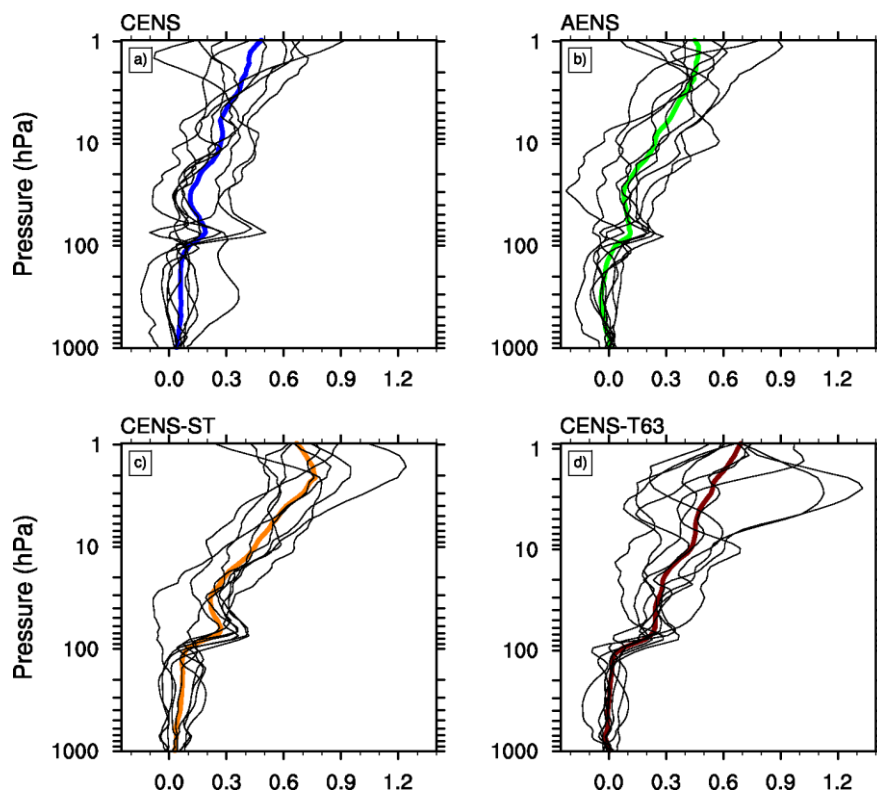
Figure 4.12: Profiles of tropical temperature solar regression coefficients (K/100 sfu) during January and February in every ensemble member (black thin lines) and the associated ensemble averages (thick colored lines) in a) CENS, b) AENS, c) CENS-ST, and d) CENS-T63.

Figure 4.13 displays the ensemble-mean temperature profiles of every experiment. The effect of the amplified UV solar cycle forcing can be clearly noticed throughout the tropical stratosphere. CENS-ST and CENS-T63 exhibit about 0.1 K/100 sfu stronger warming at 70 hPa relative to CENS and AENS. The salient feature of Figure 4.13 is that the winter season, in contrast to annual averages, favors the formation of a

temperature response maximum at 70 hPa and a subsequent minimum at 30 hPa. In the coupled simulations, the dependence between the F10.7 and Nino-3.4 predictors may bias solar responses in the TLS, but a weak temperature solar maximum (~0.1 K/100 sfu) is detected even in the AENS experiment as well. A separate analysis, not shown here, identifies that anomalous downwelling during solar maxima is causing this warming. Following the mechanism of Kodera and Kuroda (2002), the warming due to anomalous downwelling should originate from wave-mean flow interactions in the extra-tropical stratosphere. If this interaction does operate in our model, positive zonal-mean zonal wind anomalies that propagate poleward and downward should be simulated during the boreal winter.
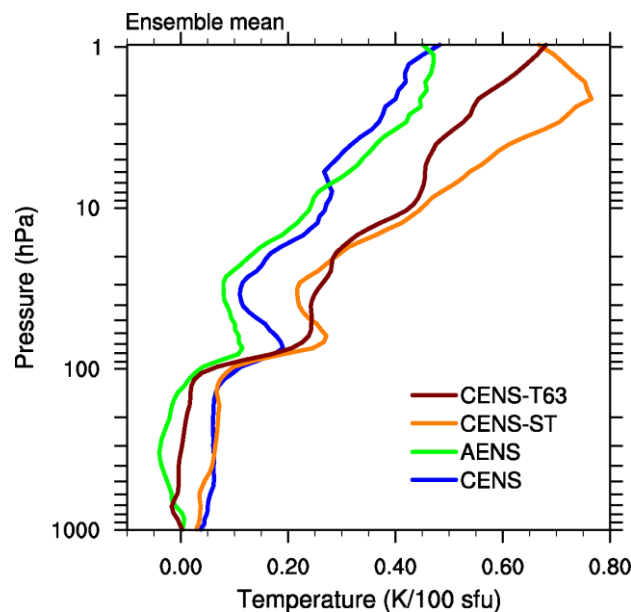
Figure 4.13: Profiles of the ensemble-mean tropical temperature solar responses (K/100 sfu) during January-February from CENS (blue), AENS (green), CENS-ST (orange), and CENS-T63 (brown).

Figure 4.14 compares the November to March evolution of the zonal-mean zonal wind responses to the increased solar cycle forcing. The similarity between CENS and AENS, particularly in late winter (January to March) is remarkable, confirming our earlier finding about the trivial sensitivity of the stratospheric solar signals on ocean coupling. The polar vortex stays anomalously weak in January but westerly anomalies that propagate poleward are simulated in the following months. The polar vortex does not react linearly to stronger UV forcing and the zonal wind anomalies in CENS-ST are considerably different from CENS. The CENS-T63 experiment shows stronger zonal winds on the order of 1.5 m/s/100 sfu in the mid-latitude lower mesosphere in December that within the next 3 months reach the troposphere. Overall, the simulated zonal wind anomalies in the extra-tropical stratosphere are weak and hardly significant since the inter-annual variability in this region (e.g. 16 m/s at 70°N and 1 hPa in February) is much higher than the solar signals.

Nevertheless, individual ensemble members show much stronger wind anomalies in February. Many members of CENS-T63, for instance, exhibit strong westerly anomalies on the order of 7 m/s/100 sfu (Figure 4.15). Yet, strong negative anomalies (~7 m/s) are also detected. This highlights that the solar responses in the NH winter stratosphere may differ drastically among individual ensemble runs. Apparently, the high internal variability of this region perplexes the simulation of robust solar responses. Our simulations suggest, therefore, that 15 ensemble runs with transient solar cycle forcing may not sufficient to untangle solar signals is the NH winter stratosphere.
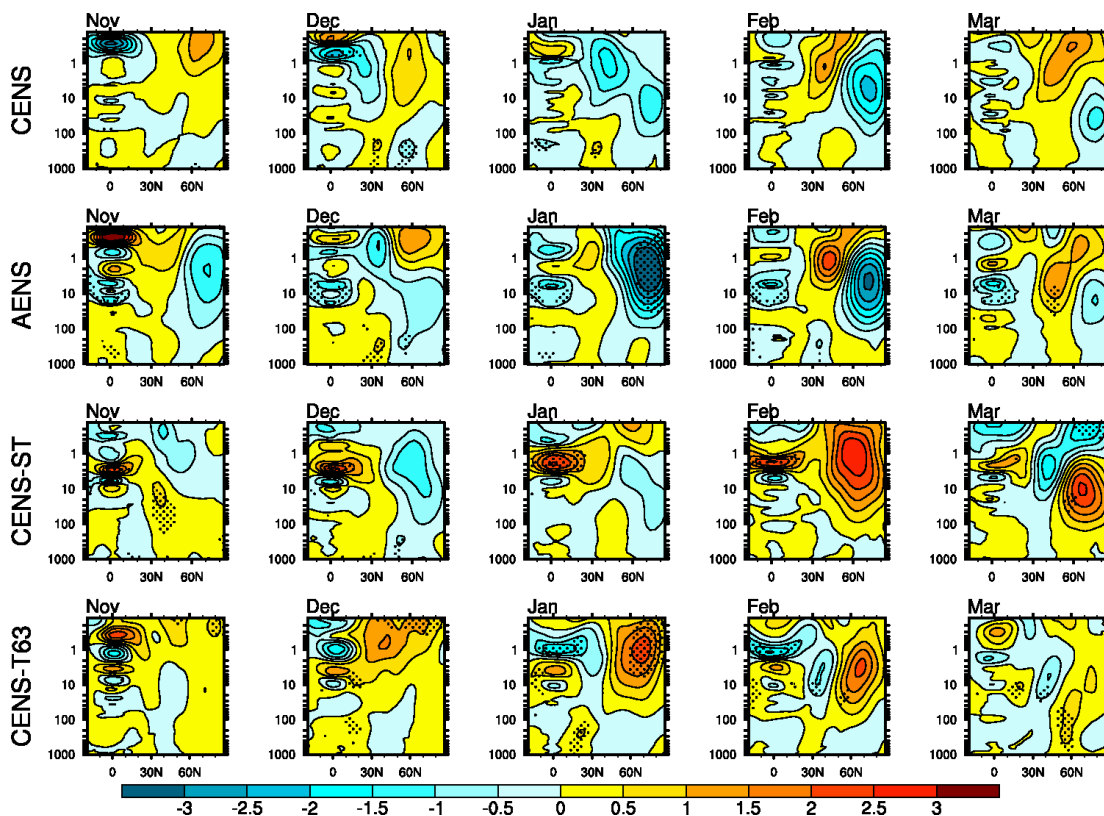
Figure 4.14: November to March evolution of the ensemble-mean zonal-mean zonal wind solar regression coefficients (m/s/100 sfu) in CENS, AENS, CENS-ST and CENS-T63.

Observation-based studies identified positive zonal wind anomalies in November that propagate poleward and downward within three months, resulting in negative anomalies in February and March (Kodera and Kuroda, 2002; Matthes et al., 2004; Frame and Gray, 2010). In our simulations, the westerly anomalies occur too late and their propagation is too slow. This is a common flaw of many GCMs (Tsutsui et al., 2009; Schmidt et al., 2010). Observations suggest that the high-latitude stratosphere is radiatively controlled in the early part of the winter and shifts to dynamical control in the late winter (Kodera and Kuroda, 2002). The low frequency of recorded SSWs in November and December compared to January highlights this transition. Our model in the coarse configuration (T31L90-GR30L40), in contrast, shows too many SSWs in November, implying that the dynamical regime is more prevalent in early winter.

Hence, in CENS, AENS, and CENS-ST the early winter polar night jet is less prone to radiative perturbations and thus the initiation of the interaction between the zonal winds and planetary waves, which amplifies the response, is delayed by couple of months. With increased horizontal resolution, the dynamical regime is established in the mid-winter season. In this case, the polar night jet should be more susceptible to radiative forcing in early winter (January). As such, the amplification of the zonal wind anomalies should start earlier. This could explain why weak westerly anomalies are simulated one month earlier in CENS-T63 compared to CENS-ST.
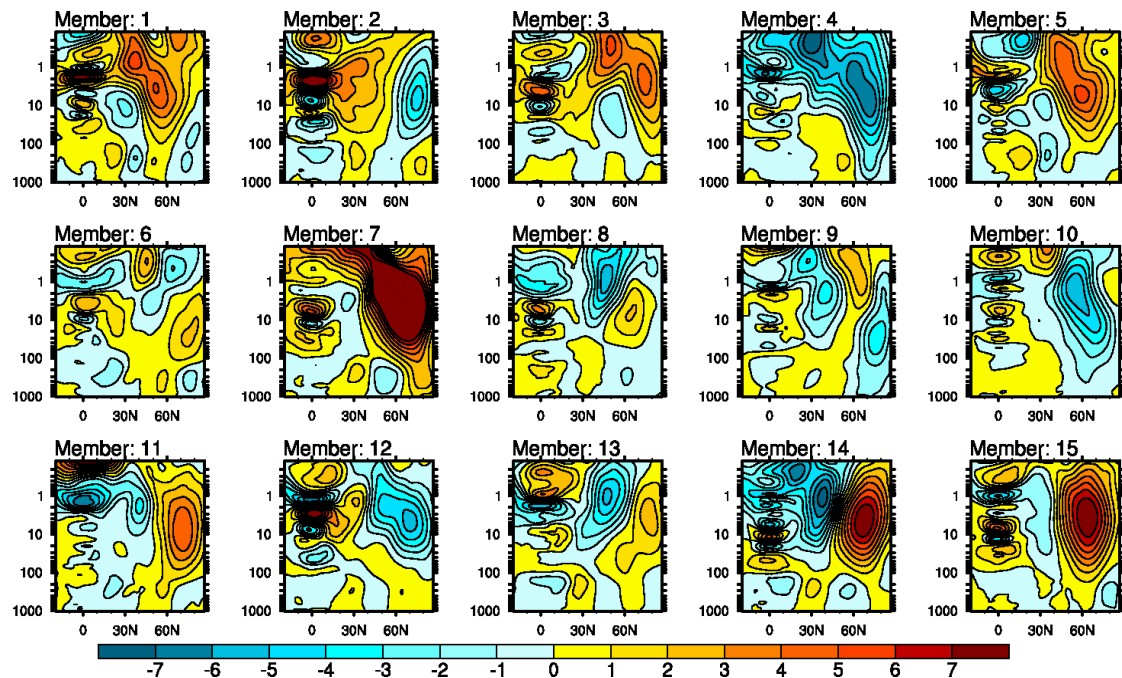
Figure 4.15: Zonal-mean zonal-wind solar regression coefficients (m/s/100 sfu) in February in every ensemble member of CENS-T63.

4.6 Discussion

It has been suggested that surface temperature changes due to the increased total solar irradiance could amplify the stratospheric responses to increased UV irradiances (van Loon et al., 2007; Meehl et al., 2009). In our simulations, the solar signals on the stratospheric temperature and zonal wind, both in annual and boreal-winter averages, do not critically depend on ocean coupling. This entails from the high resemblance of the stratospheric solar responses in CENS and AENS. Rind et al. (2008) reported similar findings but with a GCM coupled to a mixed layer ocean. In Chapter 2 we documented global mean SST anomalies on the order of 0.03 K/100 sfu and a basin-wide warming in the tropical Pacific up to 0.12 K/100 sfu. Apparently, these surface solar responses are too weak to induce any measurable change in the stratosphere. Although the magnitude of the tropospheric warming in CENS and CESN-ST is comparable, the TLS is 0.05 K/100 sfu warmer in the latter experiment in which the UV solar cycle forcing has been deliberately amplified. In our simulations, therefore,

the annually averaged solar signal in the lower stratospheric temeratures is primarily administrated by radiative changes. In boreal-winter season, however, the dynamical heating caused by weaker upwelling plays an important role, too.

Our simulations do not reproduce the observed magnitude and propagation of the solar-induced zonal wind anomalies. Matthes et al. (2004) discussed that only GCMs with accurate background conditions could simulate realistic solar signals. This argument is supported also from our experiments given that CENS-T63 demonstrates the closest correspondence to the observed solar responses. The improved distribution of the SSWs during the boreal winter in CTR-T63 compared to CTR reflects a more realistic stratospheric circulation when higher horizontal resolution is selected. Even in this case, the simulated zonal wind anomalies are very weak compared to observations (Frame and Gray, 2010). However, the observed signal is deduced from a single short realization of the real atmosphere. The variability of the simulated solar responses among individual ensemble members is high, and much stronger signals are obtained in single realizations. Hence, observations spanning over many more solar cycles may be required before definite conclusions can be made.

An unrealistic UV forcing could also affect the winter time response. Our experiments with amplified UV solar forcing (CENS and CENS-ST) demonstrate solar responses that start earlier in the boreal winter. Recent measurements with the Spectral Irradiance Monitor instrument (SIM) during the declining phase of the cycle-23 indicated much stronger UV variation between solar maximum to solar minimum than previously estimated (Harder et al., 2009). If the new estimates are accurate, we expect future simulations to demonstrate considerably different NH winter solar signals.

Concerning the solar signals in the TLS, we find a tendency towards negative or less positive temperature anomalies in ensemble members that exhibit positive correlations. Figure 4.11 demonstrates that all instances of negative temperature anomalies at 70 hPs are associated with positive correlations. The reverse is also identified in ensemble members characterized by negative correlations. Given these findings, we suggest that the positive temperature responses in the TLS indentified in the work of Frame and Gray (2010) might be overestimated since the observed Nino-3.4 correlates negatively with F10.7 over the period 1979-2003. If the correction function calculated with our ensemble simulations (0.06 K/100 sfu per 0.1 increment of correlation coefficient) is valid, we estimate a bias on the order of 0.1 K/100 sfu. Clearly, this number is small compared to the magnitude of the observed solar warming in the TLS (0.6-0.7 K).

Our analysis shows that the exclusion of the ENSO predictor from the regression model amplifies the sensitivity of the calculated solar signals in the TLS to the bias introduced by the solar cycle-ENSO collinearity. Nevertheless, the ensemble mean solar signal (intercept) remains unchanged. This feature can be exploited for extracting unbiased estimates of the solar responses in the region. We propose that

future studies with coupled models should conduct ensemble simulations. The solar signal in the TLS in a single realization can be contaminated by ENSO even in a 52 years long simulation. The comparison of the annual mean temperature response in CENS-ST and CENS-T63, indicates that in our case, 9 ensemble runs are sufficient to smear out biases from the solar cycle-ENSO collinearity.

Our model, of course, does not come without potentially important shortcomings, whereof the lack of interactive chemistry calculations is the most prominent. Hence, any possible amplification of the solar signal either in the TLS or in the NH winter stratosphere owing to circulation-chemistry interactions is neglected. If this mechanism works mainly in boreal-winter season, the anomalous downwelling simulated in the tropical stratosphere should transport ozone-reach air masses from the middle to the lower stratosphere. Consequently, the enhanced ozone UV absorption would amplify the initial adiabatic warming.

4.7 Conclusions

In this study, we used the middle atmosphere version of ECHAM5/MPIOM to investigate the response of the stratosphere to the 11-yr solar cycle forcing. A large number of ensemble simulations with and without ocean coupling in two different horizontal resolutions and two different levels of solar UV forcing were carried out. The key findings of this study are:

1) The ensemble mean stratospheric solar responses both in annual and seasonal averages do not critically depend on the solar cycle responses at the ocean surface.

2) In our model, the response of the boreal-winter stratosphere depends on the level of UV solar cycle forcing. In general, stronger heating in the upper stratosphere, as in CENS-ST, brings the time evolution of the zonal-mean zonal winds during the course of the boreal winter closer to observations. The signal is further improved in the experiment with finer horizontal resolution. Yet, the magnitudes of the simulated zonal wind anomalies are much weaker compared to those observed.

3) None of the experiments shows a temperature response maximum in the tropical lower stratosphere when ensemble-mean annual solar signals are analyzed; January-February averages demonstrate a temperature response maximum related to anomalous downwelling. Many individual ensemble members, however, do show well-formed annual temperature maxima in the tropical lower stratosphere but we call for caution in interpreting these maxima as genuine solar signals. Although the effect of collinearity between the ENSO and solar term in the multiple linear regression model is found weak in the ensemble-mean perspective, it could adversely affect any single short model realization. The same maybe true for the observed record.

Chapter 5

Conclusions and future directions

5.1 Conclusions

This thesis presents the first attempt to systematically address the response of the tropical oceans to 11-yr solar forcing by analyzing ensemble simulations. Past simulations analyzed either single realisations or small ensembles but with prescribing additional external forcings (e.g. GHGs, aerosols). Moreover, any dependence of the stratospheric solar signals on solar-induced changes at the sea surface has been thoroughly investigated. By analyzing ensemble model simulations with and without ocean coupling, in two different horizontal resolutions and with two levels of solar UV forcing, I am in the position now to answer all questions posed in Chapter 1.

- *How does the 11-yr solar cycle affect the tropical oceans?*

It must be realized first that isolating solar signals in observations is a difficult task, because natural decadal oscillations of the tropical oceans can be misinterpreted as of solar origin, when short time series are analyzed. The previously reported warming over the tropical Pacific during solar maxima should be ascribed to the Tropical Pacific Quasi-Decadal Oscillation (TPQDO), whereas the cooling in the eastern Pacific during solar maxima is likely explained by oversampling of La Niña events. In other studies, the cooling in the eastern Pacific is explained by confusing Sea Surface Temperature (SST) responses to the solar cycle with the signature of the ENSO Decadal Amplitude Modulation (EDAM).

In our coupled simulations, the tropical SSTs rise almost in phase with the 11-yr solar cycle. In the Pacific, a basin-wide warming of approximately 0.15 K is simulated, whereas the warming in the Indian and Atlantic oceans is weaker. Outside the Pacific, the surface warming is mainly explained by the water-vapor feedback, whereas atmosphere-induced changes in ocean dynamics results in a warmer Pacific.

- *Do periods of increased solar activity favor, statistically, La Niña events?*

Our model shows no evidence of more La Niña events in solar maxima. Although individual ensemble members do show a clear La Niña-like cooling with increased 11-yr solar forcing, the signal in the ensemble averaged time series is El Niño-like. However, this does not mean that the increased solar activity favors El Niño events. Contrarily, I find that the simulated warming in the Pacific is related to the TPQDO.

This oscillation, explained by the recharge/discharge ENSO mechanism, is excited naturally in many atmosphere-ocean general circulation models, and so it is in MAECHAM5/MPIOM. The 11-yr solar cycle seems to act as a pacemaker of the TPQDO in the solar-forced coupled simulations. Hence, the impact of the 11-yr solar cycle is projected on natural oscillatory modes of the atmosphere-ocean Pacific system.

In the western Pacific, the region of deep convection shifts to the east, reducing the surface easterlies. The eastward shift of the Walker circulation is the key-element to understand the solar cycle-TPQDO interaction because it happens independently of the ocean coupling; the deep convection moves to the east in the uncoupled simulations, too. The reduced surface easterlies push the Pacific system to a state where the equatorial upper ocean heat content is constantly flushed to the subtropics due to the Sverdrup divergence. This discharge of heat lifts the thermocline throughout the Pacific, initiating the negative TPQDO phase in the years to follow. In the opposite phase of the 11-yr solar cycle, the stronger equatorial easterlies push the Pacific system to a state in which heat is accumulated, favoring the positive TPQDO phase.

In our model, therefore, the increased solar forcing does not trigger La Niña episodes. I acknowledge that other coupled models may give a positive answer or no answer at all, depending on the experimental design and the model setup. However, I advocate the notion that the observed solar signals in the tropical Pacific are equally uncertain because the available datasets are admittedly too short to separate solar cycle signals from signals related to natural inter-annual and decadal oscillations.

- *Is numerical modeling supporting the observed relationships between the 11-yr solar cycle, TPQDO, and EDAM?*

Our model simulations give a positive answer. In observations from 1955 to 2009 and in our simulations alike, TPQDO synchronizes to the 11-yr solar cycle. This synchronization has statistical character in our model. Moreover, the simulated ensemble-mean EDAM lags the TPQDO by a couple of years. A low-order ENSO model provides a plausible explanation for this phase locking. In this model, weaker zonal winds are leading the positive phase of the TPQDO, whereas deeper thermocline is lagging the positive phase of the TPQDO. These changes should

increase the growth rate of ENSO, causing stronger ENSO episodes during the declining phase of the TPQDO.

Our model simulations suggest that the observed decadal oscillations of the tropical Pacific system may not be as natural as previously thought. Certainly, 11-yr solar cycle excites neither the TPQDO nor EDAM. Instead, our simulations suggest that the 11-yr solar cycle may contribute to the time evolution of these oscillations.

- *Does the stratospheric response to 11-yr solar cycle forcing depend on the solar signals in the tropical oceans?*

The simulated surface response to 11-yr solar forcing is weak. The tropical oceans warm by about 0.15 K while the global-averaged response is on the order of 0.04 K. It is not surprising, therefore, that solar signals in the stratosphere do not critically depend on ocean coupling. I find almost identical stratospheric temperature responses between ensemble simulations carried out with MAECHAM5/MPIOM and MAECHAM5 alone. Even in the tropical lower stratosphere, where the strongest influence from surface solar signals is anticipated, I find qualitatively and quantitatively comparable changes between the two model configurations. The tropospheric solar responses, however, are closely related to ocean changes given that when the Sun is more active the troposphere warms in the coupled but slightly cools in the uncoupled simulations. The latter means that solar-induced warming in the tropical oceans does play an important role on simulating solar signals in the troposphere.

- *Can we rule out the possibility that the observed solar responses in the tropical lower stratosphere originate from solar cycle-ENSO aliasing?*

No, because the solar signals in the tropical lower stratosphere isolated with multiple linear regression models are affected by the solar cycle-ENSO collinearity. I identify a clear relationship between the estimated tropical-mean temperature response to the 11-yr solar cycle forcing and the correlation coefficient between the solar and ENSO predictors. Negative correlations cause with higher solar responses and vice versa. Although the effect of collinearity is found weak in our ensemble simulations, it could adversely affect any single short realization of the model and so it could in the observed record. In other words, the observed record is too short for unambiguous identification of solar signals in the lower tropical stratosphere. This does not necessarily imply that the tropical lower stratosphere is insensitive to the 11-yr solar variations but it suggests that earlier studies may have overestimated the magnitude of the solar responses in the tropical lower stratosphere.

In addition to the above-stated findings, our model simulations show that the solar response in the extra-tropics may be sensitive to the level of solar forcing. Although

our analysis is not exhaustive in this respect, I demonstrate that the stronger solar UV heating in the upper stratosphere, brings the time evolution of the zonal-mean zonal wind anomalies during the course of the boreal winter closer to the observed changes. Increasing the horizontal resolution of the atmosphere GCM improves further the simulated solar responses. Yet, the magnitudes of the simulated zonal wind anomalies are still underestimated.

The observed warming trend in the global mean temperatures during the 20th century has not been monotonic. Temperatures reached a local maximum in the 1940s, cooled until the mid 1970s and increase ever since. It has been claimed that the secular trend of the solar variation, combined with the radiative forcing from volcanic eruptions can explain the global mean temperature changes in the first half of the 20th century. Our simulations are not designed to test this claim since we simulate solar cycle responses over the period 1955-2006. Over this period, I find no positive trend in the simulated global-mean surface temperatures. Instead, a weak quasi-periodic variation (0.04K from solar minima to solar maxima) of the global-mean surface temperature is detected. Hence, the steady temperature increase after the 1970s is not explained by variations of the incoming solar irradiance. Radiative heating from human-made greenhouse gases and to lesser extend from natural decadal variations in the climate should explain the observed global warming.

5.2 Future directions

I suggest that future research concerning the Pacific response to the 11-yr solar cycle forcing must be directed to ensemble simulations with atmosphere-ocean models. In single realizations, the solar signal in the tropical Pacific can be hidden by natural variability. In fact, the detection of solar signals is not a straightforward task even after 11 ensemble runs. Moreover, any future simulations must be carried out by considering solar cycle irradiances only. Clearly, the inclusion of additional external forcings, such as volcanic eruptions or GHG concentration increase, shall complicate the detection of solar signals.

I believe that model integrations that cover 5 solar cycles are too short for detecting robust solar signals in the tropical Pacific and thus 10 or even more solar cycles must be realized. I propose the following scheme. At first, the model should be forced with unrealistically strong 11-yr solar variability. A deliberately amplified solar cycle forcing should improve the signal-to-noise ratio, facilitating the detection of robust solar responses. In order to simulate 10 or more solar cycles, it is advised to approximate the observed solar cycle as a sinusoid. This simplification eases interpretation since the rising and declining phases of the observed solar cycle are asymmetric. Once the physical mechanism that explains the response of the Pacific system to this idealized solar cycle is established, ensemble simulations with realistic 11-yr solar forcing can be conducted as well. Obviously, our simulations cover the second step of the methodology I proposed here. I am planning to carry out ensemble

simulations with 3 times stronger spectral solar irradiances. Assuming linearity, these forthcoming simulations will reject or confirm our findings in Chapters 2 and 3.

Explaining the physics of the response of the coupled atmosphere-ocean Pacific system to periodic forcing, the 11-yr solar cycle, has far-reaching implications because it may advance our understanding of how this system will react to global warming. Herein lays a big challenge for future work. On the basis that the 11-yr solar cycle may affect natural oscillatory modes of the atmosphere-ocean Pacific system, future work employing different coupled models should aim at confirming or rejecting the relationship between solar cycle, TPQDO and EDAM identified in this study.

Concerning the solar signals in the stratosphere, I propose that future attempts to model the response of the upper stratosphere to 11-yr solar forcing will not benefit much from ocean coupling. Instead of dedicating computing resources to model ocean circulations, future simulations should be carried out with increased horizontal resolution. To simulate tropospheric changes, however, a coupled model is required. Of course, this comes at the cost of high computing demand, particularly if a model with interactive chemistry is chosen.

I examined the dependence of the temperature solar responses in the tropical lower stratosphere on the solar cycle-ENSO collinerity. Our simulations do not provide any answer about why the observed temperature solar response takes the form of two symmetric lobes. I believe that future studies should address the possibility the regression models confuse solar cycle signals with QBO-related signals. To addresses this possibility, I propose that ensemble simulations in which the observed QBO is nudged should be compared to ensemble simulations in which the QBO is naturally excited.

As many earlier modeling attempts, our ensemble simulations suffer from weak stratospheric solar responses during boreal winter when compared to observations. It is possible that observations overestimate the solar responses in the stratosphere simply because the available record is too short. It is equally possible that this inconsistency is related to the weak variation of prescribed UV solar cycle forcing when compared to stronger UV estimates from the SIM (Spectral Irradiance Monitor) instrument. Future simulations with the new estimated of the UV solar cycle forcing may improve the magnitude and time propagation of the simulated solar signals in the winter stratosphere.

Appendix 1: The Multichannel Singular Spectrum Analysis

The complexity of the analysis methodology for extracting quasi-periodic oscillations has increased considerably in the recent years and new tools have been developed. A review on advanced spectral methods frequently used in climate research is given by Ghil et al., (2002). Composite analysis, principal component analysis, single or multiple linear regression, principal oscillation patterns analysis and multi taper singular value decomposition are a few only statistical tools used in the past to isolate oscillations on various time scales. A separate data-adaptive tool (e.g. no a priori filter's shape unlike to Fourier spectral analysis with prescribed sine and cosine functions) is the Singular Spectrum Analysis (SSA) and its multichannel variant (MSSA). This method is mathematically equivalent to extended empirical orthogonal functions (EOFs) analysis of Weare and Nasstrom (1982) and it has been extensively used in many studies considering climatic fluctuations (among others Plaut and Vautard, 1994; White et al., 1997; Moron et al., 1998).

MSSA isolates quasi-periodic phenomena from a red noise background (Vautard et al., 1992; Ghil et al., 2002). Analogously to EOF expansion of the covariance matrix, MSSA is based on the EOF expansion of the temporal delayed covariance matrix constructed by embedding lagged copies of the original gridded data. The number of copies, termed embedding dimension or window length (M), determines the longest detected period and is a free parameter. Time EOFs (T-EOFs) which are M-long time sequences and the respective Time Principal Components (T-PCs) may or may not characterize oscillatory modes. A reliable oscillation is reflected in the phase quadrature of the two consecutive T-PCs as well as in the small difference of the corresponding eigenvalues. An additional criterion demands that the two associated time sequences described by the T-PCs are nearly periodic with the same period and in quadrature (Plaut and Vautard, 1994). Commonly, a traditional EOF is applied on the original time series to reduce the dimension of the delayed covariance matrix. Any analysis with MSSA is restricted to the first 15 leading T-EOFs; the rest are noise. When a T-EOF/T-PC pair, which fulfils the previous criteria, is detected, it can be used to reconstruct the gridded data associated with the selected oscillation. The MSSA toolbox is freely available at http://www.atmos.ucla.edu/tcd/ssa/.

In Chapter 1, a pair of oscillatory modes (7th and 8th T-EOFs) that show spectral peak at 12.5 years are detected with a 10-channel MSSA of 20 year window length. These modes explain 3.7% and 3.5% of the inter-annual variability of the annual tropical SST anomalies from the ERSST v3b dataset. The first 6 pairs describe the non-linear trend and ENSO-related frequencies (e.g. 3.6 years). The associated T-PCs fulfill the quadrature-relationship criterion of Plaut and Vautard (1994). This pair is used to

reconstruct SST anomalies related to the 12.5-yr oscillation. This oscillation is termed the Tropical Pacific Quasi Decadal Oscillation (TPQDO).

In Chapter 2, we are looking for 9 to 13-yr periodicities in the coupled simulations with the 11-yr solar cycle forcing. Hence we set M=14 years. Next, we calculate T-EOF and T-PCs pairs. The first 15 EOFs are considered (~78% of explained variance) but results do not depend on this number. The first six T-EOFs describe oscillatory pairs with periods of 3.7, 5.2 and 8.3 years respectively, whereas the 7th and 8th T-EOFs exhibit a clear spectral peak at 10.9 years. We note that the detected period is slightly sensitive to M. To examine if the 7th and 8th T-EOFs form a robust oscillatory pair we calculate the lag correlation function between the two T-PCs that exhibit a 10.9 years spectral peak. Both peaks in the lead/lag axis show values higher than 0.6, which exceeds the r=0.5 criterion of Plaut and Vautard (1994) as well as the most stringent (r=0.6) one of Moron et al. (1998).

Appendix 2: A low-order ENSO model

The low-order ENSO model (LO-ENSO) is a simple two-box model, which calculates the temperature anomalies in the western and eastern Pacific and thermocline depth anomalies in the western Pacific (e.g. Jin, 1996, 1997). LO-ENSO takes into account the amplification mechanism of the zonal wind-SST interaction (Bjerknes, 1966) as well as the out-of-phase, negative feedback of the heat content discharge/recharge between equatorial and off-equatorial latitudes (Wyrtki, 1985). The model reads,

$$\frac{dT_w}{dt} = -a(T_w - T_r) - u(T_e - T_w)/(L/2) \qquad \text{Eq. 1}$$

$$\frac{dT_e}{dt} = -a(T_e - T_r) - w(T_e - T_{sub})/H_m \qquad \text{Eq. 2}$$

$$\frac{dh_w}{dt} = -rh_w - \frac{rbL\tau}{2} \qquad \text{Eq. 3}$$

$$h_e = h_w + bL\tau \qquad \text{Eq. 4}$$

$$\frac{u}{L/2} = \varepsilon\beta\tau \qquad \text{Eq. 5}$$

$$\frac{w}{H_m} = -\beta\tau \qquad \text{Eq. 6}$$

$$\tau = -\mu(T_w - T_e)/\beta \qquad \text{Eq. 7}$$

$$T_{sub} = T_r - \frac{T_r - T_{r0}}{2}\left[1 - \tanh(H + h_e - z_0)/h^*\right] \qquad \text{Eq. 8}$$

The notation follows Timmerman and Jin (2002). Eqs. 1-3 are the prognostic equations of LO-ENSO. The first (second) prognostic equation describes the temperature anomalies in the well-mixed surface layer of the western (eastern) Pacific. The first terms on the right-hand side of Eqs.1 and 2 parameterize the net budget of radiative, sensible, and latent heat fluxes through the ocean surface in a form of Newtonian dumping. T_r describes the radiative-convective equilibrium temperature of western Pacific. The second term of Eq.1 represents the SST heating/cooling of western Pacific due to zonal advection. The second term of Eq.2 is responsible for dynamical cooling in the eastern Pacific due to upwelling of cold subsurface water. The temperature of the subsurface water (T_{sub}) is calculated in Eq.8. The Ekman pumping that is proportional to the zonal wind stress τ (Eq.7) controls upwelling. The third prognostic equation (Eq.3) states that the thermocline depth in the western Pacific (h_w) is controlled by wind stress τ with a damping rate of r. In this simplified version, influences on the SST variations of the wind bursts (white noise), Hadley cell dynamics, and the poleward heat transport are neglected.

We have re-written the previous equations in a simpler form with three prognostic variables, T_w, T_e, h_w and one diagnostic h_e. The new set of equations reads,

$$\frac{dT_w}{dt} = -a(T_w - T_r) + \varepsilon\mu(T_w - T_e)(T_e - T_w)$$ Eq. 9

$$\frac{dT_e}{dt} = -a(T_e - T_r) - \mu(T_e - T_{sub})(T_w - T_e)$$ Eq. 10

$$\frac{dh_w}{dt} = -rh_w + \frac{r\kappa(T_w - T_e)}{2}$$ Eq. 11

$$h_e = h_w - \kappa(T_w - T_e)$$ Eq. 12

$$T_{sub} = T_r - \frac{T_r - T_{r0}}{2}\left[1 - \tanh(H + h_2 - z_0)/h^*\right]$$ Eq. 13

Here the same terminology is used. The ε parameter measures the strength of zonal advection and normally it takes values between 0.01-0.1 (Jin, 1998). In our experiments is set to 0.0775. This value has been dictated by the physical constrain of non-negative h_e. That is, the thermocline depth in the eastern Pacific should not be lifted out of the sea surface. The rest parameters take values: a=1/180 days^{-1}, T_r=29.5 C, μ=0.0026 C^{-1}day^{-1}, L=15000000 m, h_m=50 m, H=100 m, z_0=75 m, h^*=62 m, r=1/400 days^{-1}, κ=22 m/C.

For the periodically forced experiments, Eq.10 is rewritten as follows:

$$\frac{dT_e}{dt} = -a(T_e - T_r) - \mu(T_e - T_{sub})(T_w - T_e) + A_{solar}\cos(\frac{2\pi}{T}t)$$

where A_{solar}=0.06 K and T=132 months. The last term of the right hand side describes the decadal perturbation of the temperature equation in the eastern Pacific. In the last set of simulations with LO-ENSO, a weak white noise is added in the wind stress equation (Eq.7). The probability density function (Gaussian) of the noise has zero mean and 0.005 standard deviation.

Appendix 3: The Quasi-Biennial Oscillation in MAECHAM5/MPIOM

The middle atmosphere extension of ECHAM5 (MAECHAM5) without interactive ocean coupling is one of the few general circulation models available that simulate a realistic Quasi-Biennial Oscillation (QBO) in terms of the amplitude of zonal winds and period (Giorgetta et al., 2006). MAECHAM5 generates alternating westerlies and easterlies, which descent downward to the lower equatorial stratosphere (approximately at 70 hPa) with an average period of 28 months. When the model is coupled to the Max Planck Institute Ocean Model (MPIOM), however, the simulated QBO period is unrealistically long (38 months). A 69 years control simulation with the coarse model shows a well-formed QBO but with unrealistically protracted westerlies in the lower equatorial stratosphere (Figure Ap.3-1). The model in T63L95/GR15L40 resolution fails completely to excite a QBO.
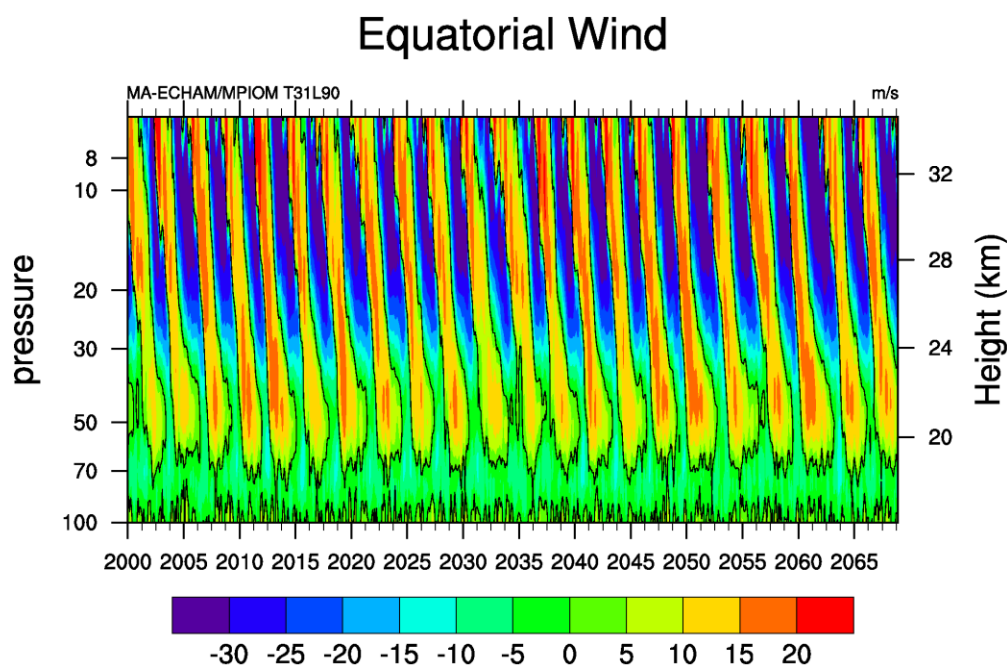
Figure Ap.3-1: The Quasi-Biennial Oscillation of the equatorial (5°S-5°N) zonal winds (m/s) simulated with the MAECHAM5/MPIOM prior to the modification in the gravity wave parameterization. A spectral analysis of zonal winds at 50 hPa shows a very sharp peak at 38 months. Time indexing is arbitrary.

The parameterized non-orographic gravity wave drag (NOGWD) in MAECHAM5 (Manzini and McFarlane, 1998) acts as a dimmer switch of the QBO period. In general, the stronger NOGWD is set the shorter the QBO period is simulated. Increasing this parameter (rmscon), however, would also impart the extra-tropical stratospheric circulation because the non-orographic gravity wave spectrum in the

default configuration is lunched uniformly in every latitude and longitude. To surpass this caveat, we implement a latitudinal variation of the NOGWD as described in Figure Ap.3-2, which pertains to T31L90/GR30L40 configuration. Details for the T63L95/GR15L40 configuration are given in Table Ap.3-1. Off the tropical band (30°S-30°N) the NOGWD takes its default value (rmscon=1), whereas it increases linearly up to a specified value (rmscon=1.07). The justification of such profile stems from the physical expectation that the amplitude of NOGWD should peak in tropical latitudes due to wave generation from deep convection. It should be noted, however, that such latitudinal enhancement is rather simplified and other, more physically meaningful profiles, have been proposed (e.g. Anstey et al., 2010). Under these modifications, the simulated QBO has average period of 28 months (not shown). In the finer horizontal resolution, the simulated QBO period is somewhat shorter (26 months).
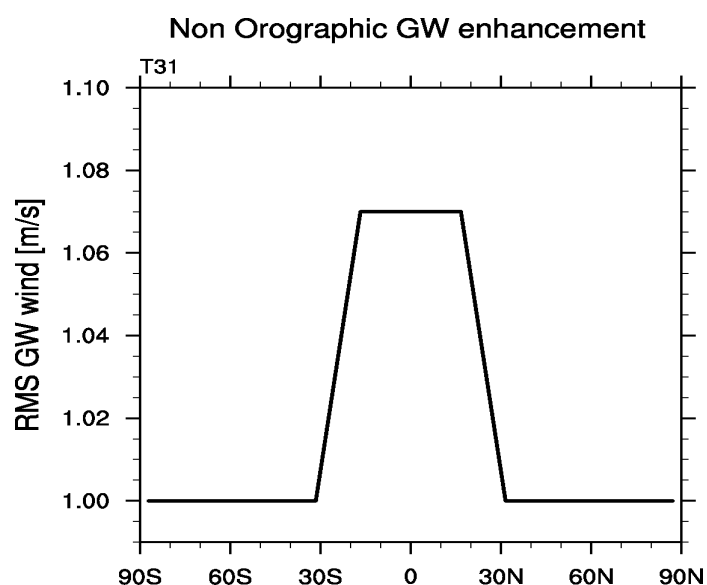
Figure Ap.3-2: Latitudinal variation of the parameter rmscon, which controls the non-orographic gravity wave drag.

Table Ap.3-1 Details of the latitudinal variation of the non-orographic gravity wave drag parameterization that is implemented in MAECHAM5/MPIOM.

	T31L90/GR30L40	T63L95/GR15L40
Modified rmscon	1.07	1.107
iheatcal	0	1
Latitude band where the modified rmscon is applied	15°S-15°N	5°S-5°N
Latitude above which the rmscon takes unit value	30°	10°

Bibliography

Allan, R. J.: ENSO and climatic variability in the last 150 years, in: El Niño and the Southern Osciallation: Multiscale Variability, Global and Regional Impacts, edited by: Diaz, H. F., and Markgraf, V., 1, Cambridge Univercity Press, Cambridge, 3-56, 2000.

An, S. I., and Wang, B.: Interdecadal change of the structure of the ENSO mode and its impact on the ENSO frequency, J. Clim., 13, 2044-2055, 2000.

Anstey, J. A., Shepherd, T. G., and Scinocca, J. F.: Influence of the Quasi-Biennial Oscillation on the Extratropical Winter Stratosphere in an Atmospheric General Circulation Model and in Reanalysis Data, J. Atmos. Sci., 67, 1402-1419, 2010.

Austin, J., Tourpali, K., Rozanov, E., Akiyoshi, H., Bekki, S., Bodeker, G., Bruhl, C., Butchart, N., Chipperfield, M., Deushi, M., Fomichev, V. I., Giorgetta, M. A., Gray, L., Kodera, K., Lott, F., Manzini, E., Marsh, D., Matthes, K., Nagashima, T., Shibata, K., Stolarski, R. S., Struthers, H., and Tian, W.: Coupled chemistry climate model simulations of the solar cycle in ozone and temperature, J Geophys Res-Atmos, 113, D11306, 2008.

Bal, S., Schimanke, S., Spangehl, T., and Cubasch, U.: On the robustness of the solar cycle signal in the Pacific region, Geophys. Res. Lett., 38, 2011.

Baldwin, M. P., and Dunkerton, T. J.: Stratospheric harbingers of anomalous weather regimes, Science, 294, 581-584, 2001.

Barnett, T. P.: A Solar-Ocean Relation - Fact or Fiction, Geophys. Res. Lett., 16, 803-806, 1989.

Bjerknes, J.: A Possible Response of Atmospheric Hadley Circulation to Equatorial Anomalies of Ocean Temperature, Tellus, 18, 820, 1966.

Burgers, G., and Stephenson, D. B.: The "normality" of El Nino, Geophys. Res. Lett., 26, 1027-1030, 1999.

Cagnazzo, C., Manzini, E., Giorgetta, M. A., Forster, P. M. D., and Morcrette, J. J.: Impact of an improved shortwave radiation scheme in the MAECHAM5 General Circulation Model, Atmos. Chem. Phys., 7, 2503-2515, 2007.

Camp, C. D., and Tung, K. K.: Surface warming by the solar cycle as revealed by the composite mean difference projection, Geophys. Res. Lett., 34, L14703, 2007.

CCMVAL: SPARC Report on the Evaluation of Chemistry-Climate Models, 2010.

Chandra, S., and McPeters, R. D.: The Solar-Cycle Variation of Ozone in the Stratosphere Inferred from Nimbus-7 and Noaa-11 Satellites, J Geophys Res-Atmos, 99, 20665-20671, 1994.

Charlton, A. J., and Polvani, L. M.: A new look at stratospheric sudden warmings. Part I: Climatology and modeling benchmarks, J. Clim., 20, 449-469, 2007.

Cibot, C., Maisonnave, E., Terray, L., and Dewitte, B.: Mechanisms of tropical Pacific interannual-to-decadal variability in the ARPEGE/ORCA global coupled model, Clim. Dyn., 24, 823-842, 2005.

Clement, A. C., Seager, R., Cane, M. A., and Zebiak, S. E.: An ocean dynamical thermostat, J. Clim., 9, 2190-2196, 1996.

Crooks, S. A., and Gray, L. J.: Characterization of the 11-year solar signal using a multiple regression analysis of the ERA-40 dataset, J. Clim., 18, 996-1015, 2005.

Deser, C., Alexander, M. A., Xie, S. P., and Phillips, A. S.: Sea Surface Temperature Variability: Patterns and Mechanisms, Annual Review of Marine Science, 2, 115-143, 10.1146/annurev-marine-120408-151453, 2010.

DiNezio, P. N., Clement, A. C., Vecchi, G. A., Soden, B. J., and Kirtman, B. P.: Climate Response of the Equatorial Pacific to Global Warming, J. Clim., 22, 4873-4892, 2009.

DiNezio, P. N., Clement, A. C., and Vecchi, G. A.: Reconciling differing views of tropical Pacific climate change, Eos, Transactions, American Geophysical Union, 91, 2010.

Douglass, D. H., and Clader, B. D.: Climate sensitivity of the Earth to solar irradiance, Geophys. Res. Lett., 29, 1786, 2002.

Eddy, J. A.: Maunder Minimum, Science, 192, 1189-1202, 1976.

Efron, B.: An Introduction to the Bootstrap, Chapman and Hall, 1993.

Fedorov, A. V., and Philander, S. G.: A stability analysis of tropical ocean-atmosphere interactions: Bridging measurements and theory for El Nino, J. Clim., 14, 3086-3101, 2001.

Flugel, M., Chang, P., and Penland, C.: The role of stochastic forcing in modulating ENSO predictability, J. Clim., 17, 3125-3140, 2004.

Frame, T. H. A., and Gray, L. J.: The 11-Yr Solar Cycle in ERA-40 Data: An Update to 2008, J. Clim., 23, 2213-2222, 2010.

Frohlich, C.: Solar irradiance variability since 1978 - Revision of the PMOD composite during solar cycle 21, Space Sci Rev, 125, 53-65, 2006.

Garcia, R. R., Marsh, D. R., Kinnison, D. E., Boville, B. A., and Sassi, F.: Simulation of secular trends in the middle atmosphere, 1950-2003, J Geophys Res-Atmos, 112, 2007.

Ghil, M., Allen, M. R., Dettinger, M. D., Ide, K., Kondrashov, D., Mann, M. E., Robertson, A. W., Saunders, A., Tian, Y., Varadi, F., and Yiou, P.: Advanced spectral methods for climatic time series, Rev. Geophys., 40, 1003, 2002.

Giorgetta, M. A., Manzini, E., Roeckner, E., Esch, M., and Bengtsson, L.: Climatology and forcing of the quasi-biennial oscillation in the MAECHAM5 model, J. Clim., 19, 3882-3901, 2006.

Gray, L. J., Beer, J., Geller, M., Haigh, J. D., Lockwood, M., Matthes, K., Cubasch, U., Fleitmann, D., Harrison, G., Hood, L., Luterbacher, J., Meehl, G. A., Shindell, D., van Geel, B., and White, W.: Solar Influences on Climate, Rev. Geophys., 48, RG4001, 2010.

Gu, D. F., and Philander, S. G. H.: Interdecadal climate fluctuations that depend on exchanges between the tropics and extratropics, Science, 275, 805-807, 1997.

Guilyardi, E., Delecluse, P., Gualdi, S., and Navarra, A.: Mechanisms for ENSO phase change in a coupled GCM, J. Clim., 16, 1141-1158, 2003.

Guilyardi, E., Wittenberg, A., Fedorov, A., Collins, M., Wang, C. Z., Capotondi, A., van Oldenborgh, G. J., and Stockdale, T.: Understanding El Nino in Ocean-Atmosphere General Circulation Models Progress and Challenges, Bull. Am. Meteorol. Soc., 90, 325, 2009.

Haigh, J. D.: The impact of solar variability on climate, Science, 272, 981-984, 1996.

Haigh, J. D.: The effects of solar variability on the Earth's climate, Philosophical Transactions of the Royal Society of London Series a-Mathematical Physical and Engineering Sciences, 361, 95-111, 2003.

Haigh, J. D., Blackburn, M., and Day, R.: The response of tropospheric circulation to perturbations in lower-stratospheric temperature, J. Clim., 18, 3672-3685, 2005.

Harder, J. W., Fontenla, J. M., Pilewskie, P., Richard, E. C., and Woods, T. N.: Trends in solar spectral irradiance variability in the visible and infrared, Geophys. Res. Lett., 36, L07801, 2009.

Hasegawa, T., and Hanawa, K.: Decadal-scale variability of upper ocean heat content in the tropical Pacific, Geophys. Res. Lett., 30, 1272, 2003.

Held, I. M., and Soden, B. J.: Robust responses of the hydrological cycle to global warming, J. Clim., 19, 5686-5699, 2006.

Holton, J. R., and Tan, H. C.: The Influence of the Equatorial Quasi-Biennial Oscillation on the Global Circulation at 50 Mb, J. Atmos. Sci., 37, 2200-2208, 1980.

Hood, L. L.: Effects of solar UV variability in the stratosphere, in: Solar variability and its effects of the Earth's atmosphere and climate system, edited by: Pap, J., Fox, P., Frohlich, C., Hudson, H., Kuhn, J., McCormack, J., North, G., Sprigg, W., and Wu, S., AGU Monograph Series, American Geophysical Union, Washington D.C., 2004.

Hood, L. L., Soukharev, B. E., and McCormack, J. P.: Decadal variability of the tropical stratosphere: Secondary influence of the El Nino-Southern Oscillation, J Geophys Res-Atmos, 115, D11113, 2010.

IPCC: Climate change 2007 : the physical science basis : contribution of Working Group I to the Fourth Assessment Report of the Intergovernmental Panel on Climate Change, Cambridge University Press, Cambridge ; New York, viii, 996 p. pp., 2007.

Jin, F. F.: Tropical ocean-atmosphere interaction, the Pacific cold tongue, and the El Nino Southern Oscillation, Science, 274, 76-78, 1996.

Jin, F. F.: An equatorial ocean recharge paradigm for ENSO .1. Conceptual model, J. Atmos. Sci., 54, 811-829, 1997.

Jin, F. F.: A simple model for the Pacific cold tongue and ENSO, J. Atmos. Sci., 55, 2458-2469, 1998.

Jungclaus, J. H., Keenlyside, N., Botzet, M., Haak, H., Luo, J. J., Latif, M., Marotzke, J., Mikolajewicz, U., and Roeckner, E.: Ocean circulation and tropical variability in the coupled model ECHAM5/MPI-OM, J. Clim., 19, 3952-3972, 2006.

Kieser, J.: The influence of precipitating energetic particles on the entire atmosphere-simulations with HAMMONIA, PhD thesis, University of Hamburg, Hamburg, 2011.

Kirtman, B. P.: Oceanic Rossby wave dynamics and the ENSO period in a coupled model, J. Clim., 10, 1690-1704, 1997.

Kirtman, B. P., and Schopf, P. S.: Decadal variability in ENSO predictability and prediction, J. Clim., 11, 2804-2822, 1998.

Klein, S. A., and Hartmann, D. L.: The Seasonal Cycle of Low Stratiform Clouds, J. Clim., 6, 1587-1606, 1993.

Knutson, T. R., and Manabe, S.: Model assessment of decadal variability and trends in the tropical Pacific Ocean, J. Clim., 11, 2273-2296, 1998.

Kodera, K., and Kuroda, Y.: Dynamical response to the solar cycle, J Geophys Res-Atmos, 107, 4749, 2002.

Kopp, G., Lawrence, G., and Rottman, G.: The Total Irradiance Monitor (TIM): Science results, Sol Phys, 230, 129-139, 2005.

Kristjansson, J. E., Stjern, C. W., Stordal, F., Fjaeraa, A. M., Myhre, G., and Jonasson, K.: Cosmic rays, cloud condensation nuclei and clouds - a reassessment using MODIS data, Atmos. Chem. Phys., 8, 7373-7387, 2008.

Langematz, U., Grenfell, J. L., Matthes, K., Mieth, P., Kunze, M., Steil, B., and Bruhl, C.: Chemical effects in 11-year solar cycle simulations with the freie universitat Berlin climate middle atmosphere model with online chemistry (FUB-CMAM-CHEM), Geophys. Res. Lett., 32, L13803, 2005.

Latif, M., Sperber, K., Arblaster, J., Braconnot, P., Chen, D., Colman, A., Cubasch, U., Cooper, C., Delecluse, P., DeWitt, D., Fairhead, L., Flato, G., Hogan, T., Ji, M., Kimoto, M., Kitoh, A., Knutson, T., Le Treut, H., Li, T., Manabe, S., Marti, O., Mechoso, C., Meehl, G., Power, S., Roeckner, E., Sirven, J., Terray, L., Vintzileos, A., Voss, R., Wang, B., Washington, W., Yoshikawa, I., Yu, J., and Zebiak, S.: ENSIP: the El Nino simulation intercomparison project, Clim. Dyn., 18, 255-276, 2001.

Lean, J.: Variations in the Suns Radiative Output, Rev. Geophys., 29, 505-535, 1991.

Lean, J., Beer, J., and Bradley, R.: Reconstruction of Solar Irradiance since 1610 - Implications for Climate-Change, Geophys. Res. Lett., 22, 3195-3198, 1995.

Lean, J., Rottman, G. J., Kyle, H. L., Woods, T. N., Hickey, J. R., and Puga, L. C.: Detection and parameterization of variations in solar mid- and near-ultraviolet radiation (200-400 nm), J Geophys Res-Atmos, 102, 29939-29956, 1997.

Lean, J.: Evolution of the sun's spectral irradiance since the Maunder Minimum, Geophys. Res. Lett., 27, 2425-2428, 2000.

Lean, J., Rottman, G., Harder, J., and Kopp, G.: SORCE contributions to new understanding of global change and solar variability, Sol Phys, 230, 27-53, 2005.

Lean, J., and Rind, D. H.: How natural and anthropogenic influences alter global and regional surface temperatures: 1889 to 2006, Geophys. Res. Lett., 35, L18701, 2008.

Lee, H., and Smith, A.: Simulation of the combined effects of solar cycle, quasi-biennial oscillation, and volcanic forcing on stratospheric ozone changes in recent decades, J Geophys Res-Atmos, 108, 2003.

Lee, J. N., Shindell, D. T., and Hameed, S.: The Influence of Solar Forcing on Tropical Circulation, J. Clim., 22, 5870-5885, 2009.

Lin, J. L.: The double-ITCZ problem in IPCC AR4 coupled GCMs: Ocean-atmosphere feedback analysis, J. Clim., 20, 4497-4525, 2007.

Mann, M. E., and Park, J.: Joint spatiotemporal modes of surface temperature and sea level pressure variability in the northern hemisphere during the last century, J. Clim., 9, 2137-2162, 1996.

Manney, G. L., Kruger, K., Pawson, S., Minschwaner, K., Schwartz, M. J., Daffer, W. H., Livesey, N. J., Mlynczak, M. G., Remsberg, E. E., Russell, J. M., and Waters, J. W.: The evolution of the stratopause during the 2006 major warming: Satellite data and assimilated meteorological analyses, J Geophys Res-Atmos, 113, 2008.

Mantua, N. J., Hare, S. R., Zhang, Y., Wallace, J. M., and Francis, R. C.: A Pacific interdecadal climate oscillation with impacts on salmon production, Bull. Am. Meteorol. Soc., 78, 1069-1079, 1997.

Manzini, E., and McFarlane, N. A.: The effect of varying the source spectrum of a gravity wave parameterization in a middle atmosphere general circulation model, J Geophys Res-Atmos, 103, 31523-31539, 1998.

Manzini, E., Giorgetta, M. A., Esch, M., Kornblueh, L., and Roeckner, E.: The influence of sea surface temperatures on the northern winter stratosphere: Ensemble simulations with the MAECHAM5 model, J. Clim., 19, 3863-3881, 2006.

Marsh, D., and Garcia, R.: Attribution of decadal variability in lower-stratospheric tropical ozone, Geophys. Res. Lett., 34, L21807, 2007.

Marsh, D. R., Garcia, R. R., Kinnison, D. E., Boville, B. A., Sassi, F., Solomon, S. C., and Matthes, K.: Modeling the whole atmosphere response to solar cycle changes in radiative and geomagnetic forcing, J Geophys Res-Atmos, 112, 2007.

Marsh, N., and Svensmark, H.: Low cloud properties influenced by cosmic rays, Phys Rev Lett, 85, 5004-5007, 2000.

Marsland, S. J., Haak, H., Jungclaus, J. H., Latif, M., and Roske, F.: The Max-Planck-Institute global ocean/sea ice model with orthogonal curvilinear coordinates, Ocean Modelling, 5, 91-127, 2003.

Matthes, K., Langematz, U., Gray, L. L., Kodera, K., and Labitzke, K.: Improved 11-year solar signal in the freie universitat Berlin climate middle atmosphere model (FUB-CMAM), J Geophys Res-Atmos, 109, D06101, 2004.

Matthes, K., Marsh, D. R., Garcia, R. R., Kinnison, D. E., Sassi, F., and Walters, S.: Role of the QBO in modulating the influence of the 11 year solar cycle on the atmosphere using constant forcings, J Geophys Res-Atmos, 115, 2010.

McPhaden, M. J.: Genesis and evolution of the 1997-98 El Nino, Science, 283, 950-954, 1999.

Meehl, G. A., Gent, P. R., Arblaster, J. M., Otto-Bliesner, B. L., Brady, E. C., and Craig, A.: Factors that affect the amplitude of El Nino in global coupled climate models, Clim. Dyn., 17, 515-526, 2001.

Meehl, G. A., Washington, W. M., Wigley, T. M. L., Arblaster, J. M., and Dai, A.: Solar and greenhouse gas forcing and climate response in the twentieth century, J. Clim., 16, 426-444, 2003.

Meehl, G. A., Arblaster, J. M., Branstator, G., and van Loon, H.: A coupled air-sea response mechanism to solar forcing in the Pacific region, J. Clim., 21, 2883-2897, 2008.

Meehl, G. A., and Arblaster, J. M.: A Lagged Warm Event-Like Response to Peaks in Solar Forcing in the Pacific Region, J. Clim., 22, 3647-3660, 2009.

Meehl, G. A., Arblaster, J. M., Matthes, K., Sassi, F., and van Loon, H.: Amplifying the Pacific Climate System Response to a Small 11-Year Solar Cycle Forcing, Science, 325, 1114-1118, 2009.

Misios, S., and Schmidt, H.: Mechanisms involved in the amplification of the 11-yr solar cycle signal in the tropical Pacific Ocean, Submitted in Journal of Climate, 2011.

Moron, V., Vautard, R., and Ghil, M.: Trends, interdecadal and interannual oscillations in global sea surface temperatures, Clim. Dyn., 14, 545-569, 1998.

Neelin, J. D., Battisti, D. S., Hirst, A. C., Jin, F. F., Wakata, Y., Yamagata, T., and Zebiak, S. E.: ENSO theory, J Geophys Res-Oceans, 103, 14261-14290, 1998.

Newman, M., Compo, G. P., and Alexander, M. A.: ENSO-forced variability of the Pacific decadal oscillation, J. Clim., 16, 3853-3857, 2003.

North, G. R., Bell, T. L., Cahalan, R. F., and Moeng, F. J.: Sampling Errors in the Estimation of Empirical Orthogonal Functions, Mon Weather Rev, 110, 699-706, 1982.

Philander, S. G.: El Niño, La Niña, and the southern oscillation, Int. Geophys., 46, Academic Press, San Diego, ix, 293 p. pp., 1990.

Philander, S. G. H.: The Response of Equatorial Oceans to a Relaxation of the Trade Winds, J. Phys. Oceanogr., 11, 176-189, 1981.

Pittock, A. B.: Critical Look at Long-Term Sun-Weather Relationships, Rev. Geophys., 16, 400-420, 1978.

Plaut, G., and Vautard, R.: Spells of Low-Frequency Oscillations and Weather Regimes in the Northern-Hemisphere, J. Atmos. Sci., 51, 210-236, 1994.

Power, S., Casey, T., Folland, C., Colman, A., and Mehta, V.: Inter-decadal modulation of the impact of ENSO on Australia, Clim. Dyn., 15, 319-324, 1999.

Randel, W. J., and Wu, F.: A stratospheric ozone profile data set for 1979-2005: Variability, trends, and comparisons with column ozone data, J Geophys Res-Atmos, 112, 2007.

Randel, W. J., Shine, K. P., Austin, J., Barnett, J., Claud, C., Gillett, N. P., Keckhut, P., Langematz, U., Lin, R., Long, C., Mears, C., Miller, A., Nash, J., Seidel, D. J., Thompson, D. W. J., Wu, F., and Yoden, S.: An update of observed stratospheric temperature trends, J Geophys Res-Atmos, 114, 2009.

Rasmusson, E. M., and Carpenter, T. H.: Variations in Tropical Sea-Surface Temperature and Surface Wind Fields Associated with the Southern Oscillation El-Nino, Mon Weather Rev, 110, 354-384, 1982.

Reichler, T., and Kim, J.: How well do coupled models simulate today's climate?, Bull. Am. Meteorol. Soc., 89, 303, 2008.

Rienecker, M. M., Suarez, M. J., Gelaro, R., Todling, R., Bacmeister, J., Liu, E., Bosilovich, M. G., Schubert, S. D., Takacs, L., Kim, G. K., Bloom, S., Chen, J. Y., Collins, D., Conaty, A., Da Silva, A., Gu, W., Joiner, J., Koster, R. D., Lucchesi, R., Molod, A., Owens, T., Pawson, S., Pegion, P., Redder, C. R., Reichle, R., Robertson, F. R., Ruddick, A. G., Sienkiewicz, M., and Woollen, J.: MERRA: NASA's Modern-Era Retrospective Analysis for Research and Applications, J. Clim., 24, 3624-3648, 2011.

Rind, D., Lean, J., and Healy, R.: Simulated time-dependent climate response to solar radiative forcing since 1600, J Geophys Res-Atmos, 104, 1973-1990, 1999.

Rind, D., Lean, J., Lerner, J., Lonergan, P., and Leboissitier, A.: Exploring the stratospheric/tropospheric response to solar forcing, J Geophys Res-Atmos, 113, D24103, 2008.

Rodgers, K. B., Friederichs, P., and Latif, M.: Tropical pacific decadal variability and its relation to decadal modulations of ENSO, J. Clim., 17, 3761-3774, 2004.

Roeckner, E., and Coauthors: The atmospheic general circulation model ECHAM5. Part I. Model description, Max-Planck-Institut für Meteorologie, Hamburg, Germany, 127 pp., 2003.

Roeckner, E., Brokopf, R., Esch, M., Giorgetta, M., Hagemann, S., Kornblueh, L., Manzini, E., Schlese, U., and Schulzweida, U.: Sensitivity of simulated climate to horizontal and vertical resolution in the ECHAM5 atmosphere model, J. Clim., 19, 3771-3791, 2006.

Roy, I., and Haigh, J. D.: Solar cycle signals in sea level pressure and sea surface temperature, Atmos. Chem. Phys., 10, 3147-3153, 2010.

Rozanov, E., Schraner, M., Schnadt, C., Egorova, T., Wild, M., Ohmura, A., Zubov, V., Schmutz, W., and Peter, T.: Assessment of the ozone and temperature variability during 1979-1993 with the chemistry-climate model SOCOL, Greenhouse Gases, Ozone, and Electrodynamics; Their Changes in the Middle Atmosphere and Lower Thermosphere, 35, 1375-1384, 2005.

Salby, M. L., and Callaghan, P. F.: Evidence of the solar cycle in the tropical troposphere, J Geophys Res-Atmos, 111, -, 2006a.

Salby, M. L., and Callaghan, P. F.: Relationship of the quasi-biennial oscillation to the stratospheric signature of the solar cycle, J Geophys Res-Atmos, 111, D06110, 2006b.

Schmidt, H., Brasseur, G. P., Charron, M., Manzini, E., Giorgetta, M. A., Diehl, T., Fomichev, V. I., Kinnison, D., Marsh, D., and Walters, S.: The HAMMONIA chemistry climate model: Sensitivity of the mesopause region to the 11-year solar cycle and CO_2 doubling, J. Clim., 19, 3903-3931, 2006.

Schmidt, H., Brasseur, G. P., and Giorgetta, M. A.: Solar cycle signal in a general circulation and chemistry model with internally generated quasi-biennial oscillation, J Geophys Res-Atmos, 115, D00I14, 2010.

Schmidt, H., Kieser, J., Misios, S., and Gruzdev, A. M.: The Atmospheric Response to Solar Variability: Simulations with a General Circulation and Chemistry Model for the Entire Atmosphere, in: Climate and Weather of the Sun Earth System, edited by: Lübken, F.-J., Springer, 2011.

Shindell, D. T., Faluvegi, G., Miller, R. L., Schmidt, G. A., Hansen, J. E., and Sun, S.: Solar and anthropogenic forcing of tropical hydrology, Geophys. Res. Lett., 33, L24706, 2006.

Smith, T. M., Reynolds, R. W., Peterson, T. C., and Lawrimore, J.: Improvements to NOAA's historical merged land-ocean surface temperature analysis (1880-2006), J. Clim., 21, 2283-2296, 2008.

Soukharev, B. E., and Hood, L. L.: Solar cycle variation of stratospheric ozone: Multiple regression analysis of long-term satellite data sets and comparisons with models, J Geophys Res-Atmos, 111, D20314, 2006.

Sun, F. P., and Yu, J. Y.: A 10-15-Yr Modulation Cycle of ENSO Intensity, J. Clim., 22, 1718-1735, 2009.

Thompson, D. W. J., Kennedy, J. J., Wallace, J. M., and Jones, P. D.: A large discontinuity in the mid-twentieth century in observed global-mean surface temperature, Nature, 453, 646-U645, 2008.

Timmermann, A., and Jin, F. F.: A nonlinear mechanism for decadal El Nino amplitude changes, Geophys. Res. Lett., 29, 1003, 2002.

Timmermann, A.: Decadal ENSO amplitude modulations: a nonlinear paradigm, Global Planet. Change, 37, 135-156, 2003.

Torrence, C., and Webster, P. J.: Interdecadal changes in the ENSO-monsoon system, J. Clim., 12, 2679-2690, 1999.

Tourpali, K., Schuurmans, C. J. E., van Dorland, R., Steil, B., and Bruhl, C.: Stratospheric and tropospheric response to enhanced solar UV radiation: A model study, Geophys. Res. Lett., 30, 1231, 2003.

Tourpali, K., Zerefos, C. S., Balis, D. S., and Bais, A. F.: The 11-year solar cycle in stratospheric ozone: Comparison between Umkehr and SBUVv8 and effects on surface erythemal irradiance, J Geophys Res-Atmos, 112, 2007.

Tourre, Y. M., Rajagopalan, B., and Kushnir, Y.: Dominant patterns of climate variability in the Atlantic Ocean during the last 136 years, J. Clim., 12, 2285-2299, 1999.

Tourre, Y. M., Cibot, C., Terray, L., White, W. B., and Dewitte, B.: Quasi-decadal and inter-decadal climate fluctuations in the Pacific Ocean from a CGCM, Geophys. Res. Lett., 32, L07710, 2005.

Tsutsui, J., Nishizawa, K., and Sassi, F.: Response of the middle atmosphere to the 11-year solar cycle simulated with the Whole Atmosphere Community Climate Model, J Geophys Res-Atmos, 114, D02111, 2009.

Tung, K. K., and Camp, C. D.: Solar cycle warming at the Earth's surface in NCEP and ERA-40 data: A linear discriminant analysis, J Geophys Res-Atmos, 113, D05114, 2008.

Tung, K. K., and Zhou, J. S.: The Pacific's Response to Surface Heating in 130 Yr of SST: La Nina-like or El Nino-like?, J. Atmos. Sci., 67, 2649-2657, 2010.

Uppala, S., and Coauthors: ERA-40: ECMWF 45-year reanalysis of the global atmosphere and surface conditions 1957-2002, ECMWF, Reading, United Kingdom, 2-21, 2004.

Uppala, S. M., Kallberg, P. W., Simmons, A. J., Andrae, U., Bechtold, V. D., Fiorino, M., Gibson, J. K., Haseler, J., Hernandez, A., Kelly, G. A., Li, X., Onogi, K., Saarinen, S., Sokka, N., Allan, R. P., Andersson, E., Arpe, K., Balmaseda, M. A., Beljaars, A. C. M., Van De Berg, L., Bidlot, J., Bormann, N., Caires, S., Chevallier, F., Dethof, A., Dragosavac, M., Fisher, M., Fuentes, M., Hagemann, S., Holm, E., Hoskins, B. J., Isaksen, L., Janssen, P. A. E. M., Jenne, R., McNally, A. P., Mahfouf, J. F., Morcrette, J. J., Rayner, N. A., Saunders, R. W., Simon, P., Sterl, A., Trenberth, K. E., Untch, A., Vasiljevic, D., Viterbo, P., and Woollen, J.: The ERA-40 re-analysis, Q. J. Roy. Meteorol. Soc., 131, 2961-3012, 2005.

Valcke, S., Caubel, D., Declat, D., and Terray, L.: OASIS Ocean Atmosphere Sea Ice Soil user's guide 85, 2003.

van Loon, H., Meehl, G. A., and Arblaster, J. M.: A decadal solar effect in the tropics in July-August, J. Atmos. Sol. Terr. Phys., 66, 1767-1778, 2004.

van Loon, H., Meehl, G. A., and Shea, D. J.: Coupled air-sea response to solar forcing in the Pacific region during northern winter, J Geophys Res-Atmos, 112, D02108, 2007.

van Loon, H., and Meehl, G. A.: The response in the Pacific to the sun's decadal peaks and contrasts to cold events in the Southern Oscillation, J. Atmos. Sol. Terr. Phys., 70, 1046-1055, 2008.

Vautard, R., Yiou, P., and Ghil, M.: Singular-Spectrum Analysis - a Toolkit for Short, Noisy Chaotic Signals, Physica D, 58, 95-126, 1992.

Vecchi, G. A., and Soden, B. J.: Global warming and the weakening of the tropical circulation, J. Clim., 20, 4316-4340, 2007.

Vimont, D. J.: The contribution of the interannual ENSO cycle to the spatial pattern of decadal ENSO-like variability, J. Clim., 18, 2080-2092, 2005.

Weare, B. C., and Nasstrom, J. S.: Examples of Extended Empirical Orthogonal Function Analyses, Mon Weather Rev, 110, 481-485, 1982.

White, W., Lean, J., Cayan, D. R., and Dettinger, M. D.: Response of global upper ocean temperature to changing solar irradiance, J Geophys Res-Oceans, 102, 3255-3266, 1997.

White, W., Cayan, D., and Lean, J.: Global upper ocean heat storage response to radiative forcing from changing solar irradiance and increasing greenhouse gas/aerosol concentrations, J Geophys Res-Oceans, 103, 21355-21366, 1998.

White, W., and Liu, Z.: Non-linear alignment of El Nino to the 11-yr solar cycle, Geophys. Res. Lett., 35, L19607, 2008a.

White, W. B., Dettinger, M. D., and Cayan, D. R.: Sources of global warming of the upper ocean on decadal period scales, J Geophys Res-Oceans, 108, 3248, 2003a.

White, W. B., and Tourre, Y. M.: Global SST/SLP waves during the 20th century, Geophys. Res. Lett., 30, 1651, 2003.

White, W. B., Tourre, Y. M., Barlow, M., and Dettinger, M.: A delayed action oscillator shared by biennial, interannual, and decadal signals in the Pacific Basin, J Geophys Res-Oceans, 108, 3070, 2003b.

White, W. B., and Liu, Z.: Resonant excitation of the quasi-decadal oscillation by the 11-year signal in the Sun's irradiance, J Geophys Res-Oceans, 113, C01002, 2008b.

Wyrtki, K.: Water Displacements in the Pacific and the Genesis of El-Nino Cycles, J Geophys Res-Oceans, 90, 7129-7132, 1985.

Yamashita, Y., Sakamoto, K., Akiyoshi, H., Takahashi, M., Nagashima, T., and Zhou, L. B.: Ozone and temperature response of a chemistry climate model to the solar cycle and sea surface temperature, J Geophys Res-Atmos, 115, D00M05, 2010.

Yeh, S. W., and Kirtman, B. P.: Tropical Pacific decadal variability and ENSO amplitude modulation in a CGCM, J Geophys Res-Oceans, 109, C11009, 2004.

Yeh, S. W., and Kirtman, B. P.: Pacific decadal variability and decadal ENSO amplitude modulation, Geophys. Res. Lett., 32, L05703, 2005.

Yule, G. U.: Why do we sometimes get nonsense-correlations between time-series? - A study in sampling and the nature of time-series., J R Stat Soc, 89, 1-69, 1926.

Zhang, Y., Wallace, J. M., and Battisti, D. S.: ENSO-like interdecadal variability: 1900-93, J. Clim., 10, 1004-1020, 1997.

Zhou, J. S., and Tung, K. K.: Solar Cycles in 150 Years of Global Sea Surface Temperature Data, J. Clim., 23, 3234-3248, 2010.

Acknowledgements

First and foremost, I wish to express my gratitude to my advisor, Dr. Hauke Schmidt, for his constant support during my studies, and for he always found time to address my countless questions. Thank you for giving me the opportunity to work in such a vivid and inspiring environment as the Max-Planck Institute for Meteorology. Many thanks to Dr. Marco Giorgetta for stimulating discussions and generous help. I trully appreciate the careful supervision of Prof. Bjorn Stevens, who guided my research with many insightful suggestions.

I would like to thank all members of the Middle and Upper Atmosphere group and particularly Manu Anna, Ulrike and Felix with whom I shared the same office. The positive spirit within the group made the work fun. I thank Felix for providing the software to calculate SSWs.

I am glad to participate on the International Max Planck Research School on Earth system Modelling. I deeply appreciate the administrative and moral support of Antje and Conni.

I must thank all the colleagues and friends who helped during my PhD in various aspects and in particular: Seethalla, Heinz Jurgen, Katrin, Christine, Fanny, Steffen, Rossi, Freja, Nils, Florian, Daniel, Daniel-Hernandez, Veronika, Chao, Natasha, Dmitri, Leonida, Thomas, Mario and Olga[2]. I thank Suvarchal for proof reading my thesis. I must thank Eleftheria, who was the other member of the Greek-connection of the MPI.

I am grateful to my parents, Michali and Sofia, and to my sisters, Vaggelitsa and Kiparissia, for their love. I am convinced that without Eleni, I would have not carried out this research. Thank you from the deep of my heart for supporting and waiting…